Image Analysis for Software-Separation and Classification of Touching Grains

by
Pankaj Shatadal

A THESIS
SUBMITTED TO THE FACULTY OF GRADUATE STUDIES
THE UNIVERSITY OF MANITOBA
IN PARTIAL FULFILMENT OF THE REQUIREMENTS FOR THE DEGREE OF

Doctor of Philosophy

Department of Agricultural Engineering
University of Manitoba
Winnipeg, Manitoba

ISBN 0-315-98980-7

Name PANKAJ SHATADAL

Dissertation Abstracts International is arranged by broad, general subject categories. Please select the one subject which most nearly describes the content of your dissertation. Enter the corresponding four-digit code in the spaces provided.

AGRICULTURAL ENGINEERING
SUBJECT TERM

0539
SUBJECT CODE

U·M·I

Subject Categories

THE HUMANITIES AND SOCIAL SCIENCES

COMMUNICATIONS AND THE ARTS
Architecture 0729
Art History 0377
Cinema 0900
Dance 0378
Fine Arts 0357
Information Science 0723
Journalism 0391
Library Science 0399
Mass Communications 0708
Music 0413
Speech Communication 0459
Theater 0465

EDUCATION
General 0515
Administration 0514
Adult and Continuing 0516
Agricultural 0517
Art 0273
Bilingual and Multicultural 0282
Business 0688
Community College 0275
Curriculum and Instruction 0727
Early Childhood 0518
Elementary 0524
Finance 0277
Guidance and Counseling 0519
Health 0680
Higher 0745
History of 0520
Home Economics 0278
Industrial 0521
Language and Literature 0279
Mathematics 0280
Music 0522
Philosophy of 0998
Physical 0523
Psychology 0525
Reading 0535
Religious 0527
Sciences 0714
Secondary 0533
Social Sciences 0534
Sociology of 0340
Special 0529
Teacher Training 0530
Technology 0710
Tests and Measurements 0288
Vocational 0747

LANGUAGE, LITERATURE AND LINGUISTICS
Language
- General 0679
- Ancient 0289
- Linguistics 0290
- Modern 0291

Literature
- General 0401
- Classical 0294
- Comparative 0295
- Medieval 0297
- Modern 0298
- African 0316
- American 0591
- Asian 0305
- Canadian (English) 0352
- Canadian (French) 0355
- English 0593
- Germanic 0311
- Latin American 0312
- Middle Eastern 0315
- Romance 0313
- Slavic and East European 0314

PHILOSOPHY, RELIGION AND THEOLOGY
Philosophy 0422
Religion
- General 0318
- Biblical Studies 0321
- Clergy 0319
- History of 0320
- Philosophy of 0322

Theology 0469

SOCIAL SCIENCES
American Studies 0323
Anthropology
- Archaeology 0324
- Cultural 0326
- Physical 0327

Business Administration
- General 0310
- Accounting 0272
- Banking 0770
- Management 0454
- Marketing 0338

Canadian Studies 0385
Economics
- General 0501
- Agricultural 0503
- Commerce-Business 0505
- Finance 0508
- History 0509
- Labor 0510
- Theory 0511

Folklore 0358
Geography 0366
Gerontology 0351
History
- General 0578
- Ancient 0579
- Medieval 0581
- Modern 0582
- Black 0328
- African 0331
- Asia, Australia and Oceania 0332
- Canadian 0334
- European 0335
- Latin American 0336
- Middle Eastern 0333
- United States 0337

History of Science 0585
Law 0398
Political Science
- General 0615
- International Law and Relations 0616
- Public Administration 0617

Recreation 0814
Social Work 0452
Sociology
- General 0626
- Criminology and Penology ... 0627
- Demography 0938
- Ethnic and Racial Studies 0631
- Individual and Family Studies 0628
- Industrial and Labor Relations 0629
- Public and Social Welfare 0630
- Social Structure and Development 0700
- Theory and Methods 0344

Transportation 0709
Urban and Regional Planning 0999
Women's Studies 0453

THE SCIENCES AND ENGINEERING

BIOLOGICAL SCIENCES
Agriculture
- General 0473
- Agronomy 0285
- Animal Culture and Nutrition 0475
- Animal Pathology 0476
- Food Science and Technology 0359
- Forestry and Wildlife 0478
- Plant Culture 0479
- Plant Pathology 0480
- Plant Physiology 0817
- Range Management 0777
- Wood Technology 0746

Biology
- General 0306
- Anatomy 0287
- Biostatistics 0308
- Botany 0309
- Cell 0379
- Ecology 0329
- Entomology 0353
- Genetics 0369
- Limnology 0793
- Microbiology 0410
- Molecular 0307
- Neuroscience 0317
- Oceanography 0416
- Physiology 0433
- Radiation 0821
- Veterinary Science 0778
- Zoology 0472

Biophysics
- General 0786
- Medical 0760

EARTH SCIENCES
Biogeochemistry 0425
Geochemistry 0996
Geodesy 0370
Geology 0372
Geophysics 0373
Hydrology 0388
Mineralogy 0411
Paleobotany 0345
Paleoecology 0426
Paleontology 0418
Paleozoology 0985
Palynology 0427
Physical Geography 0368
Physical Oceanography 0415

HEALTH AND ENVIRONMENTAL SCIENCES
Environmental Sciences 0768
Health Sciences
- General 0566
- Audiology 0300
- Chemotherapy 0992
- Dentistry 0567
- Education 0350
- Hospital Management 0769
- Human Development 0758
- Immunology 0982
- Medicine and Surgery 0564
- Mental Health 0347
- Nursing 0569
- Nutrition 0570
- Obstetrics and Gynecology .. 0380
- Occupational Health and Therapy 0354
- Ophthalmology 0381
- Pathology 0571
- Pharmacology 0419
- Pharmacy 0572
- Physical Therapy 0382
- Public Health 0573
- Radiology 0574
- Recreation 0575
- Speech Pathology 0460
- Toxicology 0383

Home Economics 0386

PHYSICAL SCIENCES
Pure Sciences
Chemistry
- General 0485
- Agricultural 0749
- Analytical 0486
- Biochemistry 0487
- Inorganic 0488
- Nuclear 0738
- Organic 0490
- Pharmaceutical 0491
- Physical 0494
- Polymer 0495
- Radiation 0754

Mathematics 0405
Physics
- General 0605
- Acoustics 0986
- Astronomy and Astrophysics 0606
- Atmospheric Science 0608
- Atomic 0748
- Electronics and Electricity 0607
- Elementary Particles and High Energy 0798
- Fluid and Plasma 0759
- Molecular 0609
- Nuclear 0610
- Optics 0752
- Radiation 0756
- Solid State 0611

Statistics 0463

Applied Sciences
Applied Mechanics 0346
Computer Science 0984
Engineering
- General 0537
- Aerospace 0538
- Agricultural 0539
- Automotive 0540
- Biomedical 0541
- Chemical 0542
- Civil 0543
- Electronics and Electrical 0544
- Heat and Thermodynamics ... 0348
- Hydraulic 0545
- Industrial 0546
- Marine 0547
- Materials Science 0794
- Mechanical 0548
- Metallurgy 0743
- Mining 0551
- Nuclear 0552
- Packaging 0549
- Petroleum 0765
- Sanitary and Municipal 0554
- System Science 0790

Geotechnology 0428
Operations Research 0796
Plastics Technology 0795
Textile Technology 0994

PSYCHOLOGY
General 0621
Behavioral 0384
Clinical 0622
Developmental 0620
Experimental 0623
Industrial 0624
Personality 0625
Physiological 0989
Psychobiology 0349
Psychometrics 0632
Social 0451

Nom _____

Dissertation Abstracts International est organisé en catégories de sujets. Veuillez s.v.p. choisir le sujet qui décrit le mieux votre thèse et inscrivez le code numérique approprié dans l'espace réservé ci-dessous.

_____ ☐☐☐ U·M·I

SUJET — CODE DE SUJET

Catégories par sujets

HUMANITÉS ET SCIENCES SOCIALES

COMMUNICATIONS ET LES ARTS
Architecture 0729
Beaux-arts 0357
Bibliothéconomie 0399
Cinéma 0900
Communication verbale 0459
Communications 0708
Danse 0378
Histoire de l'art 0377
Journalisme 0391
Musique 0413
Sciences de l'information 0723
Théâtre 0465

ÉDUCATION
Généralités 515
Administration 0514
Art 0273
Collèges communautaires 0275
Commerce 0688
Économie domestique 0278
Éducation permanente 0516
Éducation préscolaire 0518
Éducation sanitaire 0680
Enseignement agricole 0517
Enseignement bilingue et multiculturel 0282
Enseignement industriel 0521
Enseignement primaire. 0524
Enseignement professionnel 0747
Enseignement religieux 0527
Enseignement secondaire 0533
Enseignement spécial 0529
Enseignement supérieur 0745
Évaluation 0288
Finances 0277
Formation des enseignants 0530
Histoire de l'éducation 0520
Langues et littérature 0279
Lecture 0535
Mathématiques 0280
Musique 0522
Orientation et consultation 0519
Philosophie de l'éducation 0998
Physique 0523
Programmes d'études et enseignement 0727
Psychologie 0525
Sciences 0714
Sciences sociales 0534
Sociologie de l'éducation 0340
Technologie 0710

LANGUE, LITTÉRATURE ET LINGUISTIQUE
Langues
- Généralités 0679
- Anciennes 0289
- Linguistique 0290
- Modernes 0291

Littérature
- Généralités 0401
- Anciennes 0294
- Comparée 0295
- Médiévale 0297
- Moderne 0298
- Africaine 0316
- Américaine 0591
- Anglaise 0593
- Asiatique 0305
- Canadienne (Anglaise) 0352
- Canadienne (Française) 0355
- Germanique 0311
- Latino-américaine 0312
- Moyen-orientale 0315
- Romane 0313
- Slave et est-européenne 0314

PHILOSOPHIE, RELIGION ET THÉOLOGIE
Philosophie 0422
Religion
- Généralités 0318
- Clergé 0319
- Études bibliques 0321
- Histoire des religions 0320
- Philosophie de la religion 0322

Théologie 0469

SCIENCES SOCIALES
Anthropologie
- Archéologie 0324
- Culturelle 0326
- Physique 0327

Droit 0398
Économie
- Généralités 0501
- Commerce-Affaires 0505
- Économie agricole 0503
- Économie du travail 0510
- Finances 0508
- Histoire 0509
- Théorie 0511

Études américaines 0323
Études canadiennes 0385
Études féministes 0453
Folklore 0358
Géographie 0366
Gérontologie 0351
Gestion des affaires
- Généralités 0310
- Administration 0454
- Banques 0770
- Comptabilité 0272
- Marketing 0338

Histoire
- Histoire générale 0578
- Ancienne 0579
- Médiévale 0581
- Moderne 0582
- Histoire des noirs 0328
- Africaine 0331
- Canadienne 0334
- États-Unis 0337
- Européenne 0335
- Moyen-orientale 0333
- Latino-américaine 0336
- Asie, Australie et Océanie 0332

Histoire des sciences 0585
Loisirs 0814
Planification urbaine et régionale 0999
Science politique
- Généralités 0615
- Administration publique 0617
- Droit et relations internationales 0616

Sociologie
- Généralités 0626
- Aide et bien-être social 0630
- Criminologie et établissements pénitentiaires 0627
- Démographie 0938
- Études de l' individu et de la famille 0628
- Études des relations interethniques et des relations raciales 0631
- Structure et développement social 0700
- Théorie et méthodes. 0344
- Travail et relations industrielles 0629

Transports 0709
Travail social 0452

SCIENCES ET INGÉNIERIE

SCIENCES BIOLOGIQUES
Agriculture
- Généralités 0473
- Agronomie. 0285
- Alimentation et technologie alimentaire 0359
- Culture 0479
- Élevage et alimentation 0475
- Exploitation des pâturages 0777
- Pathologie animale 0476
- Pathologie végétale 0480
- Physiologie végétale 0817
- Sylviculture et faune 0478
- Technologie du bois 0746

Biologie
- Généralités 0306
- Anatomie 0287
- Biologie (Statistiques) 0308
- Biologie moléculaire 0307
- Botanique 0309
- Cellule 0379
- Écologie 0329
- Entomologie 0353
- Génétique 0369
- Limnologie 0793
- Microbiologie 0410
- Neurologie 0317
- Océanographie 0416
- Physiologie 0433
- Radiation 0821
- Science vétérinaire 0778
- Zoologie 0472

Biophysique
- Généralités 0786
- Medicale 0760

SCIENCES DE LA TERRE
Biogéochimie 0425
Géochimie 0996
Géodésie 0370
Géographie physique 0368
Géologie 0372
Géophysique 0373
Hydrologie 0388
Minéralogie 0411
Océanographie physique 0415
Paléobotanique 0345
Paléoécologie 0426
Paléontologie 0418
Paléozoologie 0985
Palynologie 0427

SCIENCES DE LA SANTÉ ET DE L'ENVIRONNEMENT
Économie domestique 0386
Sciences de l'environnement 0768
Sciences de la santé
- Généralités 0566
- Administration des hôpitaux 0769
- Alimentation et nutrition 0570
- Audiologie 0300
- Chimiothérapie 0992
- Dentisterie 0567
- Développement humain 0758
- Enseignement 0350
- Immunologie 0982
- Loisirs 0575
- Médecine du travail et thérapie 0354
- Médecine et chirurgie 0564
- Obstétrique et gynécologie 0380
- Ophtalmologie 0381
- Orthophonie 0460
- Pathologie 0571
- Pharmacie 0572
- Pharmacologie 0419
- Physiothérapie 0382
- Radiologie 0574
- Santé mentale 0347
- Santé publique 0573
- Soins infirmiers 0569
- Toxicologie 0383

SCIENCES PHYSIQUES
Sciences Pures
Chimie
- Généralités 0485
- Biochimie 487
- Chimie agricole 0749
- Chimie analytique 0486
- Chimie minérale 0488
- Chimie nucléaire 0738
- Chimie organique 0490
- Chimie pharmaceutique 0491
- Physique 0494
- PolymÈres 0495
- Radiation 0754

Mathématiques 0405
Physique
- Généralités 0605
- Acoustique 0986
- Astronomie et astrophysique 0606
- Électronique et électricité 0607
- Fluides et plasma 0759
- Météorologie 0608
- Optique 0752
- Particules (Physique nucléaire) 0798
- Physique atomique 0748
- Physique de l'état solide 0611
- Physique moléculaire 0609
- Physique nucléaire 0610
- Radiation 0756

Statistiques 0463

Sciences Appliqués Et Technologie
Informatique 0984
Ingénierie
- Généralités 0537
- Agricole 0539
- Automobile 0540
- Biomédicale 0541
- Chaleur et thermodynamique 0348
- Conditionnement (Emballage) 0549
- Génie aérospatial 0538
- Génie chimique 0542
- Génie civil 0543
- Génie électronique et électrique 0544
- Génie industriel 0546
- Génie mécanique 0548
- Génie nucléaire 0552
- Ingénierie des systèmes 0790
- Mécanique navale 0547
- Métallurgie 0743
- Science des matériaux 0794
- Technique du pétrole 0765
- Technique minière 0551
- Techniques sanitaires et municipales 0554
- Technologie hydraulique 0545

Mécanique appliquée 0346
Géotechnologie 0428
Matières plastiques (Technologie) 0795
Recherche opérationnelle 0796
Textiles et tissus (Technologie) 0794

PSYCHOLOGIE
Généralités 0621
Personnalité 0625
Psychobiologie 0349
Psychologie clinique 0622
Psychologie du comportement 0384
Psychologie du développement 0620
Psychologie expérimentale 0623
Psychologie industrielle 0624
Psychologie physiologique 0989
Psychologie sociale 0451
Psychométrie 0632

IMAGE ANALYSIS FOR SOFTWARE-SEPARATION AND CLASSIFICATION OF TOUCHING GRAINS

BY

PANKAJ SHATADAL

A Thesis submitted to the Faculty of Graduate Studies of the University of Manitoba in partial fulfillment of the requirements for the degree of

DOCTOR OF PHILOSOPHY

ABSTRACT

A mathematical morphology based algorithm was developed and tested for disconnecting the conjoint kernel regions in an image of touching grains. The algorithm found a marker for each grain present in the image. It constructed the image of disconnected kernels by growing the markers within the boundaries of the kernels in the original image with a logic which prevented the merging of the neighbouring regions. The logic was implemented via a sequential thickening operation. The algorithm was tested on the images of the touching kernels of hard red spring (HRS) wheat, durum wheat, barley, oats, and rye. Random touching patterns of the kernels were used in testing the algorithm. The algorithm was successful in disconnecting 95% HRS wheat and durum wheat, 94% barley, 89% rye, and 79% oats conjoint kernel regions.

The kernels used for a touching grains image were separated physically and another image of the kernels was acquired. A feature measurement routine was developed to compute the area, perimeter, length, width, maximum and minimum radii, rectangular aspect ratio, thinness ratio, radius ratio, area ratio, and the ratio of mean to standard deviation of all the radii of a kernel. Except for the area of oats, the change in the geometrical features of the software-separated kernels from the corresponding features of the physically-separated kernels was less than or equal to the variation between the tolerance limits of the measurement system. Hard red spring wheat was successfully discriminated from durum wheat and other cereal grains using the geometrical features of the software-separated kernels. An overall classification success of 93.3% was

achieved in a five-way classification among HRS wheat, durum wheat, barley, oats, and rye. Only 1.7% additional kernels were correctly classified when the features from the physically-separated kernels were used.

ACKNOWLEDGEMENTS

I wish to express my gratitude to Dr. D.S. Jayas for giving me the opportunity to work in the area of Digital Image Processing and for his guidance, encouragement, and support during the course of this study.

I thank Dr. H.D. Sapirstein for his valuable comments and suggestions to my research. I also thank Drs. N.D.G. White and E. Shwedyk for serving on my thesis committee and Dr. N.R. Bulley for his cooperation and guidance.

I thank Dr. T.P. McDonald for serving as my external examiner.

I acknowledge Prince Rupert Grain Ltd., Natural Sciences and Engineering Research Council of Canada, Agriculture Canada, University of Manitoba Graduate Fellowship Committee, University of Manitoba Research Grants Committee, and University of Manitoba Research Development Funds Committee for financial support of this study.

Many special thanks to Jeff Hehn, Atul Verma, and G.K. Adil for their help and cooperation. I also thank Samir Majumdar and X. Luo for their help.

I thank Messrs. Jack G. Putnam, Rob Ataman, and M. McDonald, for their technical assistance.

Special thanks are due to Dr. K. Alagusundaram for being a constant source of encouragement and help.

I dedicate this thesis to my parents and family for their endless love and support.

TABLE OF CONTENTS

LIST OF FIGURES

LIST OF TABLES

NOTATIONS

1. SETS

$\{x \mid *\}$	Set of points x satisfying property *
A,B,X,Y,Z	Digital sets under study

2. LOGIC AND SET TRANSFORMATIONS

$x \in A$	Point x belongs to set A
$A \subseteq B$	Set A is contained in (or equals) set B
A^c	Complement of set A, i.e. set of points which do not belong to A
$(A)_x$	Translate of set A by vector x
$A \cup B$	Set union, i.e. set of points belonging to A or to B
$A \cap B$	Set intersection, i.e. set of points belonging to both A and B
A/B	Set difference, i.e. set of points belonging to A and not to B
$\bigcup_{b \in B} A_b$	Union of all the translates A_b with $b \in B$
$\bigcap_{b \in B} A_b$	Intersection of all the translates A_b with $b \in B$
$A \oplus B$	Dilation of A by B
$A \ominus B$	Erosion of A by B
$A \circledast B$	Hit or Miss transform of A by B
$A \otimes B$	Thinning of A by B

$A \odot B$	Thickening of A by B
$A \circ B$	Opening of A by B
$A \bullet B$	Closing of A by B

CHAPTER 1: INTRODUCTION

There is a growing interest in applying machine vision technology to develop a fast, accurate, and automatic system for information acquisition on the content and quality of a grain sample. The term machine vision embodies the process in which a physical image sensor (instead of the human eye) is used to acquire images of given objects and dedicated computing hardware (instead of the human brain) is used to analyze the images with the objective of performing a pre-defined visual task. The important reasons behind the enhanced interest in utilizing machine vision technology for grain sample analysis are the increased awareness of the benefits of an automatic inspection system, the superior performance of microprocessors, and the continued lowering of electronics cost. Machine vision inspection is already in commercial use in automotive, electronics, and other industries. Many of the industrial objects are of defined size, shape, color, and texture. Agricultural or biological objects, on the other hand, are of variable size, shape, color, and texture. It is, therefore, more challenging to adapt machine vision technology to the plethora of inspection tasks in the agri-food sector (Tillet, 1990; Kranzler, 1985; Sarkar, 1986).

The important applications of machine vision to the grain industry include the design and development of an objective, fast, and reliable grain grading system and the on-line monitoring of grain in continuous flow at delivery points such as a terminal elevator. Grading decisions on grains and other agricultural products, by and large, require visual inspection of the product sample by trained personnel. Inspection tasks are

repetitive in nature and, in some cases, are performed in an uncomfortable environment. Fatigue of personnel is, therefore, likely. Despite training, the grading decisions are inherently subjective and are influenced by the individual experience of an inspector. Human visual inspection is prone to errors in applying the numerous grading criteria consistently (Kohler, 1991). An automatic visual inspection system which can apply the grading specifications consistently, objectively, and without fatigue will be an invaluable tool for the grain industry.

Fast and accurate information on the contents of a grain sample can be used to increase the efficiency of most grain handling operations (such as grain unloading, cleaning, binning, and shipping) at a terminal elevator. For example, such information can be used to optimize the selection and adjustment of the cleaning machines. This would lead to increased cleaning throughput and enhanced recovery of salvageable grains. Use of machine-vision-guided controls and robotics can lead to complete automation of modern terminal elevators. Efforts in this direction are underway at Prince Rupert Grain Ltd., a modern terminal elevator on the west coast of Canada.

The machine vision system was found to be more precise and efficient in measuring the dimensions of seeds than trained human inspectors working with a microscope (Churchill et al., 1990). Certain cracks and blemishes on a kernel surface may not be easily detected by human visual inspection but algorithms can be developed to detect them by machine vision (Kim et al., 1989, 1990; Paulsen et al., 1989). Another advantage of machine vision inspection is that it can make use of the radiometric information from outside the visible band of the electromagnetic spectrum. For example,

soft x-ray images can be used to gain information on internal anatomical changes (Bulley et al., 1984) and quality of grain. Imaging techniques which use energy other than electromagnetic radiation, such as nuclear magnetic resonance (NMR) imaging, can also be used. The NMR imaging technology, however, is expensive and its use in the grain industry is not economically feasible at this time.

The development of a machine vision inspection system for a given application begins with the initial research to examine the specific problems involved in the application, usually in a laboratory setting. At this stage, the application specific algorithms can be developed using a general purpose computer. The on-line inspection in the field or industrial setting may, however, require the use of hard-wired logic or special purpose computing architecture to achieve inspection at a realistic speed (Marchant, 1985).

Wheat is the major crop of Canada and contributes significantly to the economy of prairie provinces of Canada. A machine-vision-based wheat grading and monitoring system is awaited by the grain industry of Canada and other wheat producing western nations. Several researchers (Neuman et al., 1987, 1989a, 1989b; Sapirstein and Bushuk, 1989; Sapirstein et al., 1987; Kohler, 1991; Symons and Fulcher, 1988a, 1988b; Chen et al., 1989; Thomson and Pomeranz, 1991; Myers and Edsall, 1989; Barker et al., 1992a, 1992b, 1992c, 1992d; Keefe, 1992; Keefe and Draper, 1986; Zayas et al., 1985, 1986, 1989) have applied digital image analysis and statistical pattern recognition techniques to test whether certain decisions required in grading wheat can be successfully made using machine vision. One of the constraints in these studies was that the grain feature

extraction algorithms required the kernels to be presented to the camera in a scattered or non-touching manner or one kernel at a time. This was necessary because two or more kernels which were touching resulted in an image in which regions corresponding to the kernels (hereafter called kernel regions; not to be confused with different anatomical parts of a kernel) joined together making the feature measurement on an individual kernel region impossible. An algorithm which can disconnect the merged kernel regions (in a sense that pixels joining the two kernel regions are removed) will facilitate the practical implementation of automatic grain feature measurements on multiple kernels. In practice, a sample presentation device, such as a vibrating bed, may be required to present the kernels in a single-kernel-deep layer. An automatic grain grading or monitoring system is expected to possess the capability of identifying the individual kernels when the kernel regions are joined. This is possible if conjoint kernel regions are disconnected. To my knowledge, an algorithm to disconnect conjoint regions of touching grain kernels has not been reported.

It was shown by Chermant et al. (1981) that "watershed" algorithm could disconnect the conjoint circular or approximately circular regions. It was, therefore, hypothesized that the watershed algorithm could be modified to disconnect the conjoint grain kernel regions if the kernels are of approximately convex shape. It was further hypothesized that the geometrical features of the disconnected kernels can be used in the discrimination of different grain species using statistical pattern recognition techniques.

The objectives of my thesis research were (i) to develop and implement an algorithm to disconnect the conjoint regions of touching grain kernels and to test the

effectiveness of the algorithm on hard red spring (HRS) wheat, durum wheat, barley, oats, and rye kernels; (ii) to develop software for feature measurements on grain kernels (the features of interest were: area, perimeter, length, width, maximum and minimum radii, thinness ratio, rectangular aspect ratio, radius ratio, and ratio of mean to standard deviation of all the radii); (iii) to test the integrity of the features after software separation of kernels (*i.e.* after disconnecting the touching kernels using the algorithm developed for objective (i)); and (iv) to test the discriminating ability of the geometrical features of software separated kernels for the classification of HRS wheat from durum wheat, barley, oats, and rye.

CHAPTER 2: REVIEW OF LITERATURE

2.1 Background

The application of automated visual inspection (AVI) to the grain industry is a new development. A machine vision system especially tailored to grain grading and monitoring tasks is not available commercially and many of the special needs and problems in applying AVI to these visual inspection tasks have yet to be solved. The research effort in this area, however, has grown rapidly and substantially in the past eight to nine years. Determining the potential of the geometrical, gray level, and color features to classify different grain species, class, variety, damage status, and impurities using statistical pattern recognition techniques has been the main focus of the reported research. This chapter briefly reviews the results of the research in applying the AVI to grain grading. Knowledge of digital image processing and computer vision is fundamental to AVI. A very brief introduction to this subject is included at the beginning.

This thesis is a study on the software approach to separate or disconnect the touching kernel regions. The study depends heavily on the image transforms from the discipline of binary mathematical morphology. Thus a detailed introduction to binary mathematical morphology is included.

2.2 Introduction to Digital Image Processing and Computer Vision

An image is a two dimensional (2-D) function generated by sensing the radiometric information from a scene. A scene is a collection of three dimensional (3-D) object(s) with some geometrical arrangement and governed by the physical laws of nature.

The image is represented by a function f(x,y) where arguments x,y are spatial coordinates and f is the intensity or gray level at (x,y) for a gray-tone image. In a color image, f is a vector with three components representing hue, saturation, and intensity or red, blue, and green. The extension of the concepts and techniques developed for gray-tone images to color images may not be trivial.

In most cases the functional form of f(x,y) is unknown on a global basis (it may be possible to approximate it for a limited range of x,y) which presents much difficulty in algorithm development because there is a lack of underlying mathematical rigor.

In practice the image function, f, has a finite range of values and the arguments x,y have finite extent and they all must be quantized. Quantization is essential for computer processing of the image data. The discrete version of f(x,y) is called a digital image.

Digital image processing and computer vision deal with developing the models underlying the images and with the design and analysis of algorithms which, based on image models, give useful and usually application-dependent results.

The models and algorithms can be broadly categorized into three groups: image pre-processing, image analysis, and image understanding. The image pre-processing aims at enhancing the image quality either for a better (subjective) interpretation of the image by a human or for making the image more suitable for subsequent steps in computer processing. Noise removal using median filter or frame averaging, contrast enhancement by histogram equalization or histogram specification, image smoothing using a low-pass filter, edge enhancement using unsharp masking or gradient operators (high-pass filtering)

are some typical operations used in image pre-processing. The concepts involved in the image pre-processing are closely related with those in signal processing. An image is a 2-D signal, therefore, the concepts of 2-D signal transformations are required.

Image analysis concerns with the segmentation and low-level description of the image. The objective in the segmentation process is to group pixels to form higher-level regional image structures which after subsequent processing may lead to meaningful interpretations. A typical application example where segmentation is an essential processing step is in the discrimination of the objects from the background. Schalkoff (1989) commented that the success of the segmentation algorithm often determines the success or failure of the overall image analysis algorithm. In many cases further segmentation of the already segmented image regions may be required to reach the desired correspondence between the segmented image regions and the objects they represent. There are several approaches to image segmentation. Thresholding, region growing, splitting and merging, template matching, and edge detection are some examples. A good summary on segmentation can be found in Zenzo (1983), Pratt (1991, pp. 597-623), Gonzalez and Woods (1992, pp. 413-478), and Haralick and Shapiro (1992, pp. 509-550).

Subsequent to segmentation, it may be desirable to describe the segmented set of pixels. Description may be based on only the boundary pixels or may involve computations based on all the pixels of a region. Regional geometric properties, frequency characteristics, intensity statistics (for example, co-occurrence matrix) or other regional features can be used for description. Ideally the description should be invariant

to changes in position, scale, and rotation. A summary and general discussion on image analysis is given by Rosenfeld (1984).

Image understanding involves image-based knowledge manipulation, including procedural or rule-based manipulation of image data, 3-D modelling and hierarchical image analysis. A great amount of non-image-related knowledge underlying the scene representation may have to be used in image understanding.

Comprehensive coverage of the subject of digital image processing and computer vision can be found in Gonzalez and Woods (1992), Haralick and Shapiro (1992), Jähne (1991), Jain (1989), Schalkoff (1989), Ballard and Brown (1982), and Rosenfeld and Kak (1982).

2.3 Introduction to Binary Mathematical Morphology

The word, "morphology" generally refers to the study of forms and structure. The word is used in this sense in the thesis to refer to shape and size of objects. In computer vision, the word "morphology" or "mathematical morphology" refers to specific methodologies of image analysis to study the structure of images using the concepts and theories from random set theory and integral geometry.

The basic approach in mathematical morphology is to study the unknown structure of an image based on its spatial relationship to a simple image of pre-defined structure. The simple image is called a structuring element or a morphological kernel.

The language of mathematical morphology is that of set theory. A binary digital image is represented as a subset of the 2-D integer plane, Z^2. A binary image is composed of white and black pixels. As a convention, let white pixels be the pixels of

the foreground or pixels that are "ON" and black pixels be the pixels of the background or pixels that are "OFF". This convention is used throughout the thesis. A set may be defined to include only the foreground pixels or only the background pixels of an image.

A gray-scale image is represented as a subset of 3-D integer space where the third dimension corresponds to the gray value of a pixel. Color and time varying components of an image can be represented by sets of higher dimensions.

2.3.1 Basic Operations

Morphological image transforms make extensive use of set-theoretic operations. Before introducing the morphological transforms, brief definitions of important set-theoretic operations are presented.

Translation of a set A by a vector x in Z^2, denoted A_x, is defined as:

$$A_x = A + x = \{a+x \mid \forall\ a \in A\} \tag{2.1}$$

where x is a vector from a fixed and specified origin to a given point. In most cases, it is the foreground that contains the information of the image. Therefore, set A is used to represent the pixels that are "ON" or the foreground pixels of an image A. The plus sign in Eq. 2.1 refers to vector addition. The translation of an image, therefore, causes shifting of all foreground pixels of the image by a given length and along a specified direction. A_x is called the translate of A by x.

Reflection of a set A, denoted $\hat{A}$, is defined as:

$$\hat{A} = \{x \mid x = -a, \forall\ a \in A\} \tag{2.2}$$

Reflection, therefore, rotates all the points in the image by 180° with respect to a specified origin.

2.3.1.1 Dilation and Erosion

Dilation and erosion are the two basic morphological transforms. All other transforms are based on these two.

Dilation of a set A by a structuring element B, denoted $A \oplus B$, is defined as:

$$A \oplus B = \{x \mid x = a + b, \forall\ a \in A, \forall\ b \in B\} \tag{2.3}$$

The shape, size, and origin of the structuring element are pre-defined. Let set A represent the pixels that are "ON" in an image A. The vector addition of all foreground points in the image A with all the points of the structuring element B has an effect of expanding the foreground regions of the image A. For example, given a set A = {(1,1), (2,1), (3,1), (1,2), (2,2)} and a structuring element B = {(0,0), (1,0)}, the dilation yields, $A \oplus B$ = {(1,1), (2,1), (3,1), (4,1), (1,2), (2,2), (3,2)} thus expanding set A by two additional points.

An alternative definition of dilation is:

$$\mathbf{A \oplus B} = \bigcup_{b \in B} (\mathbf{A})_b \tag{2.4}$$

The definition in Eq. 2.4 states that dilation of set A with B is a union of all the translates of set A with all the points of set B.

Erosion of a set A with set B, denoted $A \ominus B$, is defined as:

$$A \ominus B = \{x \mid (B)_x \subseteq A\} \tag{2.5}$$

In words, Eq. 2.5 states that erosion of a set A with set B yields a set of points such that the translate of set B with any of the points in the set $A \ominus B$ is contained in set A. In other words, at each point of the eroded set, $A \ominus B$, set B fits in set A. For non-

trivial cases, erosion shrinks the foreground regions of an image. For example, erosion of set A={(1,1), (2,1), (3,1), (1,2), (2,2)} with set B={(0,0), (1,0)}, gives the eroded set $A \ominus B$={(1,1), (2,1), (1,2)}.

An alternative definition of erosion is:

$$\mathbf{A} \ominus \mathbf{B} = \bigcap_{b \in B} (\mathbf{A})_{-b} \tag{2.6}$$

where -b is the point b after it is rotated by 180° about the origin.

Detailed description of erosion and dilation transforms and their mathematical properties can be found in Serra (1982, pp. 43-50), Haralick et al. (1987), Haralick and Shapiro (1992, pp. 158-167), and Heijmans and Ronse (1990).

2.3.2 Opening and Closing

Opening of a set A by set B, denoted $A \circ B$, is defined as:

$$A \circ B = (A \ominus B) \oplus B \tag{2.7}$$

Opening tends to remove sharp thin peaks and small islands, smooth contours, and break narrow isthmuses. An alternative definition of opening is:

$$A \circ B = \bigcup \{(B)_x \mid (B)_x \subset A\} \tag{2.8}$$

Equation 2.8 shows the fitting property of the opening transform. Union of all the translates of set B which fit in set A, constitute $A \circ B$.

Closing of set A by set B, denoted $A \bullet B$, is defined as:

$$A \bullet B = (A \oplus B) \ominus B \tag{2.9}$$

Closing tends to fill small holes and sharp thin gulfs, and fuse narrow breaks. An important geometric property of the closing transform is that a point x belongs to $A \bullet B$,

if and only if, all translates of B containing x have at least one point common with set A. Graphical illustrations of opening, closing, dilation, and erosion can be found in Haralick and Shapiro (1992, pp. 174-185), Haralick et al. (1987), Serra (1982, pp. 50-53) and McDonald and Chen (1990a).

Opening and closing are idempotent operations. That is, after a set A is opened or closed with set B, subsequent opening or closing by set B does not change the result of either operation. Also, $A \circ B$ is a subset of set A (*i.e.* opening is antiextensive) and set A is a subset of $A \bullet B$ (*i.e.* closing is extensive). These properties play an important role when these operations are used in an image processing algorithm.

2.3.3 Hit-or-Miss Transform, Thinning, and Thickening

The hit-or-miss transform uses a mixed structuring element (also called compact structuring element) B made up of a pair of structuring elements B_1 and B_2. For non-trivial results, B_1 and B_2 must be disjoint, and the origin should belong to one of them. The hit-or-miss transform of set A by a mixed structuring element $B=(B_1,B_2)$, denoted $A \circledast B$, is defined as:

$$A \circledast B = (A \ominus B_1) \cap (A^c \ominus B_2) \tag{2.10}$$

Hit-or-miss transform, therefore, gives a set of points x such that B_1 translated by x fits in the set A and B_2 translated by x fits in the complement of the set A, simultaneously. In other words, hit-or-miss transform is a set of points at which B_1 hits the set A and B_2 misses the set A. The transform probes the spatial relationship of the foreground pixels to the background pixels relative to the structuring element pair.

Thinning of a set A by mixed structuring element B, denoted $A \otimes B$, is defined as:

$$A \otimes B = A / (A \circledast B) \tag{2.11}$$

Thickening, denoted $A \odot B$, is defined as:

$$A \odot B = A \cup (A \circledast B) \tag{2.12}$$

For non-trivial results, the origin must belong to B_1 for thinning and to B_2 for thickening. Thinning and thickening yield useful results when the operation is performed sequentially as described below. Sequential operation is denoted by enclosing the structuring element in braces. Sequential thinning, denoted $A \otimes \{B\}$, is represented as:

$$A \otimes \{B\} = (((...((A \otimes B^1) \otimes B^2)..) \otimes B^n)...) \tag{2.13}$$

where B^1, B^2,...B^n are all mixed structuring elements such that any one of them can be obtained by rotating the other.

For a mixed structuring element defined on a 3×3 window of a square lattice, there are eight possible rotations. The image A is thinned with B^1 and its output with B^2 and so on, until thinning with B^n is complete, *i.e.* the entire sequential operation of thinning with B^1, B^2,...B^n is repeated until no further changes occur.

Sequential thickening of an image does not converge and can fill the entire image frame. In practice, the result of sequential thickening after each pass with B^1, B^2,...B^n is often intersected with another set, C. The intersection operation does not let the sequential thickening result to grow beyond the set C. Sequential thickening followed by an intersection with another set is called conditional sequential thickening.

Details on hit-or-miss transform, thinning, and thickening can be found in Serra (1982, pp. 390-394) and Haralick and Shapiro (1992, pp. 168-173).

2.3.4 Choice of Structuring Element

The results desired by morphological operations and algorithms dictate the choice of the structuring element. For example, erosion by a small disc (say, of three pixel diameter) can clean the isolated noise points and smooth the contours whereas erosion by a larger disc (say, of twenty five pixel diameter) can remove the entire foreground.

A general discussion on the choice of the structuring element can be found in Serra (1982, pp. 57-59). Serra (1982, pp. 392) also described a set of mixed structuring elements and named them Golay's alphabets. These structuring elements were especially designed to give useful results when used in hit-or-miss transform, sequential thinning, and sequential thickening. Serra (1982), however, used a hexagonal grid which makes the interpretation difficult (Giardina and Dougherty, 1988). In the thesis, I have used the equivalent of Golay's alphabets for a square grid.

2.3.5 Applications in Agriculture

The usefulness of mathematical-morphology-based image transforms and algorithms in machine vision related applications in agriculture is demonstrated by McDonald and Chen (1990a). Corn kernel size distribution, plant leaf identification, and texture analysis of marbling in beef longissimus dorsi muscle using simple morphological operations and algorithms were shown. The authors commented that many machine vision related applications can be addressed using a small set of basic operators. In another study, McDonald and Chen (1990b) developed algorithms to separate muscle tissues connected to beef carcass ribeye. The algorithms did not perform well for

separating connected wheat kernel regions (Dr. T.P. McDonald: personal communication, 1992).

From an application viewpoint, morphological transforms can be implemented in parallel architecture for real time analysis (Haralick et al., 1987; McCubbery and Lougheed, 1985; Kimmel et al., 1985). Another advantage of morphological transforms is that they are global in scope (McDonald and Chen, 1990a) and do not require isolation of objects in an image before their analysis.

2.4 Automated Grain Sample Analysis

2.4.1 Potential for Objective Wheat Grading

A substantial body of literature is available on the use of digital image processing and computer vision techniques for deriving characteristics or features of grains, and subsequent classification analysis using statistical pattern recognition (Neuman et al., 1987, 1989a, 1989b; Sapirstein and Bushuk, 1989; Sapirstein et al., 1987; Kohler, 1991; Symons and Fulcher, 1988a, 1988b; Chen et al., 1989; Thomson and Pomeranz, 1991; Myers and Edsall, 1989; Barker et al., 1992a, 1992b, 1992c, 1992d; Keefe, 1992; Keefe and Draper, 1986; Brogan and Edison, 1974; Zayas et al., 1985, 1986, 1989). From a grain grading viewpoint, a classification task dealt within any one study was a small subset of various classification decisions required in grain grading. Primary and export grade determinants for Canada Western Red Spring (CWRS) wheat are given in Appendix A. Tolerances for other cereal grains in export grades of CWRS wheat are 0.4% for grade 1, 0.75% for grade 2, and 1.25% for grade 3 (Canadian Grain Commission, 1987). The export grade tolerances for wheat of contrasting classes are 0.3% for grade 1, 1.5%

for grade 2, and 2.5% for grade 3. Similarly export grade tolerances for hard red spring (HRS) wheat of varieties lower than 'Neepawa' (a HRS wheat cultivar considered the standard for milling and baking characteristics) are also very low (1.5, 3.0, and 5.0% wheat of other classes and varieties permitted for grade 1, 2, and 3, respectively). Tolerances for damaged kernels are extremely low. Because of these tight tolerances, an objective grain grading system based on digital imaging and pattern recognition must strive to achieve a near perfect classification of sound HRS wheat kernels from other cereal grains (such as barley, rye, and oats), wheat of other classes (such as hard red winter, soft white winter, and amber durum), wheat of varieties lower in quality to a pre-determined standard variety, impurities (such as stones and earth pellets), and damaged kernels. Also, the method of sample presentation to the camera should be practically implementable.

The most promising results for objective determination of other cereal grains in wheat were reported by Sapirstein and Bushuk (1989). For a sample size of more than 1000 kernels, 99% of HRS wheat were correctly identified using a linear discriminant function and assuming Gaussian patterns. It is worth mentioning that a large sample size (1000 or more kernels) is essential if the estimated error of misclassification is expected to be close to the "true" error (Duda and Hart, 1973, pp.73-76). Out of 900 kernels of other cereal grains, 2% were misclassified as HRS wheat. For wheat versus other cereal grains, the classification results using plan-form geometrical features were similar to the results when mean reflectance feature (measured via mean gray level) was added. Adding mean reflectance, however, improved the classification of oats from 78% to 95%. In a

previous study, Sapirstein et al. (1987) obtained a near perfect classification among HRS wheat, barley, oats, and rye using a sample size of 580 kernels. Backlighting was used for easy and accurate segmentation of images. Plan-form size and shape features were used in the classification model. In both studies, grain samples were prepared from pedigreed seed samples and, therefore, may have contained less variability than expected in commercial grain samples.

Chen et al. (1989) used additional features from the depth profile of kernels, measured using a laser range finder, for the classification of other cereal grains. A sample size of 850 kernels was used. They reported 16% misclassification of rye kernels as wheat. This level of misclassification is not satisfactory. Also, 6% of hulless barley were misclassified as wheat. Higher errors for rye may have occurred because the feature selection was based on minimizing the classification error between wheat of two different classes. Differences in classification results among different studies suggest that any classification scheme must be thoroughly tested on commercial grain samples to confirm its reliability. Sample presentation for laser scanning was tedious. The kernels were positioned manually, one at a time, under the fixed laser scanning line, once crease down and then crease up. Such sample presentation may be difficult, if not impossible, to automate. Thomson and Pomeranz (1991) improved the instrumentation of Chen et al. (1989) to obtain a 3-D profile of a grain in one laser scan.

Chen et al. (1989) also reported misclassifications of 8-12% among wheat of different classes and 20-26% among wheat of different cultivars within the same class. There were, however, no misclassifications of dent corn, flint corn, sorghum, soybean, and

wild oats. Export tolerance for wild oats in CWRS wheat is very low at 0.05% for grade 1, 2, and 3 (Appendix A). Ability to identify them with 100% accuracy is required for meeting the current grading criteria. Neuman et al. (1987) used plan-form size and shape features obtained using backlighting to discriminate among wheat of different classes and wheat of different cultivars within the same class. Using a sample size of 672 kernels, no misclassifications were found for CWRS and Canada Amber Durum Wheat (CADW). These two wheat classes are the most important in Canada accounting for 90% of wheat production in western Canada in 1992 (Canadian Grain Commission, 1992). There were, however, substantial misclassifications (up to 43%) among Canada Utility (CU), Canada Prairie Spring (CPS), Canada Western Red Winter (CWRW), and Canada Western Soft White Spring (CWSWS) wheat classes. Misclassifications among various cultivars of a single wheat class were greater. Errors ranged from 8% for cultivar 'Neepawa' to 85% for cultivar 'Columbus'. The authors suggest that features of anatomical parts of the kernels, such as size and shape of germ area, cheek and brush shape, and depth and width of crease, may be essential for varietal identification. The higher classification success reported by Zayas et al. (1986) in pairwise discrimination between wheat of certain cultivars from two different classes may be due to a very low sample size of 10 kernels. "True" error of misclassification of up to 8% can occur if no errors are made in a sample size of 50 (Duda and Hart, 1973, pp. 73-76). Symons and Fulcher (1988a) conducted a study similar to Neuman et al. (1987) for Eastern Canadian wheat classes and varieties. Shape and size features derived from backlit images were used. For a sample size of 225 kernels, they found that 94% of soft white winter (SWW) wheat were correctly classified

using a 4-way classification among SWW, hard red winter (HRW), hard red spring originated from Europe (HRS_E), and hard red spring wheat originated from western Canada (HRS_W). Sixteen percent of HRS_W were confused as HRW. The HRS_W sample was comprised of cultivars 'Katepwa' and 'Columbus'. These cultivars were also included in the study by Neuman et al. (1987). HRW wheat cultivars used by Symons and Fulcher (1988a) were different from HRW cultivars used by Neuman et al. (1987). It can be mentioned again that Neuman et al. (1987) found no confusion between HRS and HRW wheat classes. Such comparisons suggest that there is a need for a large data-base to develop a robust classifier.

Symons and Fulcher (1988a) also experienced the inadequacy of the plan-form size and shape features for discriminating among different cultivars of a wheat class. For three of the wheat cultivars of SWW, correct classifications of less than 60% were reported. In a subsequent study, Symons and Fulcher (1988b) used additional features derived from the bran layer and crease from the image of transverse section of kernels to aid in classification among different cultivars of the SWW class. Classification results were unsatisfactory with errors of more than 50%. Myers and Edsall (1989) also used additional features derived from the side view of the kernels to improve the classification among Australian wheat varieties. Errors up to 22% were reported. Barker et al. (1992a, 1992b, 1992c, 1992d) used features derived from the contour of a wheat kernel positioned in a fixed orientation to discriminate among Australian wheat varieties. Overall correct classification among eight varieties was less than 65%.

Another problem when using plan-form geometrical features was reported by Zayas et al. (1989). The study on classification of weeds and stone from wheat found that 12% of the stone pieces were confused as wheat kernels. It is expected that the addition of color and gray-level based features will improve the identification of stones.

The use of color features for discrimination among wheat of different classes and cultivars was tried by Neuman et al. (1989b). Red, green, and blue values were used as discriminating features. The results were unsatisfactory with errors ranging from 10 to 66%.

Sapirstein and Bushuk (1989) studied the vitreosity of durum wheat by taking the image of transilluminated kernels and specifying the frequency distribution of gray level. They found 95% correlation between vitreosity computed by digital image processing method and replicated official grain inspection of hard vitreous kernels. They also found a good linear relationship (correlation coefficient = 0.88) between grain hardness (measured in particle size index or PSI) predicted by computed vitreosity and the measured PSI score.

Features based on whole kernel size, shape, and color, and features of anatomical parts of a kernel may be essential to meet current grading criteria. An interesting alternative approach to objective wheat grading may be to find a completely new set of grading factors which can be easily administered by machine-vision-based grading. Work reported by Kohler (1991) suggests that variabilities of size, shape, and reflectance features derived from kernels of a sample can serve as important grading factors. Cargo samples of CWRS grades 1, 2, and 3 were successfully classified using the mean and

variance of the features as quantitative classification variables (Kohler, 1991). On carlot samples, however, only grades 1 and 3 could be successfully discriminated from each other.

2.4.2 Potential for Automated Grain Monitoring

Unlike grain grading, tolerances in grain monitoring can be relaxed. An approximate knowledge on the contents of small and large seeds (such as canola, mustard, peas, beans, domestic buckwheat, wild oats) and roughage (such as threshed wheat heads, stones) in a wheat sample can help in automatically selecting an optimum cleaning strategy thereby increasing the cleaning throughput.

It is known that different grains of similar shape and size can be classified with more than 90% accuracy. Hehn and Sokhansanj (1990) found 99% correct classification between canola and mustard seeds. This and the results cited in section 2.4.1 suggest that classification of small and large seeds in wheat or barley samples can be achieved by AVI.

2.4.3 Sample Presentation

The presentation of grain kernels in the field of view (FOV) of an image sensor was manually controlled in all of the studies cited in section 2.4.1 and 2.4.2. Especially, it was ensured that kernels did not touch one another. An automated grain grading or grain monitoring system would, however, require an automated seed presentation device. Few studies have been reported on automating a sample presentation system.

Casady and Paulsen (1989) developed an automated corn kernel positioning device for machine vision analysis. The device used a vibratory bowl feeder coupled with a

gating arrangement. An optical sensor at the gating arrangement controlled the metering of single kernels onto a conveyor belt. The system worked well for singulating sound corn kernels. Ni et al. (1993) used the mechanism of Casady and Paulsen (1989) to place the kernels onto a rotating transparent table. A strobe light was used to time the image capture. The system worked at a throughput rate of 12 kernels/min and was 97% successful in singulating corn kernels. It was suggested by Casady (1987) that the vibratory bowl feeding mechanism would not work for wheat and other small grains. The device was not tested for more realistic grain samples containing grains of more than one species.

Craig (1993) developed a seed singulation mechanism using a vacuum drum with rows of radially directed orifices at the drum surface. The seeds were held at the orifices by vacuum as the drum rotated through a grain sample. An air blast was applied to remove seeds which were not tightly held, thus improving the singulation. A positive pressure was later applied to remove the seeds and scavenge the orifices. The device was tested on samples of wheat, barley, lentils, and canola. The device worked well for singulating wheat, barley, lentils, and canola. Singulation success was 89 to 94% for wheat and 78 to 81% for barley. A failure in singulation occurred when more than one kernel or no kernel appeared on a single orifice. The major drawback of the device was that it was biased towards small seeds. In a mixed sample of wheat and canola with 5% canola, the device picked 23% canola. Design and development of an improved seed presentation device is currently under progress at the Department of Agricultural Engineering, University of Manitoba.

Development of software to carry out feature measurements on the touching kernels (Shatadal et al., 1992, 1993) would help in the design of the sample presentation device. The requirement of the device would then be limited to presenting the kernels in a one-kernel-layer thickness.

CHAPTER 3 : DISCONNECT ALGORITHM

3.1 Introduction

An image of touching wheat kernels is shown in Fig. 3.1. The kernel regions in the image are connected to one another by narrow and small isthmuses or bridges. In developing the disconnect algorithm, the objective was to break the isthmuses without distorting or changing the shape and size of the individual kernel regions.

Serra (1982, pp. 415-416) described an algorithm, known as watershed segmentation, which could disconnect conjoint circular regions with short and narrow isthmuses (Chermant et al., 1981; Lantuéjoul, 1980). The watershed segmentation did not work for disconnecting conjoint kernel regions because of inherent concavities in the kernel shapes and the unpredictable manner in which an isthmus could be formed. I used the logic of the watershed segmentation and added heuristics to arrive at the disconnect algorithm. A separate description of the watershed segmentation is not included here because it is a subset of the disconnect algorithm. Instead, references are made wherever a step or equation used in the disconnect algorithm is the same as or similar to a step or equation in the watershed segmentation.

The image shown in Fig. 3.1 is used as an example for showing the image processing steps of the disconnect algorithm.

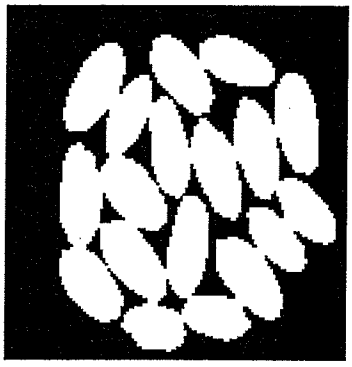

Fig. 3.1. An image of touching wheat kernels, X(0).

3.2 Algorithm

3.2.1 Step 1: Progressive Erosion

The image of touching kernels (Fig. 3.1), X(0), is eroded by progressively larger disc structuring elements, D(i), (the disc structuring elements are digital circles) giving a family of set X(i) (Eq. 3.1):

$$X(i) = X(0) \ominus D(i) \qquad (3.1)$$

$$i = 1,2,3,4.....m,m+1$$

Erosion is stopped when the eroded image reduces to a null set, $\varnothing$. That is, $X(m + 1) = \varnothing$. The null image contains only the background pixels or pixels that are "OFF".

Erosion by a disc shrinks the foreground components in the image by turning "OFF" or removing the pixels from the periphery of the components. Figure 3.2 shows the erosions of the image, X(0), with disc structuring elements of 5, 9, 14, 16, 17 and 18 pixel diameter. Those pixels of a region are removed where the structuring element does not completely fit in the region. As illustrated by Fig. 3.2, erosion with progressively larger discs removes progressively larger areas leaving only the more distant pixels from the original boundary of the regions. The isthmuses are broken before any one kernel region completely disappears. The inherent concavities on the kernel shape, however, leads to breaking of some of the kernel regions themselves. For the image X(0), shown in Fig 3.1, the value of m was 18. That is, the image X(0) when eroded by a disc of 19 pixel diameter reduced to a null image. The components which appear in eroded set X(i-1) but disappear in the subsequent eroded set X(i), are called ultimately eroded components or UEC. The UECs, therefore, are the most distant pixel(s) from the

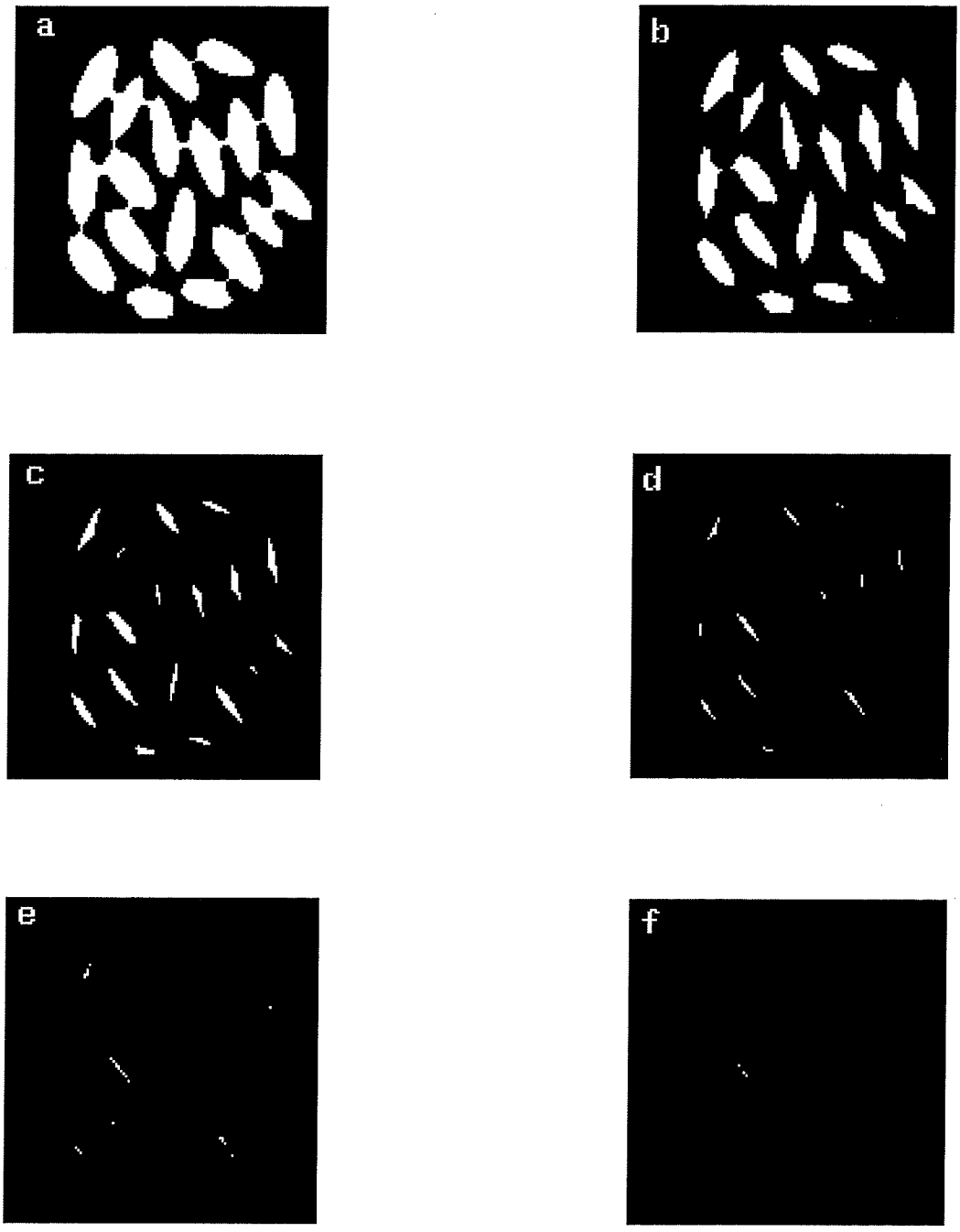

Fig. 3.2. Erosions of image X(0). (a) - X(5); (b) - X(9); (c) - X(14); (d) - X(16); (e) - X(17); (f) - X(18).

boundary of a kernel region in the original image. For an image containing kernels of similar shapes and sizes, disappearing of components during progressive erosion occurs in the last few erosions with bigger discs (Fig 3.2). The image of X(18) (Fig. 3.2 f) shows the UECs derived from the kernel regions of X(0) at which a disc of eighteen pixel diameter could fit.

The progressive erosion (Eq. 3.1) is the same in the watershed segmentation. In the watershed algorithm, each UEC represents a centre or marker for each convex region in the original image and the image of disconnected convex regions is constructed by growing these markers with a logic which prevents joining of already disconnected growing regions. For the images of touching kernels, however, one kernel region can yield more than one UEC (Fig. 3.2). If the UECs are not merged, growing them with the logic which prevents joining of neighbouring expanding components would lead to bisected kernels in the final image of disconnected kernels.

In the disconnect algorithm, the UECs are dilated with the objective of merging the UECs derived from a single kernel region. The UECs appearing in the last eroded set, X(m), are dilated (Eq. 3.2):

$$Y(0) = X(m) \oplus D(11) \tag{3.2}$$

where D(11) is a disc of 11 pixel diameter.

Dilation with relatively larger discs improves the chances of merging UECs derived from a single kernel region but increases the risk of merging UECs from two or more neighbouring kernel regions. Trials on several images of touching HRS wheat, barley, durum, rye, and oat kernels revealed that dilation with an eleven pixel diameter

in Eq. 3.2 was optimum. Figure 3.3 depicts Y(0). The dilated UECs serve as markers in the disconnect algorithm.

3.2.2 Step 2: Sequential Thickening

The logic which grows the markers but prevents the neighbouring expanding components from joining together is implemented via sequential thickening operation with mixed structuring element, $L = (L_1, L_2)$. On a square grid the mixed structuring element for thickening is

$$\begin{matrix} \ell_2 & \ell_2 & \ell_2 \\ * & \ell_2 & * \\ \ell_1 & \ell_1 & \ell_1 \end{matrix}$$

where ℓ_1s belong to L_1, ℓ_2s to L_2, and * are "don't care" locations. That is, only those pixels are included in the hit-or-miss transform of an image with the mixed structuring element, L, where simultaneously the L_1 locations hit the foreground of the image and L_2 locations miss the foreground. There are no restrictions on the "don't care" locations. The origin of the mixed structuring element, L, is located at the centre and, therefore, belongs to L_2. For sequential thickening, the above configuration of the structuring element, L, and its seven other rotations on the grid are used. The result of thickening is the union of the input image and its hit-or-miss transform.

The conditional sequential thickening of Y(i-1) is limited to growing it within X(m-i) and is given by:

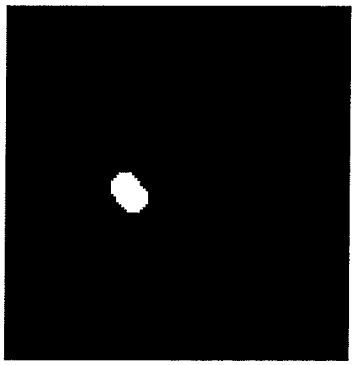

Fig. 3.3. Image of Y(0).

$$S(i) = Y(i - 1) \odot \{L\} \cap X(m - i) \qquad (3.3)$$

$$i = 1,2,3,4.....m$$

Equation 3.3 grows the components in Y(i-1) to the size they were in X(m-i) without allowing them to join one another. The conditional sequential thickening is stopped when S(i) converges. The image of Y(i-1) for an incremented value of i is obtained after steps 2 to 7 are implemented. The steps 3 to 7 are described in sections 3.2.2 to 3.2.7.

The sequential thickening adds those background pixels to the set Y(i-1) where ℓ_1s fit in the background and the ℓ_2s fit in the foreground. In other words, an "OFF" pixel can be turned "ON" as a result of thickening with mixed structuring element, L, if from eight of its neighbours at least three neighbours as defined by ℓ_1 locations are "ON" and at least three other neighbours as defined by ℓ_2 locations are "OFF". Pixels satisfying this criterion can only occur at the interface of foreground components with the background. The logic thus imposed in growing the components prevents their merger. The image S(1) is shown in Fig. 3.4. The conditional sequential thickening operation of Eq. 3.3 is the same as given in the watershed segmentation (Serra, 1982, pp. 415-416).

3.2.3 Step 3: Pruning of Dendrites

As was noted earlier, the criterion for an "OFF" pixel to turn "ON" as a result of thickening with structuring element, L, was that at least three of its eight neighbours must be "OFF" and three others must be "ON". The thickening criterion may not be met at certain pixel patterns along a single-pixel-thick protrusions or dendrites of one or more components in S(i). For example, two pixels in a dendrite which are connected

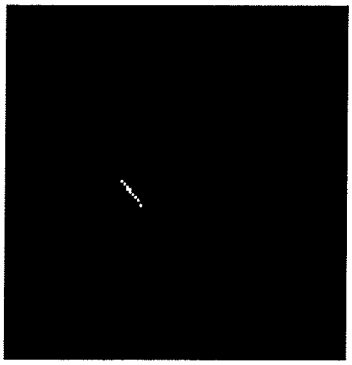

Fig. 3.4. Image of S(1).

diagonally present such a pattern. The dendrites in S(i) are, therefore, removed or pruned by sequential thinning of S(i) with mixed structuring element E=(E_1, E_2):

$$T(i) = S(i) \otimes \{E\} \tag{3.4}$$

where structuring element, E, is given by:

$$\begin{matrix} e_2 & e_2 & e_2 \\ e_1 & e_1 & e_2 \\ e_2 & e_2 & e_2 \end{matrix}$$

where e_1 locations belong to E_1, e_2 locations belong to E_2, and the origin is at the centre.

The interpretation of the subscripts is the same as it was for the mixed structuring element, L. That is, only those pixels of the input image are included in its hit-or-miss transform with the structuring element, E=(E_1, E_2), where simultaneously E_1 locations hit the foreground of the image and E_2 locations miss the foreground. The thinning operation gives the set difference of the input image with its hit-or-miss transform. Thinning, therefore, removes those pixels of the input image where e_1s fit in the foreground and e_2s fit in the background. For sequential thinning, the above configuration of structuring element, E, and its seven other rotations on the grid are used. The image T(1) is shown in Fig. 3.5. Note that the dendrite appearing in S(1) is removed in T(1) (Figs. 3.4 and 3.5).

3.2.4 Step 4: Dilation of Small Components

Thickening around certain small pixel patterns (*e.g.* four pixels arranged to form a 2×2 square pattern) is not possible. Such small components can occur in image T(i).

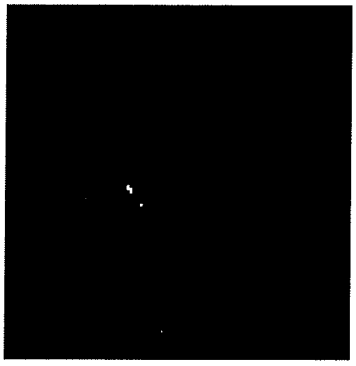

Fig. 3.5. Image of T(1).

Small components are, therefore, located (Eq. 3.5) and replaced in the image after dilating them by a small disc (Eq. 3.6). The size of the small disc depends on the current value of i. For values of i less than 12, a disc of eight pixel diameter is used; for other i values a disc of five pixel diameter is used.

$$W(i) = T(i) / [(T(i) \circ P(3)) \oplus \{D(3)\} \cap T(i)] \tag{3.5}$$

where P(3) is a three pixel long and one pixel thick structuring element. The origin of P(3) is located on the middle pixel. The sequential dilation within T(i) is performed until it converges.

$$U(i) = T(i) \cup (W(i) \oplus D(s)) \tag{3.6}$$

The opening of T(i) with P(3) removes components in which P(3) can not entirely fit. Opening with P(3) ensures removal of all such patterns which are not suitable for thickening. Sequential dilation on the result of opening within T(i) on the right hand side (R.H.S.) of Eq. 3.5 restores any component made smaller by opening to its size and shape in T(i). W(i), therefore, contains components which were removed by opening. The image U(1) is shown in Fig. 3.6.

Let the k_{th} erosion in Eq. 3.1 represent the erosion step which gives the UECs for a given kernel region. A single kernel region may split into more than one component in the k_{th}, $(k-1)_{th}$, or $(k-2)_{th}$ erosion step. If split components are not merged, the logic of the sequential thickening (Eq. 3.3) would cause sectioning of a single kernel region into more than one region. The merging of components which split in the k_{th} erosion is attempted by dilating the UECs. The merging of components which split in the $(k-1)_{th}$ or $(k-2)_{th}$ erosion can occur as a result of step 4, as a result of step 3 and 4 combined, or

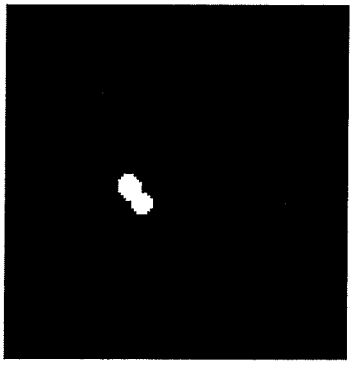

Fig. 3.6. Image of U(1).

as a result of step 5 described in section 3.2.5. Generally, the components split from a single kernel region in $(k-1)_{th}$ or $(k-2)_{th}$ erosion are small (*i.e.* 2×2 pixel pattern or smaller) or they are made small by pruning the dendrites (Eq. 3.4). Such small components are detected (Eq. 3.5) and dilated (Eq. 3.6). Dilation of small components tends to merge split components from a single kernel region. In some cases, dilation of the UECs may fail to merge split components from a single kernel but steps 3 and 4 may merge them.

3.2.5 Step 5: Adding Dendrites

To further reduce the risk of bisecting a kernel region, the dendrites removed by pruning (Eq. 3.4) are dilated and placed back in the image (Eq. 3.7).

$$Q(i) = U(i) \cup [\, (S(i) / T(i)) \oplus D(2) \,] \qquad (3.7)$$

Figure 3.7(a) shows the components split from a single kernel region in the $(k-1)_{th}$ erosion. Split components became far apart after a dendrite is removed (Fig. 3.7 (b)) and could not be merged as a result of step 4 (Fig. 3.7(c)). Figure 3.7(d) shows the result of adding the dilated dendrite. The components were merged in Fig. 3.7(d). Adding dilated dendrites, however, increases the risk of merging the neighbouring kernel regions which were disconnected as a consequence of progressive erosion. To reduce the risk of merging the neighbouring kernel regions, Eq. 3.7 is used for i values less than 10.

3.2.6 Step 6: Finding UECs

Various kernel regions in the image of touching kernels may be of different sizes. Upon progressive erosion (Eq. 3.1), therefore, different regions may completely erode or disappear at different stages of erosion. Equation 3.8 finds the UECs that disappeared in

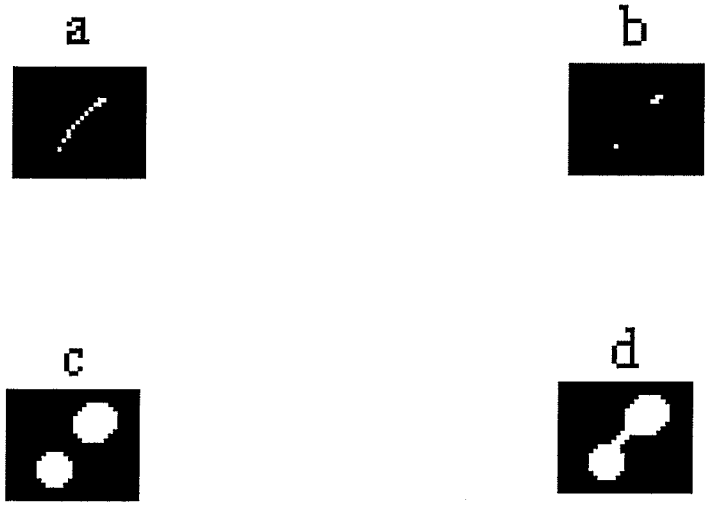

Fig. 3.7. Effect of adding the dilated dendrite. (a) - Split components; (b) - Components after pruning the dendrites; (c) - After small components are dilated; (d) - Components merge after adding the dilated dendrite.

the $(m\text{-}i+1)_{th}$ erosion. These components are added to Q(i) after they are appropriately dilated (Eq. 3.9).

$$V(i) = X(m\text{-}i) \,/\, [Y(i-1) \oplus \{D(3)\} \cap X(m-i)] \tag{3.8}$$

$$R(i) = Q(i) \cup (V(i) \oplus D(s)) \tag{3.9}$$

Sequential dilation of Y(i-1) within X(m-i) brings the components in it to their size in X(m-i). Taking the set difference (Eq. 3.8), therefore, gives those components which are present in X(m-i) but not in Y(i-1). Figure 3.8 shows V(1), the UECs which disappeared in the m_{th} erosion. Note that the components appearing in V(1) (Fig. 3.8) are those which appear in X(17) but disappear in X(18) (Fig. 3.2). Figure 3.9 shows R(1).

The disc structuring element used for dilating the UECs in Eq. 3.8 is reduced in size with increasing value of i. For i = 1 to 4 a disc of eleven pixel diameter is used. The size is reduced to a nine pixel disc for i = 5 to 9; a seven pixel disc for i = 10 to 14; and a five pixel diameter disc for i > 14. Such a scheme of dilating the UECs with lower size disc with increasing i is used to reduce the risk of merging the neighbouring components as a consequence of dilation. In the watershed segmentation, the UECs are not dilated.

3.2.7 Step 7: Eliminating the Corners

If a corner pixel of one block of pixels is connected diagonally to a corner pixel of another block of pixels (Fig. 3.10(a)), thickening around such corner pixels is not possible (Fig. 3.10(b)). The corner locations are, therefore, eliminated by locating and dilating them (Eq. 3.10).

$$Y(i) = R(i) \cup [\, ((R(i) \circledast G^1) \cup (R(i) \circledast G^2)) \oplus D(3)] \tag{3.10}$$

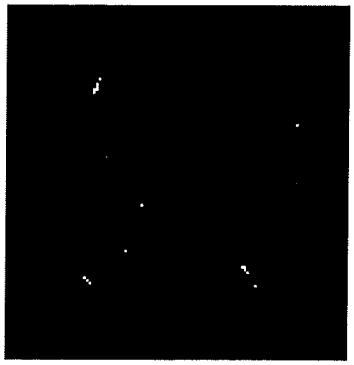

Fig. 3.8. Image of V(1).

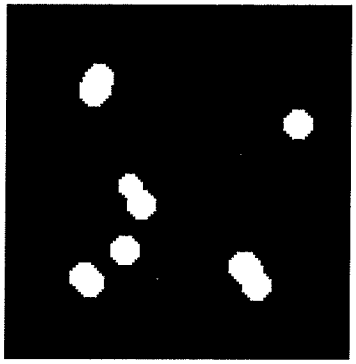

Fig. 3.9. Image of R(1).

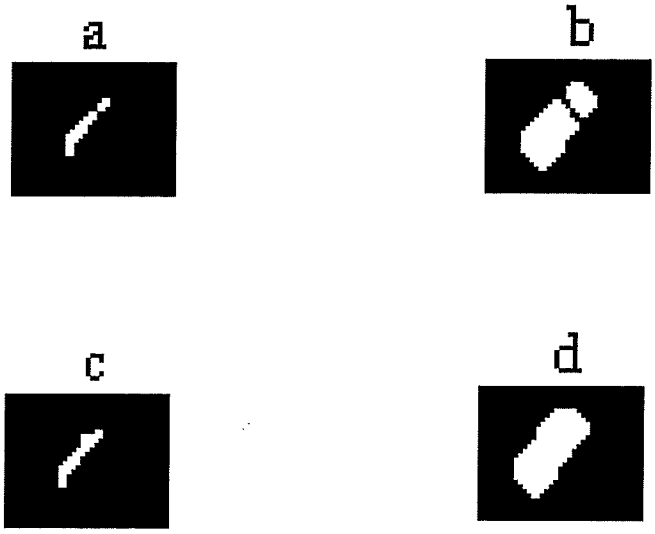

Fig. 3.10. Effect of eliminating the corners. (a) - Corner between two block of pixels; (b) - Sequential thickening of the image in (a); (c) - Corner is eliminated by locating and dilating them; (d) - Sequential thickening of the image in (c).

where G^1 is a mixed structuring element as given below and G^2 is obtained by rotating G^1 on the grid.

$$g_1 \quad g_2$$

$$g_2 \quad g_1$$

Subscripts have their usual meaning. That is, only those pixels are included in the hit-or-miss transform where g_1 locations hit the foreground and g_2 locations miss the foreground simultaneously. Figure 3.10(c) shows the result of locating and dilating the corner location. Thickening can then take place without any problem (Fig. 3.10(d)).

The image of Y(1) is the same as the image of R(1) because there were no corners in the R(1) (Fig. 3.11).

Steps 2 to 7 are repeated until Y(m) is obtained. The steps of the algorithm are further illustrated in Fig. 3.12(a) to 3.12(k). Note that sequential thickening does not permit merging of components (Fig. 3.12(b) and Fig. 3.12(j)). Note also the merger of components split from a single kernel using step 4 (Fig. 3.12(c) and Fig. 3.12(e)).

3.2.8 Step 8: Removing the Notches

Preliminary trials showed that Y(m) separates the touching kernel regions but some kernels tend to have small notches or line segments extending from the boundary of the kernel towards the inside of the component (Fig. 3.12(k)). To remove the notches, thinning with the mixed structuring element F, is performed on the complement of the image:

$$Z = -(-Y(m) \otimes \{F\}) \tag{3.11}$$

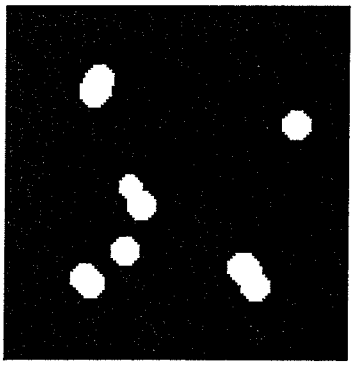

Fig. 3.11. Image of Y(1).

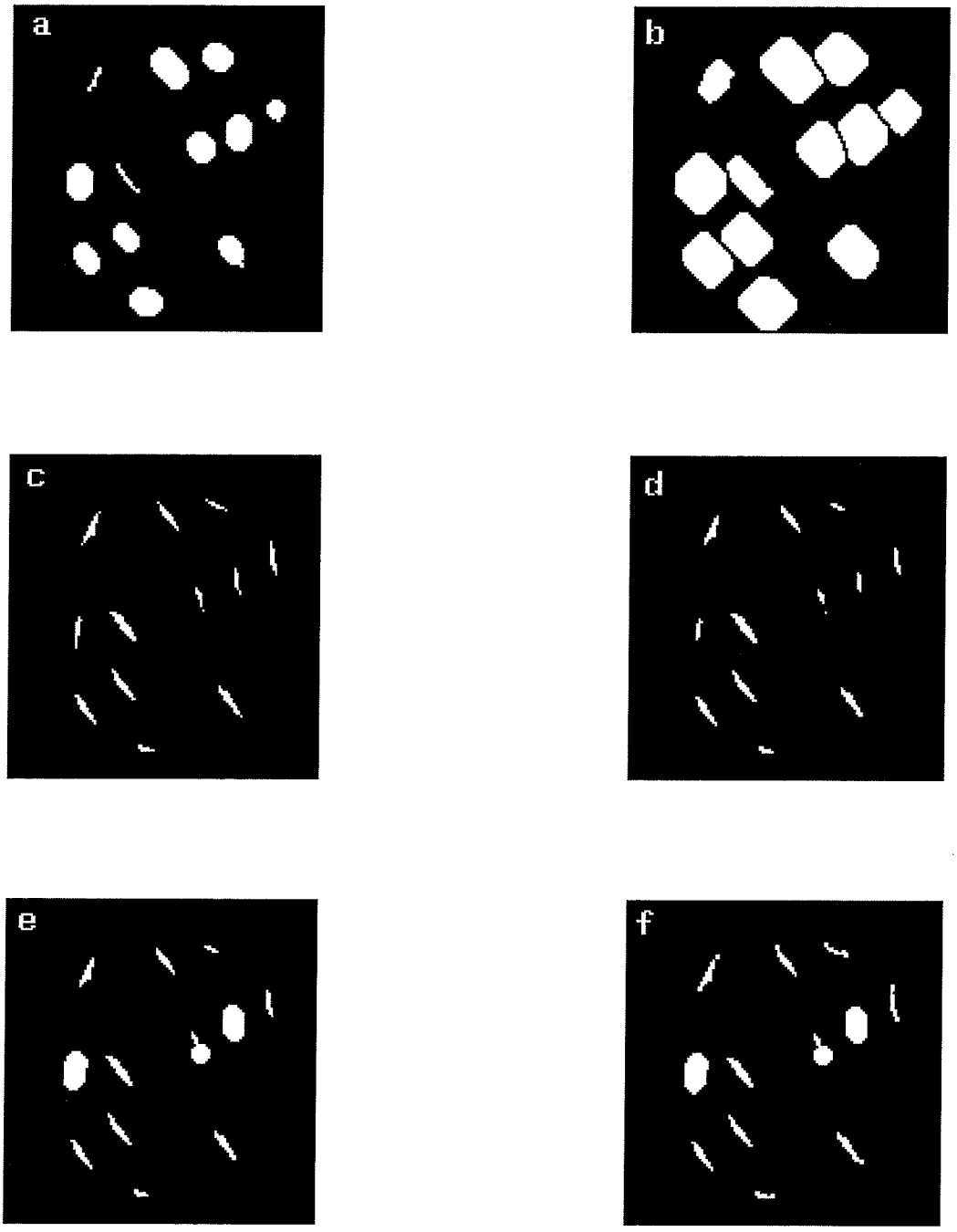

Fig. 3.12. Steps of the disconnect algorithm. (a) - Y(2); (b) - Y(2)⊙{L}; (c) - S(3); (d) - T(3); (e) - U(3); (f) Q(3). contd..

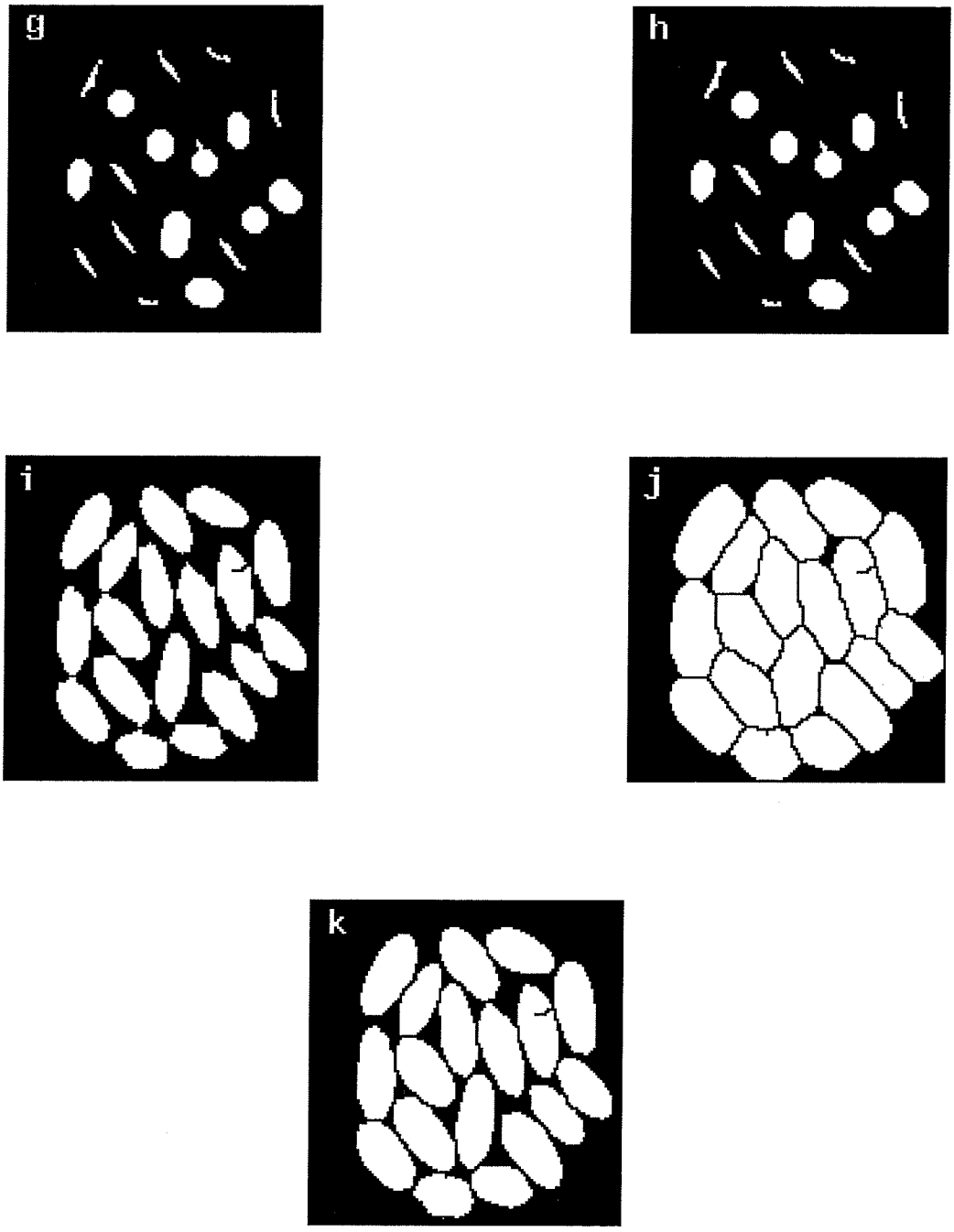

Fig. 3.12. Steps of the disconnect algorithm. (g) - R(3); (h) - Y(3); (i) - Y(17); (j) - Y(17)$\odot${L}; (k) - Y(18).

where the mixed structuring element F is given by:

$$\begin{matrix} * & f_2 & f_2 \\ f_1 & f_1 & f_2 \\ * & f_2 & f_2 \end{matrix}$$

The * are the "don't care" locations. In using the rotations of the above configuration of the structuring element F for sequential thinning, the "don't care" locations are replaced by f_2 locations when the two f_1 locations are diagonally connected.

Z is the resulting image of the separated kernels (Fig. 3.13).

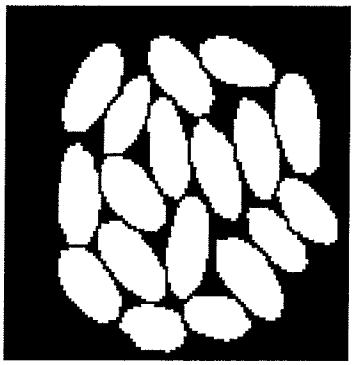

Fig. 3.13. Image of disconnected kernels, Z.

CHAPTER 4: MATERIALS AND METHODS

4.1 Vision Hardware

A 3 chip CCD (charge coupled device) color camera (Model DXC-3000A, SONY) was used to acquire images. A zoom lens (VCL-1012 BY) of 10-120 mm focal length was fitted in the camera. The camera was mounted on a stand (Model m3, Bencher Inc., Chicago, IL.) which provided easy vertical movement and a stable support for the camera. The camera was connected to a camera control unit (Model CCU-M3, SONY). The iris was selectable to manual or automatic mode. The option of the manual iris control was used to achieve repeatability in the experiments. The automatic gain control of the camera was disabled. The camera was white balanced before each imaging session.

The red (R), green, (G), and Blue (B) video signals from the camera control unit (ccu) were converted to a 24 bit color digital image by a frame grabber board (Model DT 2871, Data Translation Inc., Molboro, MA). The frame grabber board was installed on an expansion slot of a personal computer (Model 80386, UNISYS). The frame grabber could convert the R,G,B color signal to hue (H), saturation (S), and intensity (I), signal in the real time. The frame grabber had three separate 8-bit A/D (analog to digital) converters and four 512×512×8 bit frame buffers. The programs to control the frame grabber were written in C programming language using the aurora subroutine library (Aurora, Data Translation Inc., Molboro, MA). Only the intensity buffer was saved for further analysis. Image analysis was carried out on a workstation (model SPARCSTATION 2, Sun Microsystems, Inc., Mountain View, CA).

4.2 Sample Illumination

Uniform diffuse backlighting was used in all the experiments. Backlighting was preferred for easy and accurate segmentation of the grain kernels from the background. Four screw-based 100 W tungsten filament bulbs arranged in a ring configuration served as the illumination source. The ring-lamp was suspended below the object plane. The light passed through an opal acrylic plate via a centre cut window of 0.11 m diameter. A voltage regulator (Sola Canada Inc.) controlled the voltage to the lamps within ±0.5 V. A variac was used to change the illumination level by changing the voltage to the lamps. The illumination level was calibrated by repeatedly digitizing a small and fixed region of interest on the image of an opal acrylic plate and simultaneously changing the voltage to the lamps until the mean value of the region hit a pre-selected target value of 230.

4.3 Grain Samples

Grain samples of hard red spring (HRS) wheat (Grade 1 Canada Western Red Spring), durum wheat (Grade 1 Canada Western Amber Durum), barley (Special Select Malt barley), rye (Grade 1), and oats (Grade 1) used in the experiments were obtained from the Grain Inspection Division of the Canadian Grain Commission (Winnipeg, MB).

4.4 Experiment 1: The Precision

One typical kernel of each of HRS wheat, barley, durum, oats, and rye were selected for the precision experiment. Repeated backlit images of the same kernel were taken. The kernel orientation in repeated images of the same kernel was random. The randomness was ensured by dropping the kernel on the viewing plate. If a kernel bounced off the field of view (FOV), it was repositioned manually in the FOV. Care was

taken not to disturb the orientation of the kernel while moving it manually. Fifty five images of the same kernel of a HRS wheat and 65 images of the same barley, durum, oat, and rye kernels were taken. An image of a Canadian quarter coin was also acquired for the spatial calibration of the images. Feature measurements on these kernels were performed using the same software settings.

4.5 Experiment 2: Testing the Disconnect Algorithm

Samples of each cereal grain were reduced in size by Boerner divider. The Boerner divider maintains randomness in dividing a grain sample. Foreign or severely damaged kernels were removed before placing the kernels for image acquisition. The kernels were randomly dropped through a 30 mm diameter and 30 mm long tube over a viewing plate. Twenty to twenty five kernels were used for a single image. The viewing plate was tapped to bring any overlapping kernels to a one-kernel-thick layer. The kernels that were not close to any other kernel were made to touch at least one other kernel. In the image of touching kernels, however, a few kernels were not connected to other kernels. Care was taken not to disturb the random configuration of the kernels while moving any individual kernel. An image of the touching kernels was acquired and saved. The kernels were then manually separated without disturbing the orientation of the kernels. Despite the care, reorientation of some of the kernels could have occurred unintentionally. An image of the manually separated kernels was also acquired at the same hardware settings.

4.6 Image Analysis

The thresholded images of the touching kernels were first processed by the

disconnect algorithm described in Chapter 3 to disconnect the conjoint kernel regions. The disconnected kernel regions thus obtained are hereafter referred to as software-separated kernels. The term "physically-separated" is used to refer to kernels in the image of the manually separated kernels. All of the images of the software-separated kernels and the physically-separated kernels were labelled and the features of all of the kernels were extracted using the same software settings. Image analysis algorithms used for the feature extraction are described in Chapter 5.

CHAPTER 5: IMAGE ANALYSIS

5.1 Primary Segmentation

The objective in the primary segmentation of any acquired image of grains was to group together pixels participating in the background separately from the pixels participating in grain kernel regions. The images were acquired in a controlled environment and were free from noise and other aberrations. A global thresholding worked well as the primary segmentation technique for all the images. The thresholding operation assigned a value of zero (black) to all pixels which were above the threshold and a value of 255 (white) to pixels below the threshold. It was expected that pixels corresponding to touching kernels would merge forming an isthmus or bridge between touching kernel regions after primary segmentation. The thresholded images of the touching kernel images were, therefore, further segmented using the disconnect algorithm described in Chapter 3.

5.2 Region Labelling

The group of pixels obtained after segmentation did not possess any identity. Region labelling was performed to assign a unique label or an identifier to each kernel in the segmented image of physically-separated kernels and disconnected image of the touching kernels. All the features of a kernel were identified with the label value of the kernel in the image.

The region labelling algorithm scanned the segmented image once from the top-left to the bottom-right. Initially, all the pixels had no label. The first unlabelled pixel,

(i,j), was assigned a unique label value. The same label value was propagated to those 8-neighbours of pixel (i,j) which possessed the same pixel value as that of (i,j). Eight neighbours of each of the previous neighbours were examined in succession and those with the same pixel value as that of (i,j) received the same label value as that of (i,j). The propagation of the same label value continued until no more neighbouring pixels with the same pixel value as that of (i,j) could be found. The scan of the image resumed until another unlabelled pixel was encountered. Haralick and Shapiro (1992, pp. 28-48) describe this and the other region labelling algorithms.

Each 8-connected component received a unique label in one scan of the image. Regions with only one pixel were considered isolated noise points and were, therefore, removed. The output image from the labelling routine is, hereafter, referred to as a labelled image.

5.3 Feature Extraction

5.3.1 Boundary Tracking

A boundary tracking algorithm is essential to the calculation of the important features such as perimeter and length of major principal axis. The boundary of a region can be either 8-connected or 4-connected. Pixels of a region which have at least one of their 4-neighbours in the background constitute an 8-connected boundary of the region. A 4-connected boundary of a region is a set of pixels of the region which have at least one of their 8-neighbours in the background. The 8-connected boundary was used for all the images.

The boundary of a labelled component is followed as soon as the first transition

from the background pixel to the first non-zero labelled pixel is encountered in a row by row scan of the labelled image from the top-left to the bottom right. The boundary tracking of the component is completed and the scan of the image resumes until another non-zero labelled pixel is encountered.

For any component with a non-zero label, the boundary tracking begins by numbering the 8-neighbours of the first encountered pixel of the component (say, i,j). The pixel (i,j) is the first pixel of the boundary. The numbering of neighbours starts with the pixel on the left of (i,j) and proceeds in the counterclockwise direction. Let the neighbours be numbered as R_0, R_1, ..., R_7. The first non-zero neighbour pixel with the same label value as that of (i,j), R_i, becomes the next pixel of the boundary and the neighbour R_{i-1} becomes the next R_0. The neighbours are again marked in a counterclockwise direction starting with R_0. The process is repeated until the first two boundary pixels are revisited in a sequence. The boundary tracking algorithm is taken from Rosenfeld and Kak (1982, pp. 220-223).

5.3.2 Area and Perimeter

The area of a component was calculated by counting the number of pixels in the component. The perimeter was calculated by adding the Euclidean distances (hereafter referred to as distances) between all the successive pairs of pixels in the boundary of the component.

5.3.3 Centroid and Angle of Orientation

The centroid, $(\bar{x},\bar{y})$, of a region, $\Re$ is given by:

$$\bar{x}=\frac{1}{N}\sum_{(x,y)\in\Re} x \tag{5.1}$$

$$\bar{y}=\frac{1}{N}\sum_{(x,y)\in\Re} y \tag{5.2}$$

The angle of orientation, θ, of a region, $\Re$, is given by:

$$\theta=\frac{1}{2}\tan^{-1}\left[\frac{2\mu_{1,1}}{\mu_{2,0}-\mu_{0,2}}\right] \tag{5.3}$$

where $\mu_{p,q}$ is the (p,q) order central moment of the region and is defined as:

$$\mu_{p,q}=\sum_{(x,y)\in\Re}[(x-\bar{x})^p(y-\bar{y})^q] \tag{5.4}$$

The above definitions of the centroid, the angle of orientation, and the central moments are taken from Jain (1989, pp. 392-394).

The solution of Eq. 5.3 can give either the orientation of the major principal axis or the orientation of the minor principal axis.

5.3.4 Length and Width

The length of the major principal axis of a region and the width of the minimum bounding rectangle were used to represent the length and the width of a grain kernel. To measure the length and the width, the coordinates of the boundary pixels of the region were transformed as below:

$$\alpha = (x - \bar{x})\cos\theta + (y - \bar{y})\sin\theta \tag{5.5}$$

$$\beta = -(x - \bar{x})\sin\theta + (y - \bar{y})\cos\theta \tag{5.6}$$

The coordinates (α, β), therefore, were the coordinates of the boundary pixels when the origin was at the centroid and the α axis was along the angle θ. The distances between the crossing points of the boundary pixels (α,β) with the axis $\alpha = 0$ (say, ℓ_1) and with the axis $\beta = 0$ (say, ℓ_2) were determined. The greater of the two distances, ℓ_1 and ℓ_2, was the length of the major principal axis.

The distance between two boundary pixels for which the value of α were maximum and minimum (say, w_1) and the distance between pixels of maximum and minimum β (say, w_2) were determined. The shorter of the two distances, w_1 and w_2, was the width of the minimum bounding rectangle.

The radii were computed as the distances between the boundary pixels and the centroid. Maximum and minimum radii, length, width, area, and perimeter were used as the size features.

5.3.5 Shape Features

All the shape features were derived from the size features. They are defined as:

$$Thinness\ Ratio = \frac{(Perimeter)^2}{Area} \tag{5.7}$$

$$Rectangular\ Aspect\ Ratio = \frac{Length}{Width} \tag{5.8}$$

$$Area\ Ratio = \frac{(Length \times Width)}{Area} \tag{5.9}$$

$$Radius\ Ratio = \frac{MaximumRadius}{MinimumRadius} \tag{5.10}$$

$$H\ Ratio = \frac{\mu_r}{\sigma_r} \tag{5.11}$$

where μ_r and σ_r are the mean and the standard deviation of all the radii (*i.e.* distances of all the pixels on the boundary from the centroid) of a kernel region.

H ratio is a shape feature that was not used in previous studies on grain shapes. It is, however, a useful feature because it increases monotonically as a shape becomes more circular and is independent of orientation and size of a component (Haralick and Shapiro, 1992). It was expected that H ratio of HRS wheat kernels would be greater than that of durum wheat, barley, oats, and rye.

CHAPTER 6: RESULTS AND DISCUSSION

6.1 Effectiveness of the Disconnect Algorithm

Images of the touching kernels of HRS wheat, durum, barley, oats, and rye were processed with the disconnect algorithm. In total, 30 images of HRS wheat containing 746 touching or connected kernels, 20 images of durum containing 391 touching kernels, 19 images of barley containing 376 touching kernels, 15 images of oats containing 286 touching kernels, and 20 images of rye containing 393 touching kernels were used for testing the effectiveness of the disconnect algorithm in disjoining the connected kernel regions. Some of the typical results of the disconnect algorithm for HRS wheat, durum, barley, oats, and rye are illustrated in Figs. 6.1-6.10. A repository of software-separated kernel images is given in Appendix B. Any disconnected kernel region which was not bisected or visibly distorted by improper placement of the separation lines was considered successfully disconnected. The success rate in disjoining the connected kernel regions, measured as a percent of the number of kernel regions successfully disconnected out of a given total number of kernel regions that were connected, was 95% for HRS wheat and durum, 94% for barley, 79% for rye, and 71% for oats.

6.1.1 Influence of Threshold

The thresholded images of the touching kernels were the input to the disconnect algorithm. Durum kernels were relatively translucent and therefore, a high threshold of 180 was required for their proper segmentation. The threshold of 180 was selected subjectively by examining the images and histograms of the durum wheat images. Most

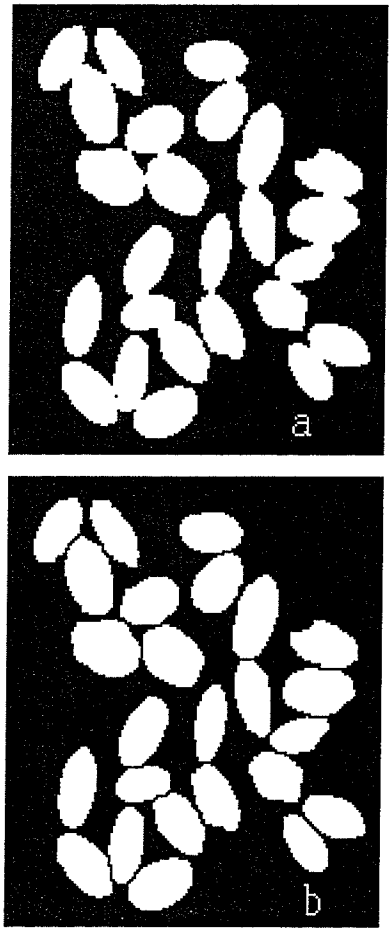

Fig. 6.1. Example of (a) touching and (b) software-separated kernels of HRS wheat.

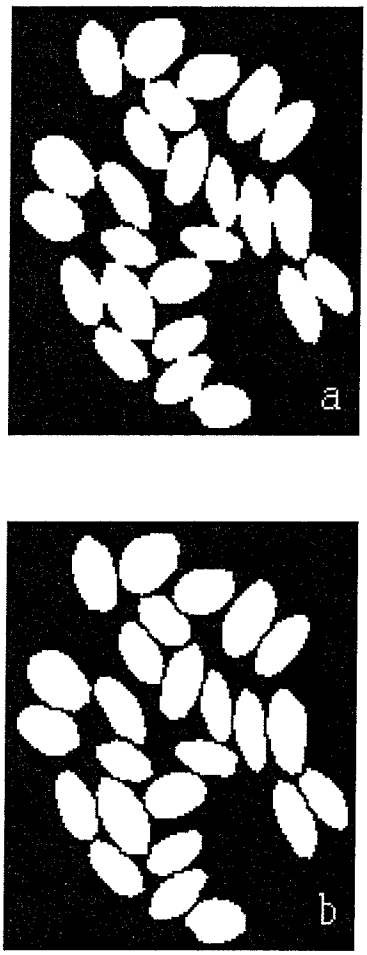

Fig. 6.2. Example of (a) touching and (b) software-separated kernels of HRS wheat.

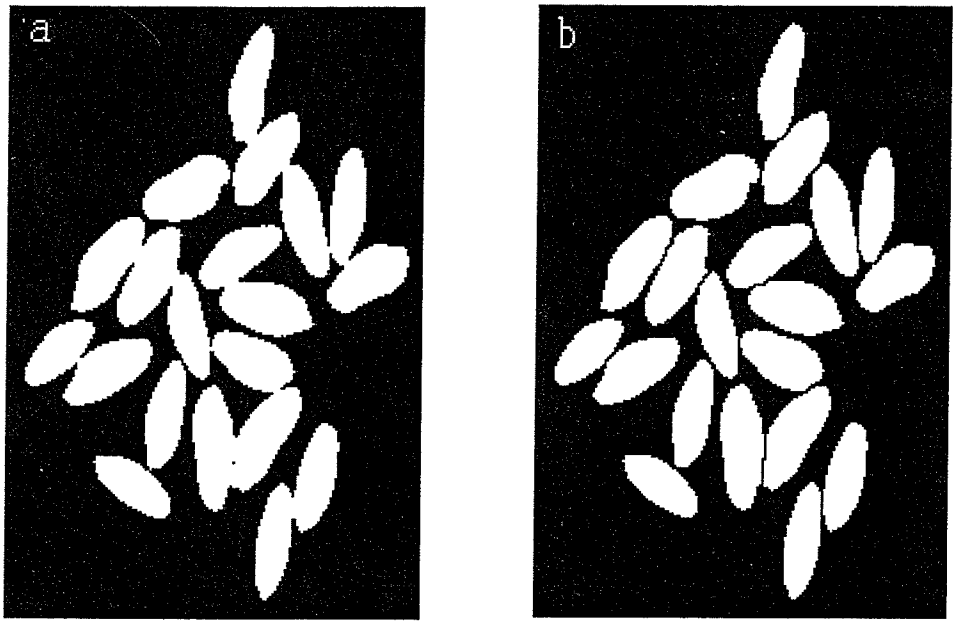

Fig. 6.3. Example of (a) touching and (b) software-separated kernels of durum wheat.

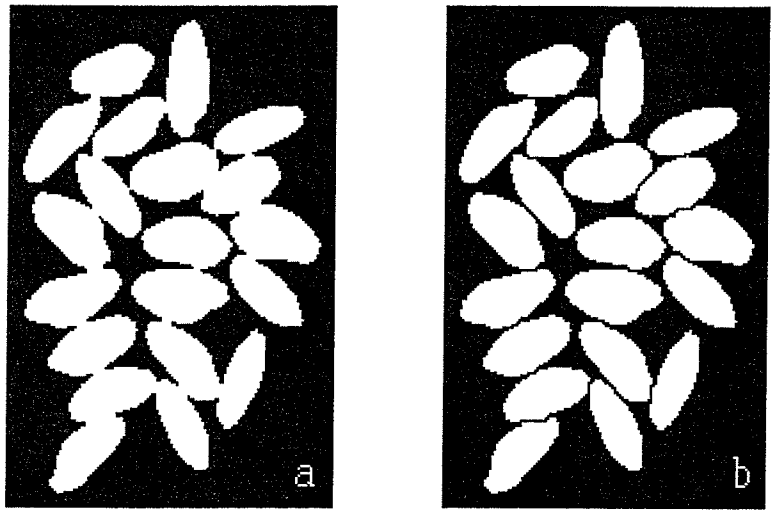

Fig. 6.4. Example of (a) touching and (b) software-separated kernels of durum wheat.

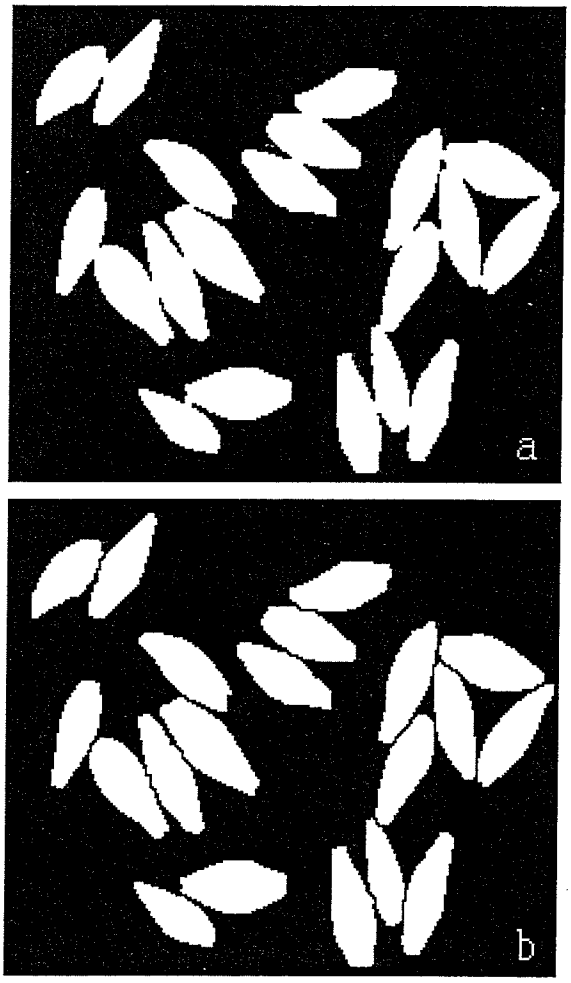

Fig. 6.5. Example of (a) touching and (b) software-separated kernels of barley.

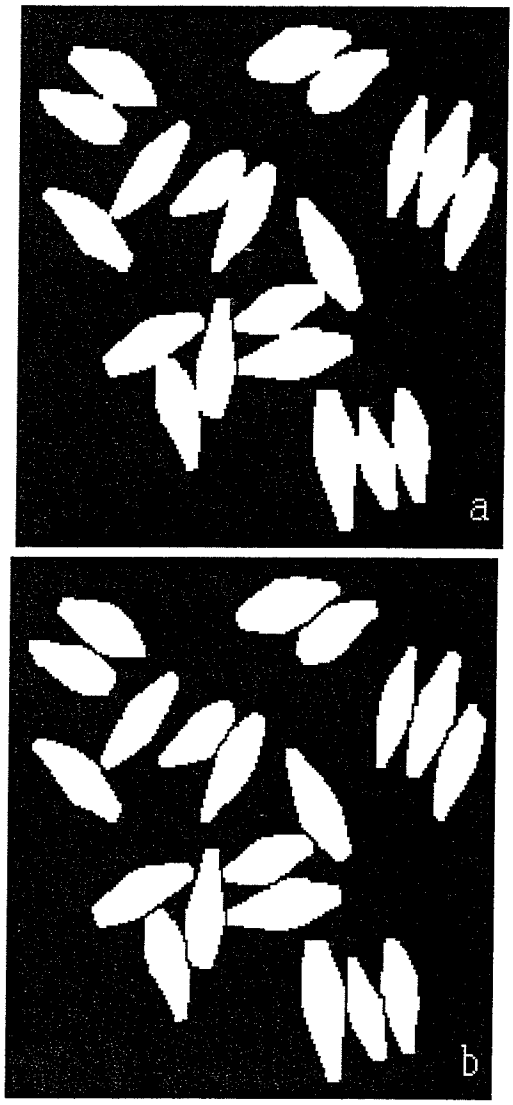

Fig. 6.6. Example of (a) touching and (b) software-separated kernels of barley.

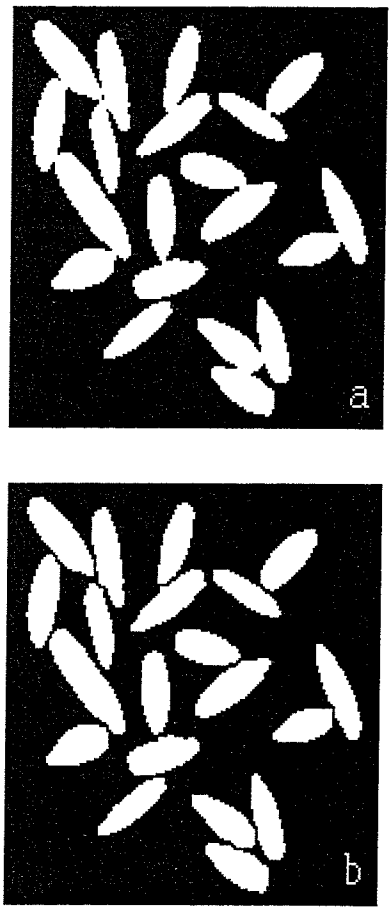

Fig. 6.7. Example of (a) touching and (b) software-separated kernels of rye.

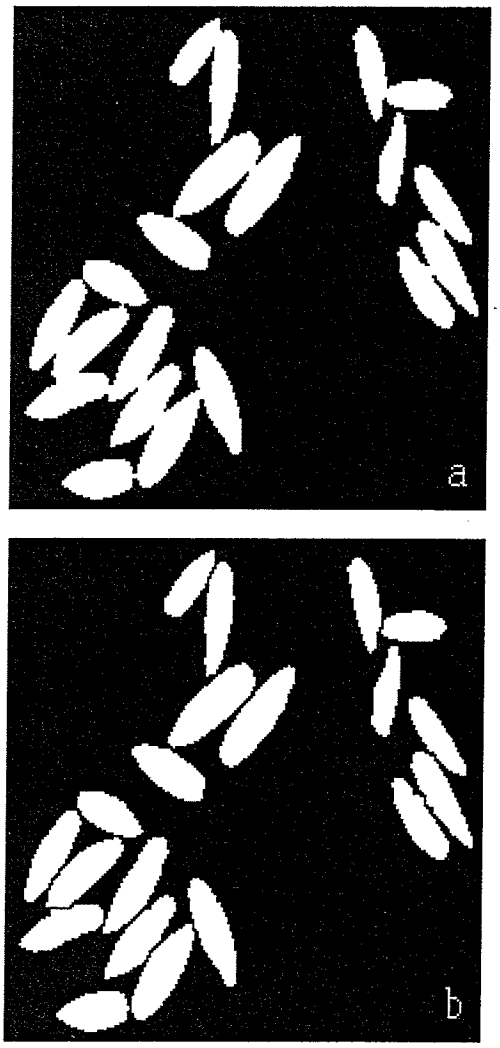

Fig. 6.8. Example of (a) touching and (b) software-separated kernels of rye.

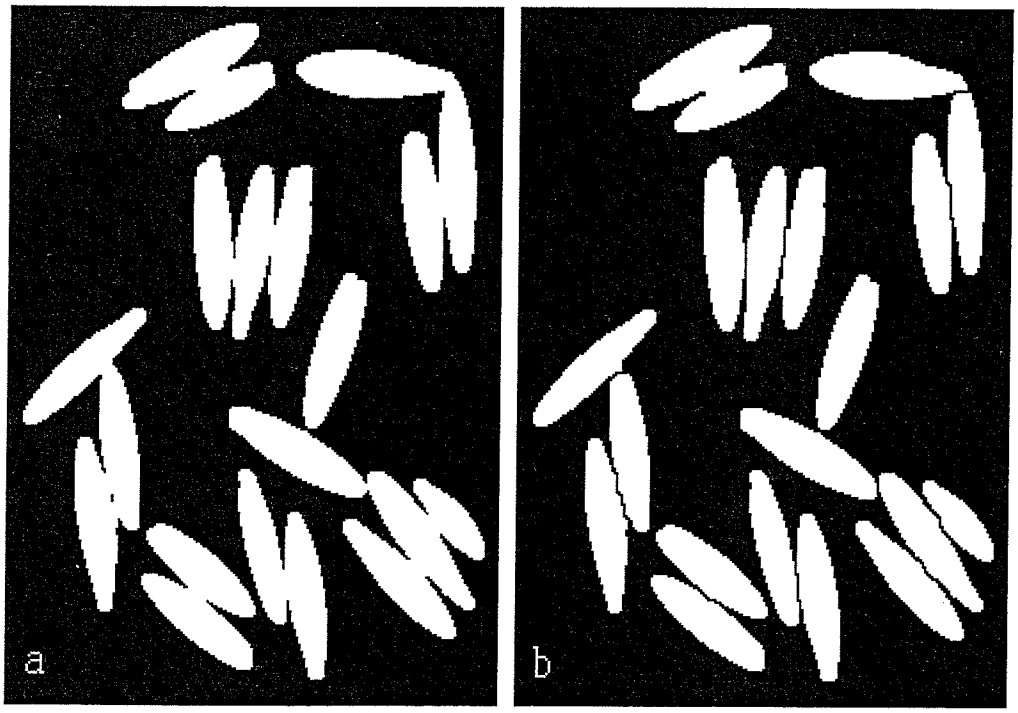

Fig. 6.9. Example of (a) touching and (b) software-separated kernels of oats; two of the kernels were not separated.

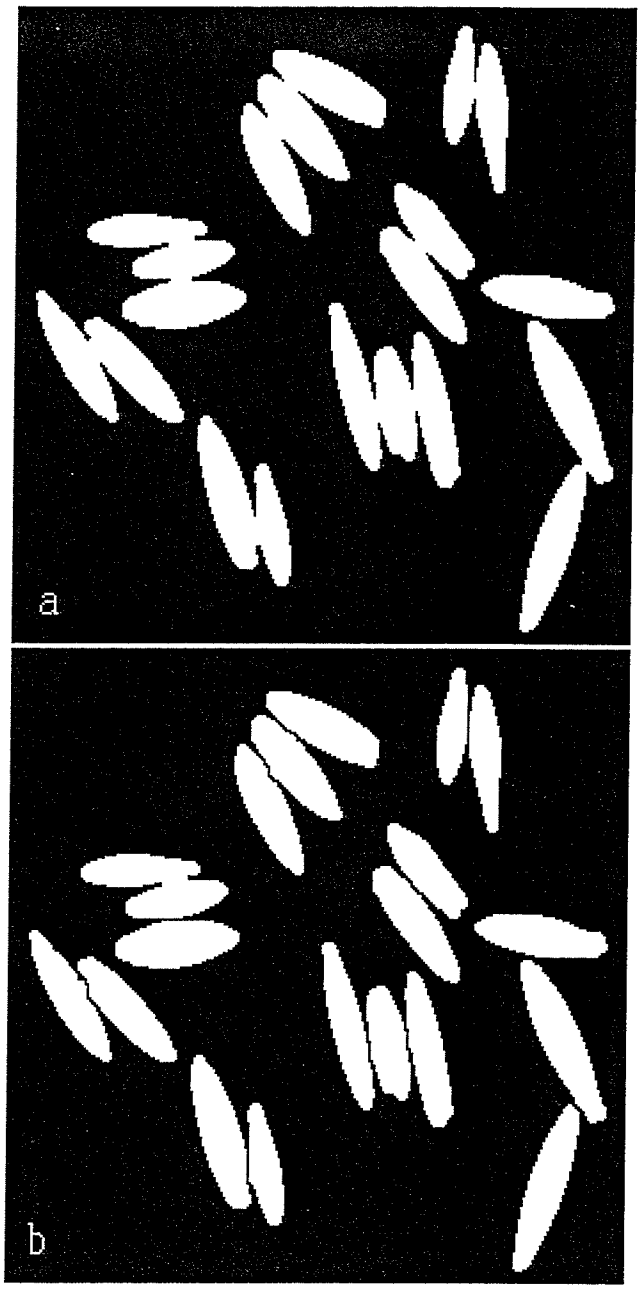

Fig. 6.10. Example of (a) touching and (b) software-separated kernels of oats; two of the kernels were not separated.

images of other grains were also segmented at threshold of 180. Two images of oats were thresholded at 190 and one at 175 because they were not properly segmented at 180.

One reason for the poor performance of the disconnect algorithm on the touching images of rye and oats was the combined effect of their slender shape and the use of high thresholds for their primary segmentation. At high thresholds, several pixels at the isthmus between kernel regions became part of the isthmus when, in fact, they belong to the background. Use of a lower threshold can make the isthmus short and narrow. Conjoint kernels can be more easily disconnected if the isthmus is short and narrow. A bigger isthmus may not be broken by the disconnect algorithm, especially if the kernels are slender in shape (such as kernels of rye and oats). The kernels of rye and oats are opaque and it was possible to segment them at lower thresholds. Success rate in disjoining kernel regions improved to 79% (from 71%) for oats and 89% (from 79%) for rye when lower thresholds in the range of 110 to 140 were used.

6.1.2 Limitations of the Disconnect Algorithm

In the disconnect algorithm, heuristics was added (such as dilating the UECs, adding the dilated dendrite) to reduce the chances of bisecting a kernel. This, however, could not be done without increasing the risk of leaving some kernels connected. The important limitation of the disconnect algorithm, therefore, was that a few of the conjoint kernels could not be disconnected (Figs. 6.9-6.12).

As was noted earlier, the area of an isthmus joining the kernel regions affects the performance of the disconnect algorithm. This influence can be explained based on the mechanism of the algorithm. The underlying logic for breaking of an isthmus is that

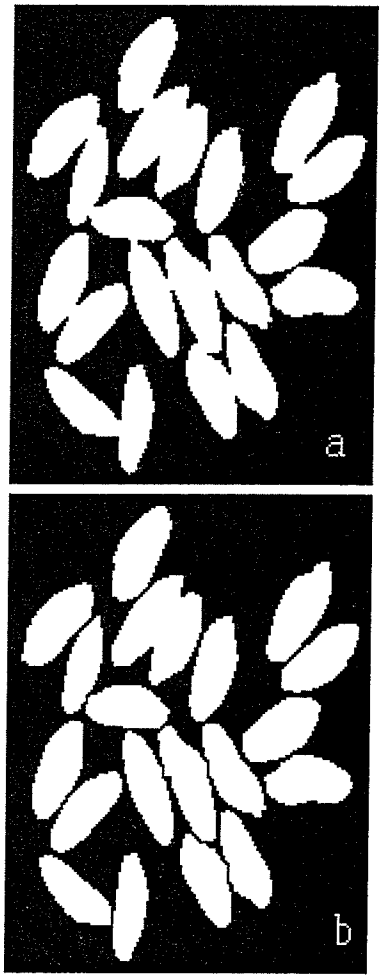

Fig. 6.11. Example of (a) touching and (b) software-separated kernels; two of the kernels were not separated.

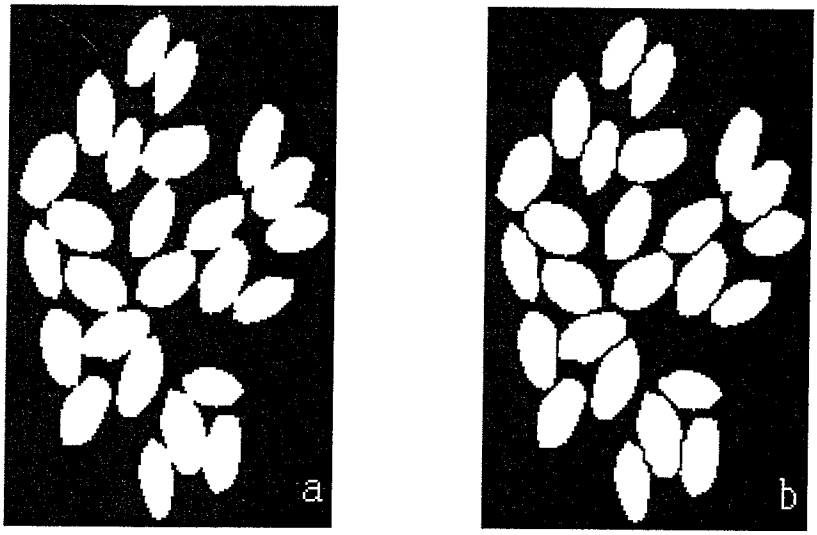

Fig. 6.12. Example of (a) touching and (b) software-separated kernels; two of the kernels were not separated.

upon successive erosions of an image of the touching kernels with progressively larger discs (Eq. 3.1), a stage of erosion comes when a disc does not fit in the isthmus area joining two or more kernel regions but fits in the kernel regions joined at the isthmus. Kernels could not be disconnected if the condition of the minimum diameter or the minimum disc fitting space in the isthmus was not met. In such a case, the region made of conjoint kernels yielded a single UEC corresponding to the isthmus. This is illustrated by Fig. 6.13. Notice that a single UEC was obtained for a conjoint kernel region in which two thin rye kernels were touching each other lengthwise (Fig. 6.13).

A more frequent cause for failure in disconnecting kernels was that a bigger isthmus area biased the location of the UECs towards it. In other words, the UECs of kernel region occurred not near the centres of the regions but rather near the centre of the isthmus (Fig. 6.13). Such biased UECs of the two kernels were close to one another and merged upon dilation (Eq. 3.2 and 3.9). Figure 6.13(c,d) show the biased UECs of the kernels in two conjoint regions where kernels could not be disconnected.

In a few cases, adding the dendrite after its dilation (Eq. 3.7) and subsequent elimination of corner locations using Eq. 3.10 also caused merging of the components which were otherwise disconnected. This is illustrated in Fig. 6.14. Notice that components (indicated by arrows) were separated before the addition of the dilated dendrites (Fig. 6.14(a)).

Another limitation of the algorithm was that the separation line, in some cases, was placed within a kernel region rather than at the isthmus (Fig.6.15). This happened because the narrowest section across which a minimum disc did not fit occurred within

Fig. 6.13. Failure in software-separation due to long isthmus (a) - Touching kernels; (b) - Kernels after software-separation; (c) - Ultimately eroded components (UECs) of the kernels which could not be separated; (d) - UEC locations superimposed on image in (b) as black pixels.

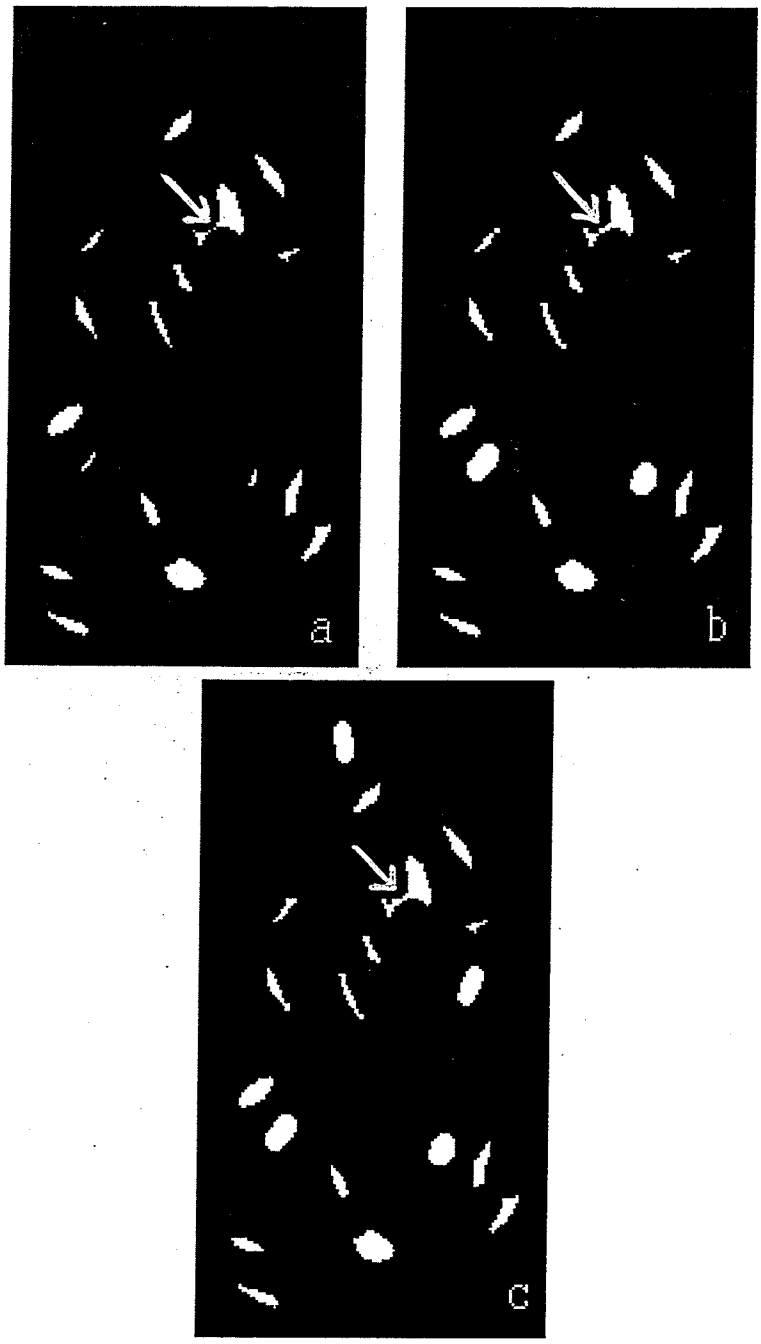

Fig. 6.14. Failure in software-separation due to addition of dilated dendrites and subsequent elimination of corners. (a) - Two of the components are separate before adding the dendrite; (b) - Components after adding the dilated dendrites; (c) - The two components merged after eliminating the corners.

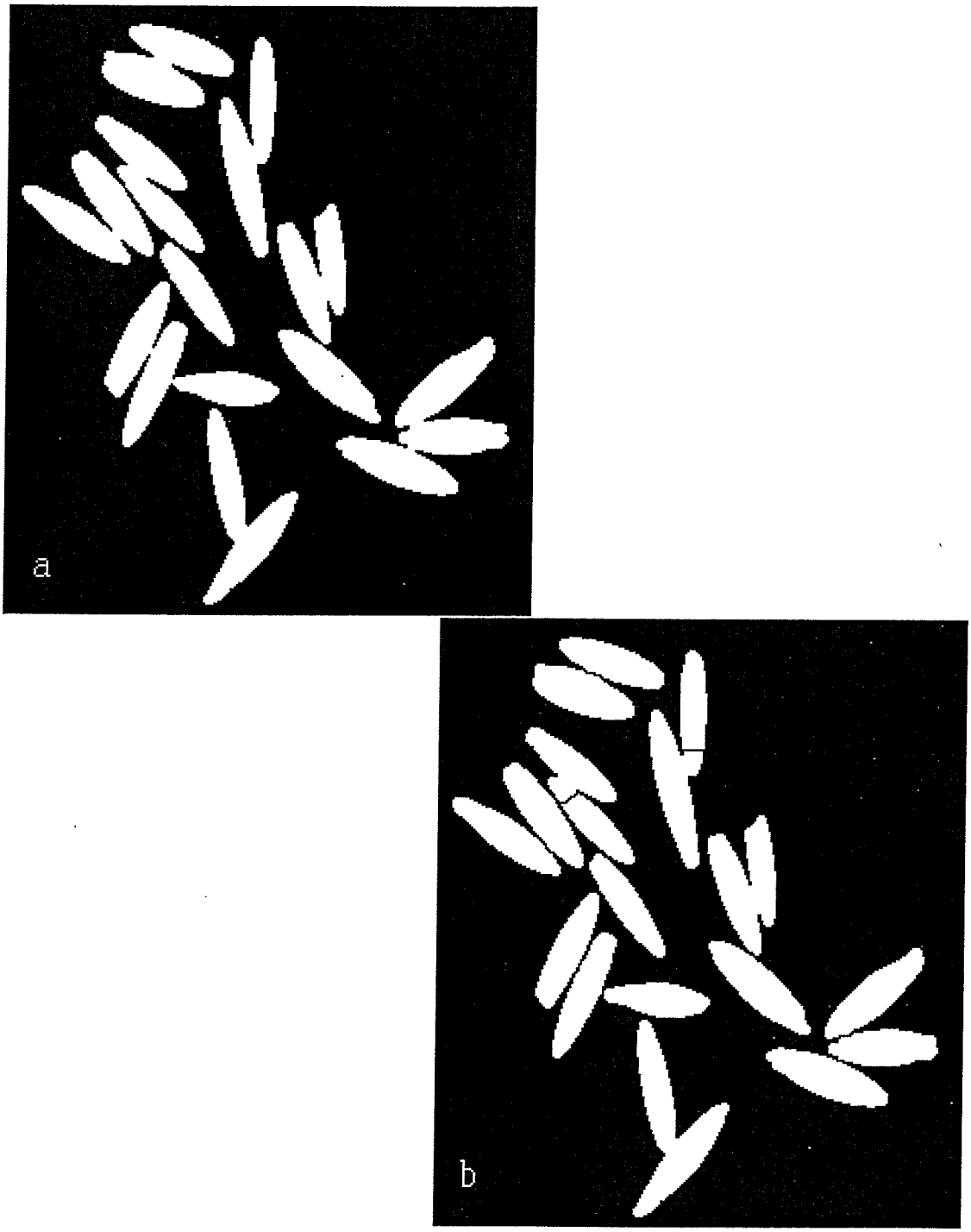

Fig. 6.15. Improper placement of the separation lines. (a) - Touching and (b) - Separated kernels of oats.

a kernel region. This was a problem, especially, when a thin tip of an oat kernel was touching another kernel.

6.2 Precision of the Measured Features

The geometrical feature data from repeated images of a single kernel (Experiment 1) of each grain type (HRS wheat, barley, durum, oats, and rye) were used to determine the tolerance limits of precision of each of the features for each of the grains. For a normal distribution of measurements with an unknown mean μ and an unknown standard deviation σ, tolerance limits are given by $x \pm k \cdot s$, where k is determined so that there is $100.\gamma\%$ confidence that the given limit contains at least $1-\alpha$ proportion of the measurements (Walpole and Myers, 1978, pp. 220-221) where x and s are the sample mean and standard deviation, respectively. The value of k depends on γ, α, and the sample size, and can be obtained from statistical tables (Walpole and Myers, 1978, pp. 520-521). The variation between the upper and lower tolerance limits is given by $2k \cdot s$. The values of $2k \cdot s$ for $\gamma = 0.99$ and $\alpha = 0.05$ were calculated for all the features of all the five grain types based on the data from repeated images of the same kernels. These values of $2k \cdot s$ were named $\gamma_{0.99}\alpha_{0.05}$ variation and are given in Table 6.1. The values of $\gamma_{0.99}\alpha_{0.05}$ variation were used as a guiding limit when comparing the differences of features between the software-separated and the physically-separated kernels.

The means and coefficient of variations of all the features for each of the grain types are given in Appendix C.

6.3 Geometrical Features of the Software-Separated Kernels

The usefulness of the disconnect algorithm in disjoining the conjoint kernel

Table 6.1. **Comparison of variation in repeated measurements on the same kernels to the differences between the software-separated and the physically-separated kernels.**

Features	Experiment 1: Precision					Experiment 2: Software Separation				
	$\gamma_{0.99}\alpha_{0.05}$ Variation					$\gamma_{0.99}\alpha_{0.05}$ Difference				
	HRS Wheat	Durum	Barley	Oats	Rye	HRS Wheat	Durum	Barley	Oats	Rye
Length (mm)	0.79	0.55	0.50	0.92	0.48	0.40	0.37	0.42	0.77	0.35
Area(mm^2)	0.98	2.06	1.70	0.93	0.84	0.84	0.91	0.94	1.20	0.84
Perimeter(mm)	0.88	1.23	1.56	2.69	1.29	0.59	0.77	0.84	1.65	0.83
Width(mm)	0.65	0.38	0.46	0.44	0.35	0.33	0.27	0.29	0.24	0.29
Min. Rad. (mm)	0.30	0.23	0.21	0.17	0.19	0.17	0.18	0.15	0.16	0.14
Max. Rad. (mm)	0.20	0.20	0.21	0.37	0.23	0.15	0.17	0.21	0.29	0.22
Thinness Ratio	1.48	1.99	2.78	5.51	2.90	1.17	1.35	1.73	2.74	2.06
Rectangular Aspect Ratio	0.42	0.26	0.32	0.71	0.45	0.20	0.18	0.24	0.41	0.38
Radius Ratio	0.41	0.45	0.39	0.82	0.63	0.26	0.41	0.40	0.65	0.52
H Ratio	2.17	0.36	0.16	0.15	0.28	0.68	0.27	0.14	0.15	0.23
Area Ratio	0.18	0.18	0.22	0.22	0.18	0.17	0.14	0.13	0.12	0.16

regions rests on the assumption that the shape or size related features do not change considerably from their true values. A true value of a feature, in this context, is a value derived from the image when kernel(s) were not touching one another.

The labelled images of the software-separated and the physically-separated kernels were visually compared to attach consistent labels to the same kernel in the software-separated and the physically-separated images. Visual comparison of labelled images was essential because feature data of a kernel were identified by its label value whereas the label values of the same kernel in the software-separated image and the physically-separated image were not the same.

The mean and the standard deviation of the difference in the features between the physically-separated and the software-separated kernels were used to calculate the tolerance limits, $x_{diff} \pm k \cdot s_{diff}$ for $\gamma = 0.99$ and $\alpha = 0.05$ for all the eleven features of the five types of grains. For each of the grain type, at least 100 randomly selected kernel data were used in calculating the mean, x_{diff}, and the standard deviation, s_{diff}, of the difference in the measured features. The bigger of the two values, $x_{diff} + k \cdot s_{diff}$ and the absolute value of $x_{diff} - k \cdot s_{diff}$, was named $\gamma_{0.99}\alpha_{0.05}$ difference. It can be interpreted as the limiting value for the absolute difference in a feature between the physically-separated and the software-separated kernels so that there is 99% confidence that the absolute difference in a feature for at least 95% of the kernels would be equal to or less than the limiting value. The $\gamma_{0.99}\alpha_{0.05}$ difference values for HRS wheat, durum, barley, oats, and rye are given in Table 6.1. It is noteworthy that except for the area of oats, the $\gamma_{0.99}\alpha_{0.05}$ difference of all other features for all the grain types were approximately equal to or less

than the $\gamma_{0.99}\alpha_{0.05}$ variation in the precision data (Table 6.1). Software separation, thus, does not distort or change the geometrical features of HRS wheat, durum, barley, oats, and rye beyond the tolerance limits of precision.

Table 6.2 shows the percent of kernels for which a feature change after software-separation was more than $\gamma_{0.99}\alpha_{0.05}$ variation based on the precision data. Note that the change in the features was prominent for more kernels of oats, rye, and barley than the kernels of HRS wheat or durum (Table 6.2).

6.4 Pattern Classification in the Software-Separated Kernels

The ultimate use of the feature data set is in pattern classification. To assess the pattern classification capability of the geometrical features from the software-separated kernels, procedure DISCRIM of SAS (1990) was used to classify the kernels into the categories of HRS wheat, durum, barley, oats, and rye. All the eleven features mentioned in Table 6.1, were used in the classification. The kernel regions that were visibly distorted due to improper placement of the separation lines and those which could not be disconnected were not used for the classification. A non-parametric probability density estimation (*viz* k-nearest neighbour) was used because the normality assumption does not hold for oats kernel population (Symmons and Fulcher, 1988c). The classification was based on the Bayes decision rule which classifies an entity (represented by its pattern vector) to a class for which the entity has maximum a posteriori probability (Hand, 1981, pp. 4-6; Duda and Hart, 1973, pp. 10-20). The confusion matrix for a cross validation or leave-one-out classification is given in Table 6.3.

Table 6.2. Percent of kernels for which a feature changed more than the $\gamma_{0.99}\alpha_{0.05}$ Variation.

Features	HRS wheat	Durum	Barley	Oats	Rye
Length	0	0	1	2	1
Area	2	1	0	8	3
Perimeter	0	0	0	0	0
Width	0	0	0	0	1
Minimum Radius	0	0	0	3	1
Maximum Radius	0	3	3	1	3
Thinness Ratio	0	0	0	0	0
Rect. Aspect Ratio	0	0	1	0	2
Radius Ratio	0	2	5	2	2
H Ratio	0	1	0	2	2
Area Ratio	3	1	0	0	3

Table 6.3. Confusion matrix for the software-separated kernels.

Categories (to)→ (from)↓	HRS Wheat	Durum	Barley	Oats	Rye
HRS Wheat (n=424)	414 (97.6%)	5	0	0	5
Durum (n=240)	2	225 (93.7%)	4	0	9
Barley (n=260)	1	9	239 (91.9%)	6	5
Oats (n=217)	0	2	11	189 (87.1%)	15
Rye (n=317)	7	10	5	2	293 (92.4%)

In the leave-one-out classification, one sample, at a time, is classified and the remaining n-1 samples serve as a training set. Among commonly used methods of error estimation in classification, the leave-one-out method yields the most unbiased estimate of the expected true error (Hand, 1981, pp. 186-190). It avoids drastically dividing the available data into training and test sets, while maintaining an independence between them (Fukunaga and Hayes, 1989).

The overall correct classification for all the five grain categories together was 93.3%. Except for the oats, the classification of software-separated kernels was satisfactory (Table 6.3). The lack of discriminatory power of the geometrical features alone for the classification of oats was reported by Sapirstein and Bushuk (1989). Sapirstein and Bushuk (1989) found that the addition of the mean gray level feature of grains improved the classification of oats. It is expected that addition of gray-level or

color dependent features will improve the classification of software-separated kernels, especially because such features would not be affected by the disconnect algorithm.

From a wheat grading perspective, a 3-way classification among HRS wheat, durum, and other cereals is more important. For the 3-way classification, correct classification for HRS wheat and durum remained the same as before. The other cereal class (including barley, oats, and rye together in one class) was correctly classified with 96.3% success. The overall correct classification into three categories was also 96.3% (Table 6.3).

The classification of the physically-separated kernels into the categories of HRS wheat, durum, barley, oats, and rye using non parametric classification (k nearest neighbour estimation) with the leave-one-out method is given in Table 6.4. The overall correct classification achieved was 95.0%. Thus, 1.7% additional kernels were correctly classified for the physically-separated kernels when compared to the classification of the software-separated kernels. Most of the additional misclassifications of the software-separated kernels occurred for oats and rye kernels (Tables 6.3 and 6.4).

Another approach to calculate the additional misclassification caused by the software-separation is to treat the physically-separated kernels as a training set and the software-separated kernels as a test set. As was mentioned above, the overall correct classification for the physically-separated kernels was 95.0%. The classification results for the software-separated kernels in this case is given in Table 6.5. The overall correct classification in this case was 93.3%, the same as that obtained with the leave-one-out method for the software-separated kernels.

Table 6.4. Confusion matrix for the physically-separated kernels.

Categories (to)→ (from)↓	HRS Wheat	Durum	Barley	Oats	Rye
HRS wheat (n=424)	418 (98.5%)	5	0	0	1
Durum (n=240)	2	227 (94.5%)	4	0	7
Barley (n=260)	1	5	241 (92.6)	10	3
Oats (n=217)	0	1	6	197 (90.7%)	13
Rye (n=317)	3	4	3	5	302 (95.2%)

Table 6.5. Confusion matrix for the software-separated kernels when they are treated as a test set.

Categories (to)→ (from)↓	HRS Wheat	Durum	Barley	Oats	Rye
HRS wheat (n=424)	416 (98.1%)	6	0	0	2
Durum (n=240)	1	229 (95.4%)	3	0	7
Barley (n=260)	1	6	241 (92.6%)	6	6
Oats (n=217)	0	3	11	183 (84.3%)	20
Rye (n=317)	5	14	3	3	292 (92.1%)

In an n-dimensional feature space, the pattern classes (classification categories) form n-dimensional hyperclouds. A sample which occurs in the vicinity of the boundaries between two or more hyperclouds is a most likely candidate for the misclassification. Only those changes in the features subsequent to the software-separation which would bring a sample's feature vector from inside of its pattern's hypercloud to the surface, can cause additional misclassification. In this respect, a small change in a feature vector which is already near the surface of its pattern's hypercloud can be more detrimental than a relatively large change in the feature vector which is deep inside the pattern's hypercloud. Also, a small change which pulls a pattern to the surface of its hypercloud is more serious compared to a relatively large change which pulls the pattern towards the centre of the hypercloud.

Results presented in Tables 6.1 to 6.5 demonstrate that the geometrical features of the software-separated kernels were not distorted and can be successfully used in discriminating HRS wheat from durum and other cereal grains.

CHAPTER 7: CONCLUSIONS

Feature measurement and classification of grain when the imaged samples contain touching kernels may be essential for automated grain sample analysis. In this study a mathematical morphology based algorithm was developed for disconnecting the conjoint regions in the image of touching kernels. A grain feature extraction routine was also developed to measure the area, perimeter, length, width, maximum and minimum radii, rectangular aspect ratio, thinness ratio, radius ratio, area ratio, and the ratio of the mean to the standard deviation of all the radii. The study shows that the software-separated kernels retain their geometrical features and can be successfully used in classification of cereal grains used in the present study. The following specific conclusions can be drawn:

1. The algorithm was successful in disconnecting 95% HRS and durum wheat, 94% barley, 89% rye, and 79% oats conjoint kernel regions.
2. Except for the area of oats, the change in the features of the software-separated kernels from the corresponding feature values of the physically-separated kernels was less than or equal to the variation within tolerance limits of the measurement system.
3. Hard red spring wheat was discriminated from durum and other cereal grains with 97.6% success using the geometrical features of the software-separated kernels.
4. The overall classification success of 93.3% was achieved in a five-way classification of the software-separated grains among HRS and durum wheat, barley, oats, and rye. A very few additional kernels (1.7%) were correctly

classified for the physically-separated grains.

CHAPTER 8: CONTRIBUTION TO KNOWLEDGE

A general solution to the image segmentation problem containing touching objects has not been reported in the published literature. In this research a heuristic algorithm was developed for the segmentation of touching grain images. The aim of the algorithm was to disconnect the conjoint kernel regions in the image. A strict convexity for the touching objects was not assumed. The algorithm, therefore, can be used in the segmentation of touching patterns of other objects of approximately convex shape if the radius of the largest circle fitting inside the connected regions when the circle is translated to the centre of the isthmus joining the objects is smaller than the radii of the largest circles fitting in the objects.

It was demonstrated that the software-separated kernels preserved their geometrical features. The design requirements for a grain sample presentation device can be simplified based on the knowledge from this research. Especially, presentation of multiple kernels to the camera will be possible so long as kernels do not overlap.

CHAPTER 9: RECOMMENDATIONS FOR FUTURE RESEARCH

The effectiveness of the disconnect algorithm developed in this study is affected by the size of the isthmus joining two or more kernel regions. Investigation into the image segmentation techniques should be made with the objective of reducing the length, width, or both of the isthmus.

The classification of the software-separated kernels should be retried after adding the color and gray level dependent features in the pattern vector.

Wheat and other cereal grains found as inseparable foreign material in wheat samples were studied. To arrive at a broad based conclusion, however, the disconnect algorithm should be tested for other small and large seeds found in commercial grades of wheat and barley.

Implementation of the disconnect algorithm in specialized image processing computer architecture (such as an array processor) to achieve realistic speed and a sample presentation device which can present the grains in a single-kernel-layer to the camera's field of view are essential for automation of grain sample analysis. Work in both these areas is needed.

REFERENCES

Ballard, D.H. and C.M. Brown. 1982. Computer Vision. Prentice Hall Inc., Englewood Cliffs, NJ. 523 p.

Barker, D. A., T.A. Vouri, M.R. Hegedus, and D.G. Myers. 1992a. The use of ray parameters for the discrimination of Australian wheat varieties. Plant Var. and Seeds **5:** 35-45.

Barker, D. A., T.A. Vouri, and D.G. Myers. 1992b. The use of slice and aspect ratio parameters for the discrimination of Australian wheat varieties. Plant Var. and Seeds **5:** 47-52.

Barker, D. A., T.A. Vouri, and D.G. Myers. 1992c. The use of Fourier descriptors for the discrimination of Australian wheat varieties. Plant Var. and Seeds **5:** 47-52.

Barker, D. A., T.A. Vouri, M.R. Hegedus, and D.G. Myers. 1992d. The use of Chebychev coefficients for the discrimination of Australian wheat varieties. Plant Var. and Seeds **5:** 47-52.

Brogan, W.L. and A.R. Edison. 1974. Automatic Classifications of grains via pattern recognition techniques. Pattern Recognition **6:** 97-103.

Bulley, N.R., N. MacDonald, and O. Sziklai. 1984. Utilizing image analysis for determining seed viability. Paper No. PNR 84-501. Am. Soc. Agric. Eng., St. Joseph, MI. 17 p.

Canadian Grain Commission. 1992. Quality of Western Canadian Wheat Exports. Crop Bulletin No. 198, ISSN 0829-8718. Grain Reseatch Laboratory, Winnipeg, MB.

28 p.

Canadian Grain Commission. 1987. Official Grain Grading Guide. Canadian Grain Commission, Winnipeg, MB.

Casady, W.W. and M.R. Paulsen. 1989. An automated kernel positioning device for computer vision analysis of grains. Transactions of the ASAE **32:** 1821-1826.

Casady, W.W. 1987. Development of an automated computer vision system for determining grain quality. Unpublished M.S. thesis, University of Illinois, Urbana, IL. 106 p.

Chen, C., Y.P. Chiang, and Y. Pomeranz. 1989. Image analysis and characterization of cereal grains with a laser range finder and camera contour extractor. Cereal Chem. **66:** 466-470.

Chermant, J., M. Coster, J. Jernot, and J. Louis. 1981. Morphological analysis of sintering. J. Microscopy **121**: 89-98.

Churchill, D.B., D.M. Bilsland, and T.M. Cooper. 1990. Comparision of machine vision with human measurement of seed dimensions. Paper No. 90-7519. Am. Soc. Agric. Eng., St. Joseph, MI.

Craig, E. M. 1993. An automated seed presentation device for use in machine vision identification of grains. Unpublished B.Sc. thesis, University of Manitoba, Winnipeg, MB. 38 p.

Duda, R.O. and P.E. Hart. 1973. Pattern Classification and Scene Analysis. John Wiley and Sons, Inc. New York, NY. 482 p.

Fukunaga, K. and R.R. Hayes, 1989. Estimation of classifier performance. IEEE Trans.

Pattern Analysis and Machine Inteligence **11:** 1087-1101.

Giardina, C.R. and E.R. Dougherty. 1988. Morphological Methods in Image and Signal Processing. Prentice Hall, Englewood Cliffs, NJ. 321 p.

Gonzalez, R.C. and R.E. Woods. 1992. Digital Image Processing. Addision-Wesley Publishing Co., Reading, MA. 716 p.

Hand, D.J. 1981. Discrimination and Classification. John Wiley and Sons, New York, NY. 218 p.

Haralick, R.M. and L. Shapiro. 1992. Computer and Robot Vision. Addision-Wesley Publishing Co., Reading, MA. 672 p.

Haralick, R.M., S.R. Sternberg, and X. Zhuang. 1987. Image analysis using mathematical morphology. IEEE Trans. PAMI **9:** 523-550.

Hehn, J.L., and S. Sokhansanj. 1990. Canola and mustard seed identification using Macintosh based imaging system. Paper No. 90-3534. Am. Soc. Agric. Eng., St. Joseph, MI. 13 p.

Heijmans, H.J.A.M. and C. Ronse. 1990. The algebraic basis of mathematical morphology. Comput. Vis. Graph. Im. Proc. **50:** 245-295.

Jain, A.K. 1989. Fundamentals of Digital Image Processing. Prentice Hall, Englewood Cliffs, NJ. 569 p.

Jähne, B. 1991. Digital Image Processing: Concepts, Algorithms and Scientific Applications. Springer-Verlag, Berlin, Germany. 383 p.

Keefe, P.D. 1992. A dedicated wheat grading system. Plant Var. and Seeds **5:** 27-33.

Keefe, P.D. and S.R. Draper. 1986. The measurement of new characters for cultivar

identification in wheat using machine vision. Seed Sci. Technol. **14:** 715-724.

Kim, C., J.F. Reid, and M.R. Paulsen. 1990. Evaluation of a machine vision system for corn stress crack detection. Paper No. 90-7051. Am. Soc. Agric. Eng., St. Joseph, MI. 12 p.

Kim, C., J.F. Reid, and M.R. Paulsen. 1989. Algorithms for automatic detection of corn stress cracks. Paper No. 89-7508. Am. Soc. Agric. Eng., St. Joseph, MI. 27 p.

Kimmel, M.J., R.S. Jaffe, J.R. Manderville, and M.A. Levin. 1985. MITE: Morphic Image Transform Engine, an architecture for reconfigurable pipelines of neighbourhood processors. Pages 493-500 in: Proc. IEEE Comput. Soc. Workshop Computer Architecture for Pattern Analysis and Image Database Management, Miami Beach, FL.

Kohler, J.M. 1991. Study of commercial grades of Canada red spring wheat by digital image processing. M.Sc. thesis, University of Manitoba, Winnipeg, MB. 131 p.

Kranzler, G.A. 1985. Applying digital image processing in agriculture. Agric. Eng. **66:** 11-13.

Lantuéjoul, C. 1980. Skeletonization in quantitative metallography. Pages 107-135 in: Issues of Digital Image Processing, R.M. Haralick and J.C. Simon (eds.). Sijthoff and Noordhoff, Groningen, The Netherlands.

McCubbery, D.L. and R.M. Lougheed. 1985. Morphological image analysis using a raster pipeline processor. Pages 444-452 in: Proc. IEEE Comput. Soc. Workshop Computer Architecture for Pattern Analysis and Image Database Management, Miami Beach, FL.

McDonald, T.P. and Y.R. Chen. 1990a. Application of morphological image processing in agriculture. Transactions of ASAE. **33:** 1345-1352.

McDonald, T.P. and Y.R. Chen. 1990b. Separating connected muscle tissues in images of beef carcass ribeyes. Transactions of ASAE. **33:** 2059-2065.

Marchant, J.A. 1985. The use of robotics in the agricultural and food industries. Div. note DN 1304, Natl. Inst. Agric. Eng., Silsoe, UK. 28 p.

Myers, D.G. and K.J. Edsall. 1989. The application of image processing techniques to the identification of Australian wheat varieties. Plant Var. and Seeds **2:** 109-116.

Neuman, M., H.D. Sapirstein, E. Shwedyk, and W. Bushuk. 1987. Discrimination of wheat class and variety by digital image analysis of whole grain samples. J. Cereal Sci. **6:** 125-132.

Neuman, M., H.D. Sapirstein, E. Shwedyk, and W. Bushuk. 1989a. Wheat grain color analysis by digital image processing I. Methodology. J. Cereal Sci. **10:** 183-188.

Neuman, M., H.D. Sapirstein, E. Shwedyk, and W. Bushuk. 1989b. Wheat grain color analysis by digital image processing II. Wheat class discrimination. J. Cereal Sci. 10:183-188.

Ni, B., M.R. Paulsen, K. Liao, and J.F. Reid. 1993. An automated corn kernel inspection system using machine vision. Paper No. 93-3032. Am. Soc. Agric. Eng., St. Joseph, MI. 10 p.

Paulsen, M.R., W.D. Wigger, J.B. Litchfield, and J.B. Sinclair. 1989. Computer image analysis for detection of maize and soybean quality factors. J. Agric. Eng. Res. **43:** 93-101.

Pratt, W.K. 1991. Digital Image Processing, Second edition. John Wiley and Sons, New York, NY. 698 p.

Rosenfeld, A. 1984. Image analysis. In Digital Image Processing Techniques. M.P. Ekstrom (ed.). Acedemic Press, Inc., Orlando, FL.

Rosenfeld, A. and A.C. Kak. 1982. Digital Picture Processing, Volume 2, Second edition. Academic Press, New York, NY. 349 p.

Sapirstein, H.D. and W. Bushuk. 1989. Quantitative determination of foreign material and vitreosity in wheat by digital image analysis. Pages 453-474 in: ICC '89 Symposium: Wheat End-Use Properties. H. Salovaara (ed.). Lahti, Finland. Pp. 453-474.

Sapirstein, H.D., M. Neuman, E.H. Wright, E. Shwedyk, and W. Bushuk. 1987. An instrumental system for cereal grain classification using digital image analysis. J. Cereal Sci. **6:** 3-14.

Sarkar, N.R. 1986. Machine vision in the food industry. ASAE (Am. Soc. Agric. Eng.) Food Engineering News. October: pp. 1, 3-5. St. Joseph, MI.

SAS. 1990. SAS User's Guide: Statistics. Statistical Analysis System Inc, Raleigh, NC. 890 p.

Schalkoff, R.J. 1989. Digital Image Processing and Computer Vision. John Wiley and Sons, Inc., New York, NY. 489 p.

Serra, J. 1982. Image Analysis and Mathematical Morphology. Academic Press, New York, NY. 610 p.

Shatadal, P., D.S. Jayas, and N.R. Bulley. 1992. Separating contiguous wheat kernel

image regions using mathematical morphology. Paper No. 92-3577. Am. Soc. Agric. Eng., St. Joseph, MI. 13 p.

Shatadal, P., D.S. Jayas, J.L. Hehn, and N.R. Bulley. 1993. Classification and feature measurement on touching kernels of wheat and barley. Paper No. 93-3031. Am. Soc. Agric. Eng., St. Joseph, MI. 9 p.

Symons, S.J. and R.G. Fulcher. 1988a. Determination of wheat kernel morphological variation by digital image analysis: I. Variation in Eastern Canadian milling quality wheats. J. Cereal Sci. **8:** 211-218.

Symons, S.J. and R.G. Fulcher. 1988b. Determination of wheat kernel morphological variation by digital image analysis: II. Variation in cultivars of soft white winter wheats. J. Cereal Sci. **8:** 219-229.

Symons, S.J. and R.G. Fulcher. 1988c. Determination of variation in oat kernel morphology by digital image analysis. J. Cereal Sci. **7:** 219-229.

Thomson W.H. and Y. Pomeranz. 1991. Classification of wheat kernels using three-dimensional image analysis. Cereal Chem. **68:** 357-361.

Tillet, R.D. 1990. Image analysis for agricultural processes. Div. note DN 1585, AFRC Inst. Eng. Res., Silsoe, UK. 15 p.

Walpole, R.E. and R.H. Myers. 1978. Probability and Statistics for Engineers and Scientists. MacMillan Publishing Inc., New York, NY. 580 p.

Zayas, I., Y. Pomeranz, and F.S. Lai. 1985. Discrimination between Arthur and Arkan wheats by image analysis. Cereal Chem. **62:** 478-480.

Zayas, I., F.S. Lai, and Y. Pomeranz. 1986. Discrimination between wheat classes and

varieties by image analysis. Cereal Chem. **63:** 52-56.

Zayas, I., Y. Pomeranz, and F.S. Lai. 1989. Discrimination of wheat and nonwheat components in grain samples by image analysis. Cereal Chem. **66:** 233-237.

Zenzo, S.D. 1983. Advances in image segmentation. Image Vis. Comput. **1:** 196-210.

Appendix A

Primary and Export Grade Determinants for red spring wheat (Canada Western)
(Source: Official Grain Grading Guide (1987), Canadian Grain Commission, Winnipeg)

RED SPRING WHEAT (Canada Western) - PRIMARY GRADE DETERMINANTS

Grade Name	Standard of Quality				Maximum Limits of			
					Foreign Material		Wheats of Other Classes or Varieties	
	Minimum Test Weight kg/hL	Variety	Minimum Hard Vitreous Kernels	Degree of Soundness	Matter Other Than Cereal Grains	Total Including Cereal Grains	Contrasting Classes	Total Including Contrasting Classes
No. 1 Canada Western Red Spring	75.0	Any variety of red spring wheat equal to Neepawa	65.0%	Reasonably well matured, reasonably free from damaged kernels	About 0.2%	0.75%	1.0%	3.0%
No. 2 Canada Western Red Spring	72.0	Any variety of red spring wheat equal to Neepawa	35.0%	Fairly well matured, may be moderately bleached or frost damaged, but reasonably free from severely damaged kernels	About 0.3%	1.5%	3.0%	6.0%
No. 3 Canada Western Red Spring	69.0	Any variety of red spring wheat equal to Neepawa	-	May be frost damaged, immature or weathered, but moderately free from severely damaged kernels	About 0.5%	3.5%	5.0%	10.0%
Canada Western Feed	No Minimum	Any type or variety of wheat excluding amber durum	No Minimum	Excluded from other grades of wheat on account of light weight or damaged kernels, but shall be reasonably sweet	1.0%	10.0%	No Limit 10.0% amber durum only	
Final Grade Name	Canada Western Feed		No. 3 C.W. Red Spring		Over 1.0% grade Wheat, Sample C.W. Account Admixture	Over 10.0% grade Mixed Grain, C.W. Wheat	Canada Western Feed Over 10.0% amber durum grade Wheat, Sample C.W. Account Admixture	

RED SPRING WHEAT - PRIMARY GRADE DETERMINANTS

Grade Name	Sprouted		Binburnt Severe Mildew Rotted Mouldy	Heated Incl. Binburnt	Fireburnt	Stones	Ergot	Sclerotinia	Smudge	Total Smudge and Blackpoint
	Severe	Total Incl. Severe Sprouted								
No. 1 C.W. Red Spring	0.1%	0.5%	2K	0.1%	Nil	3K	3K	3K	30K	10.0%
No. 2 C.W. Red Spring	-	1.5%	5K	0.75%	Nil	3K	6K	6K	1.0%	20.0%
No. 3 C.W. Red Spring	-	5.0%	10K	2.0%	Nil	5K	24K	24K	5.0%	35.0%
Canada Western Feed	No Limit		10.0%	10.0%	2.0%	10K	0.25%	0.25%	No Limit	No Limit
Final Grade Name	Canada Western Feed		Over 10.0% grade Wheat, Sample C.W. Account Heated		Over 2.0% grade Wheat, Sample C.W. Account Fireburnt	Over grade tolerance up to 2.5% grade Rejected "grade" Account Stones. Over 2.5% grade Wheat, Sample Salvage	Over 0.25% grade Wheat, Sample C.W. Account Ergot	Over 0.25% grade Wheat, Sample C.W. Account Admixture	Canada Western Feed	Canada Western Feed

Grade Name	Shrunken and Broken			* Degermed	** Grass Green	Pink Kernels	Artificial Stain No Residue	Natural Stain	*** Insect Damage		Dark Immature
	Shrunken	Broken	Total						Sawfly Midge	Grasshopper Army Worm	
No. 1 C.W. Red Spring	6.0%	6.0%	7.0%	4.0%	0.75%	1.5%	Nil	0.5%	2.0%	1.0%	1.0%
No. 2 C.W. Red Spring	10.0%	10.0%	11.0%	7.0%	2.0%	5.0%	5K	2.0%	8.0%	3.0%	2.5%
No. 3 C.W. Red Spring	No Limit	15.0%	No Limit Providing Broken Tolerances Not Exceeded	13.0%	10.0%	10.0%	10K	5.0%	25.0%	8.0%	10.0%
Canada Western Feed	No Limit	50.0%		No Limit	No Limit	No Limit	2.0%	No Limit	No Limit	No Limit	No Limit
Final Grade Name	No. 3 C.W. Red Spring	Over 50.0% grade Sample Broken Grain		Canada Western Feed	Canada Western Feed	Canada Western Feed	Over 2.0% grade Wheat, Sample C.W. Account Stained Kernels	Canada Western Feed	Canada Western Feed	Canada Western Feed	Canada Western Feed

*Degermed: Tolerances apply to kernels not classed as sprouted.

**Grass Green Kernels: Tolerances are given as a general guide and may be increased or reduced in the judgment of the inspector after consideration of the overall quality of a sample.

***Insect Damage: Tolerances are not absolute maximums. Inspectors must consider the degree of damage in conjunction with the overall quality of the sample.

NOTE: THE LETTER "K" IN THESE TABLES REFERS TO KERNEL SIZE PIECES IN 500 GRAMS.

RED SPRING WHEAT - EXPORT GRADE DETERMINANTS

Grade Name	Commercial Cleanliness				
	Broken Grain Thru 5 △	Material through 4.5 R.H. and Roughage			
		SSDS	RHGE	ATT	TOT
No. 1 C.W. Red Spring	0.30%	0.05%	0.05%	0.10%	0.10%
No. 2 C.W. Red Spring	0.30%	0.05%	0.05%	0.10%	0.10%
No. 3 C.W. Red Spring	0.30%	0.05%	0.05%	0.10%	0.10%
Canada Western Feed	0.50%	0.05%	0.10%	0.10%	0.10%

Grade Name	Total Foreign Material											
	Seeds and Wild Oats											
	LSDS	SSDS	W.O.	TOT	RHGE	ATT	Stones	Total Mineral Matter	Ergot	Sclero-tinia	Other Cereal Grains	Total Foreign Material
No. 1 C.W. Red Spring	0.20%	0.05%	0.05%	0.20%	0.05%	0.10%	0.03%	0.06%	0.01%	0.01%	0.40%	0.40%
No. 2 C.W. Red Spring	0.20%	0.05%	0.05%	0.20%	0.05%	0.10%	0.03%	0.10%	0.02%	0.02%	0.75%	0.75%
No. 3 C.W. Red Spring	0.20%	0.05%	0.05%	0.20%	0.05%	0.10%	0.06%	0.10%	0.04%	0.04%	1.25%	1.25%
Canada Western Feed	0.50%	0.05%	0.10%	0.50%	0.10%	0.10%	0.10%	0.25%	0.10%	0.10%	5.0%	5.0%

Grade Name	Wheats of Other Classes		Minimum Hard Vitreous Kernels	Sprouted		Heated and Binburnt	Shrunken and Broken		
	Contrasting Classes	Total Including Cont. Classes		Severe	Total Including Severe Sprouted		Shrunken	Broken	Total
No. 1 C.W. Red Spring	0.30%	1.5%	65.0%	0.1%	0.5%	0.05% including 1 binburnt kernel per 1000 g	6.0%	5.0%	7.0%
No. 2 C.W. Red Spring	1.5%	3.0%	35.0%		1.5%	0.4% including 4 binburnt kernels per 1000 g	10.0%	8.0%	11.0%
No. 3 C.W. Red Spring	2.5%	5.0%	No Minimum		5.0%	1.0% including 6 binburnt kernels per 1000 g	No Limit	13.0%	No Limit providing broken tolerances not exceeded
Canada Western Feed	No Limit (10.0% Amber Durum only)		No Minimum	No Limit		2.5% including 2.5% binburnt kernels	No Limit	50.0%	

90.10.1

Appendix B

A Repository of Software-Separated Kernel Images

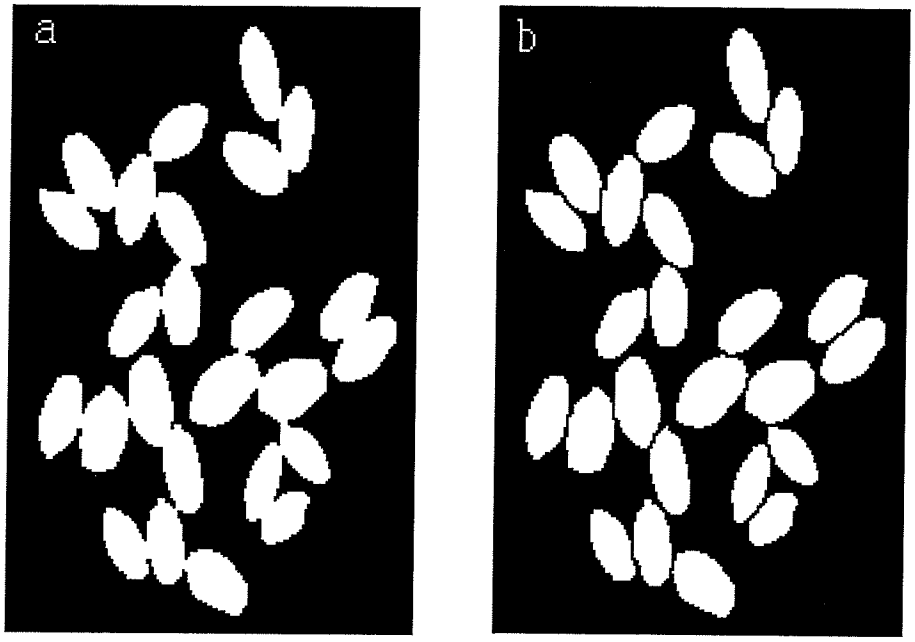

Fig. B1: Example of (a) touching and (b) separated kernels of HRS wheat

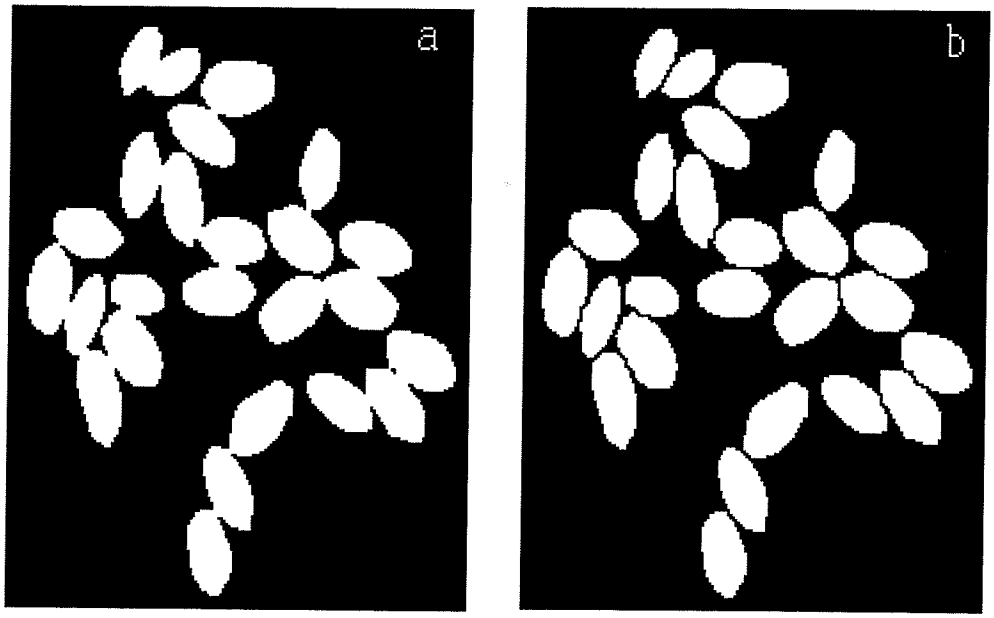

Fig. B2: Example of (a) touching and (b) separated kernels of HRS wheat

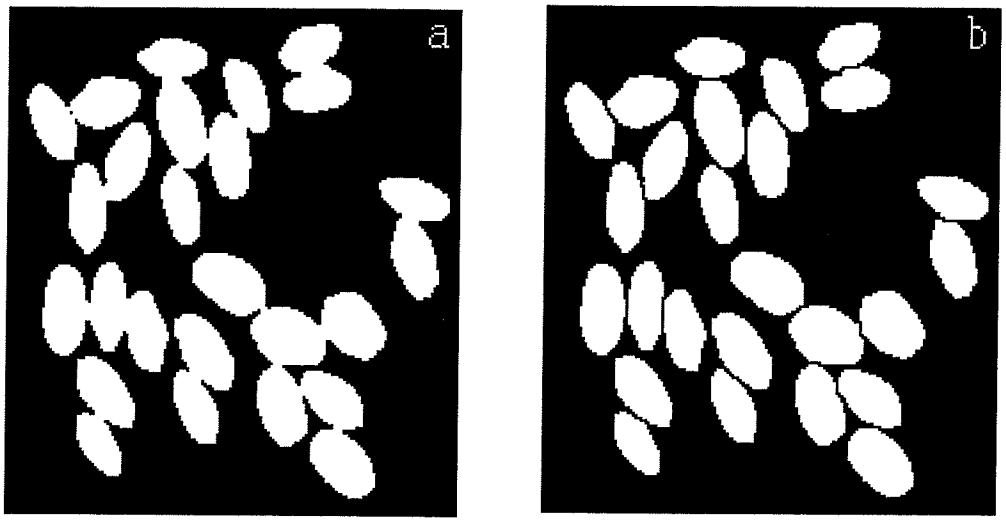

Fig. B3: Example of (a) touching and (b) separated kernels of HRS wheat

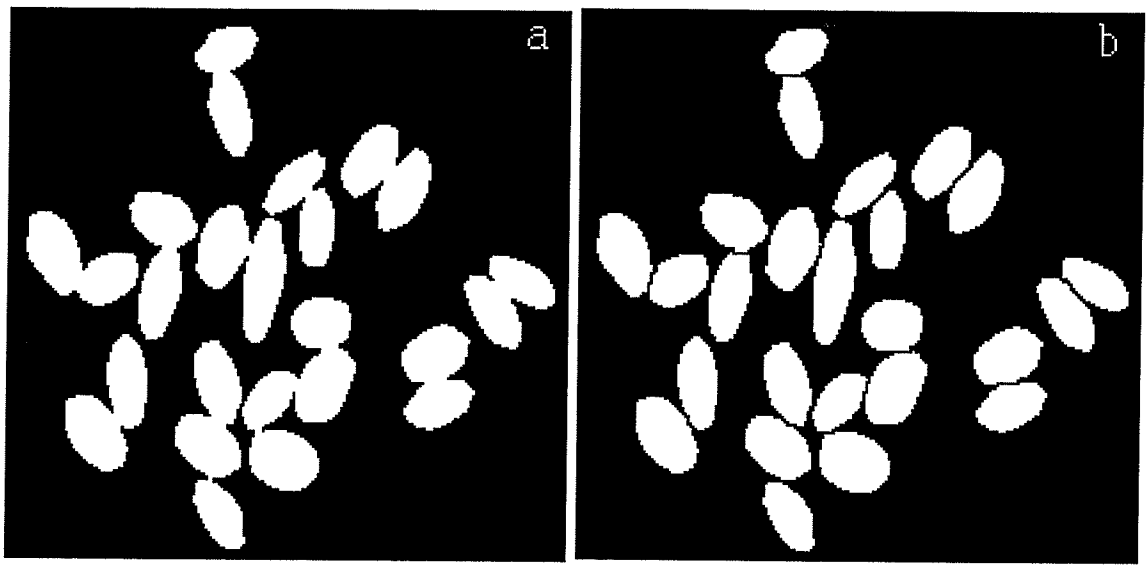

Fig. B4: Example of (a) touching and (b) separated kernels of HRS wheat

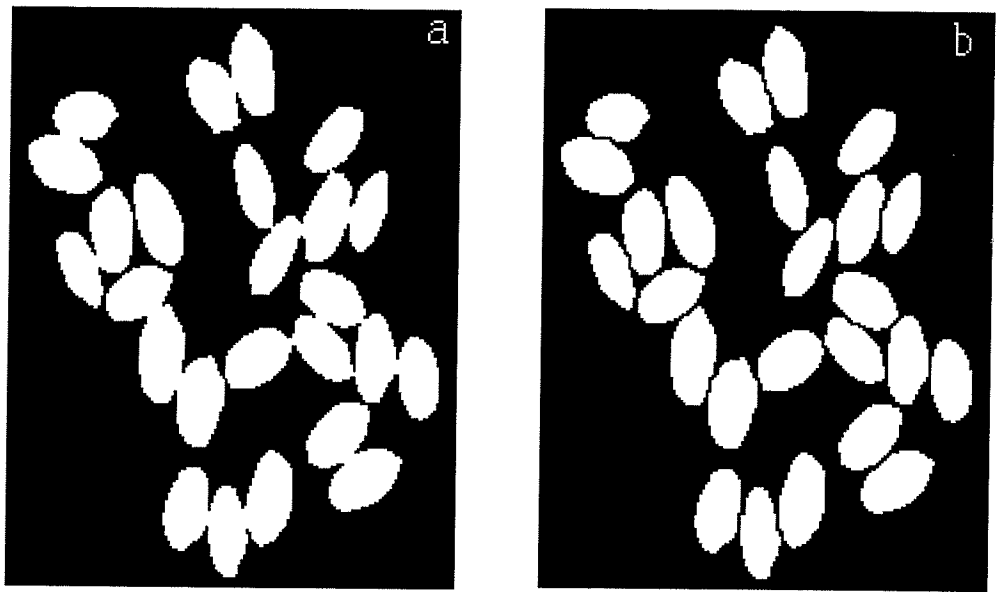

Fig. B5: Example of (a) touching and (b) separated kernels of HRS wheat

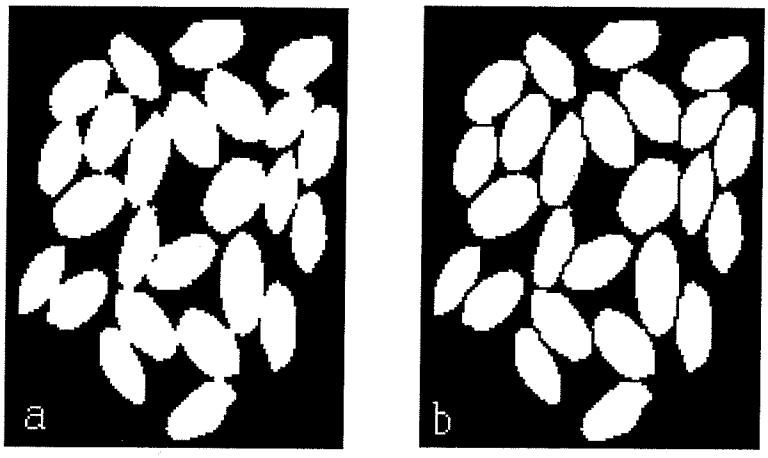

Fig. B6: Example of (a) touching and (b) separated kernels of HRS wheat

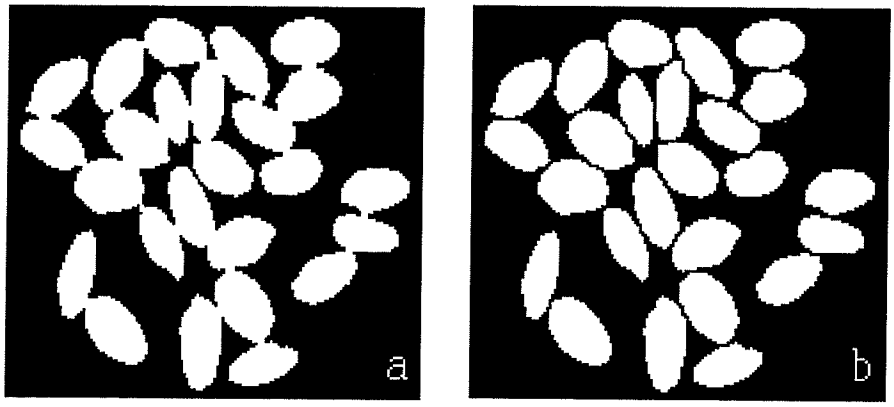

Fig. B7: Example of (a) touching and (b) separated kernels of HRS wheat

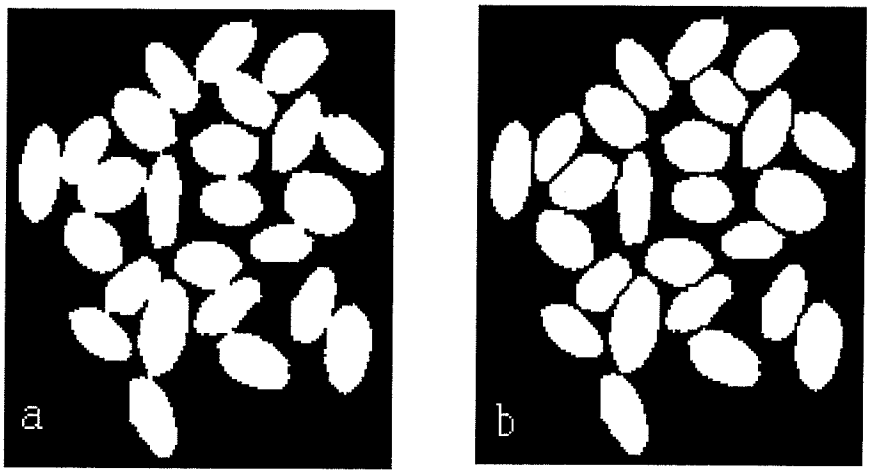

Fig. B8: Example of (a) touching and (b) separated kernels of HRS wheat

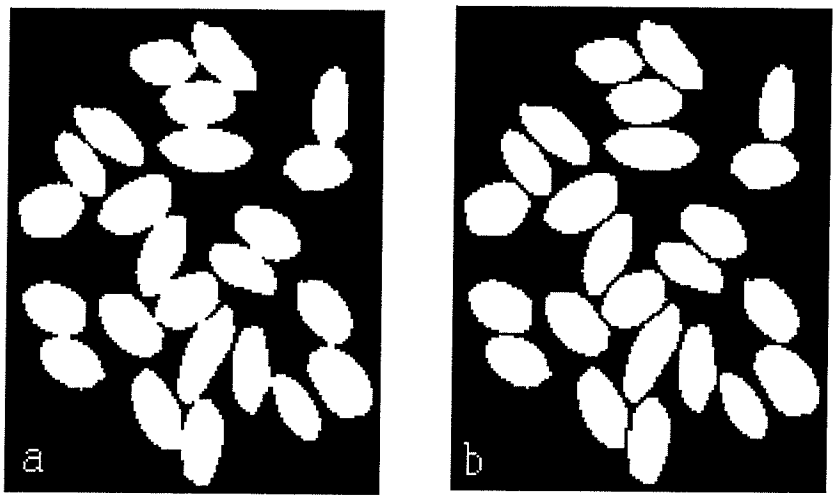

Fig. B9: Example of (a) touching and (b) separated kernels of HRS wheat

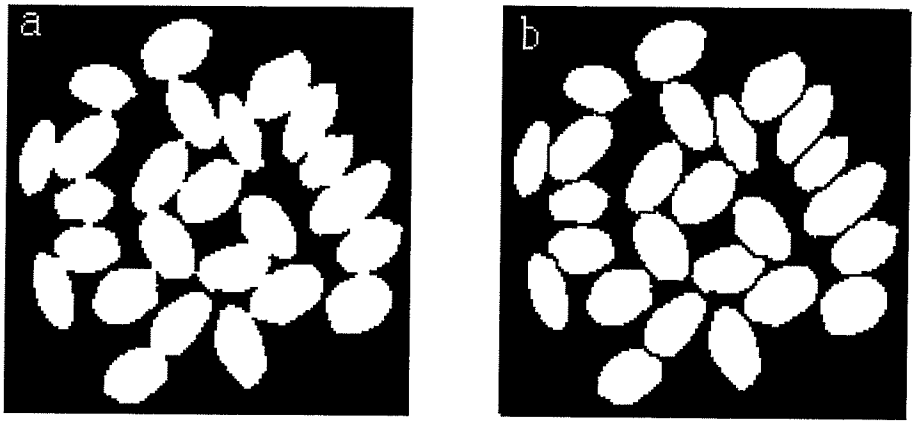

Fig. B10: Example of (a) touching and (b) separated kernels of HRS wheat

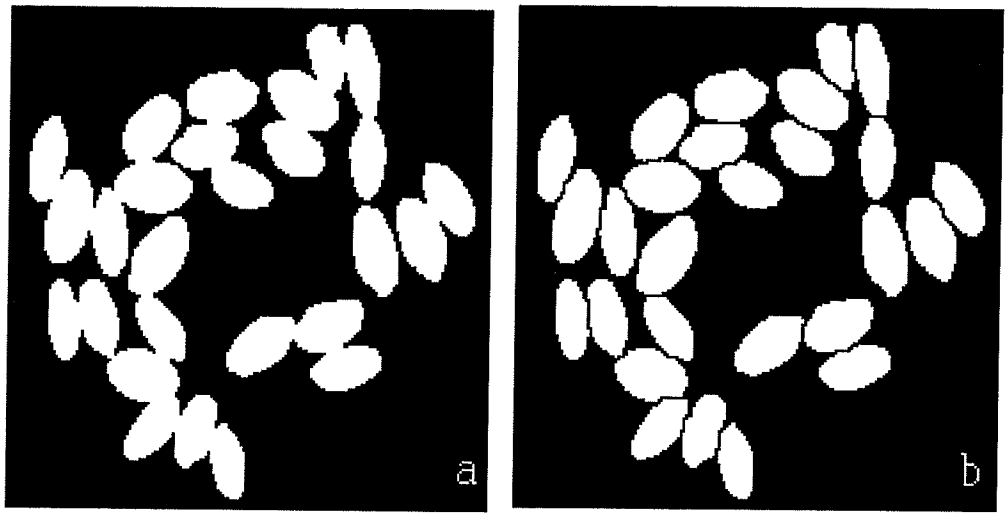

Fig. B11: Example of (a) touching and (b) separated kernels of HRS wheat

Fig. B12: Example of (a) touching and (b) separated kernels of HRS wheat

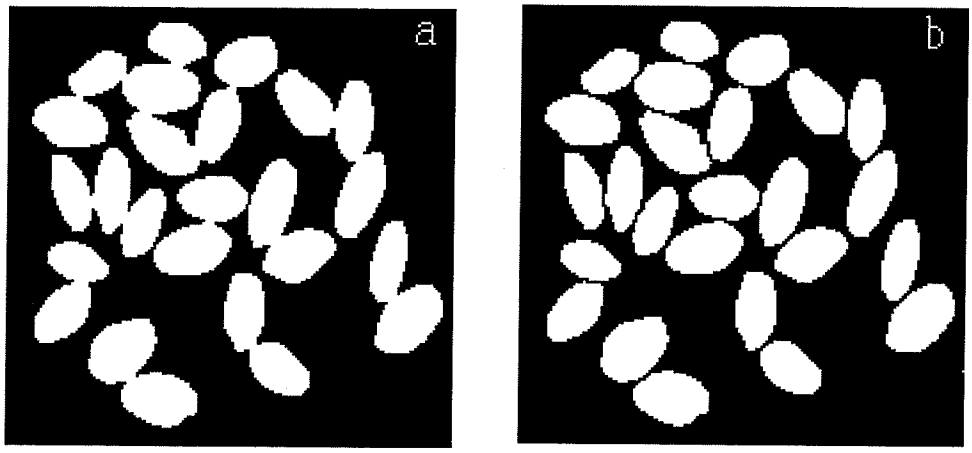

Fig. B13: Example of (a) touching and (b) separated kernels of HRS wheat

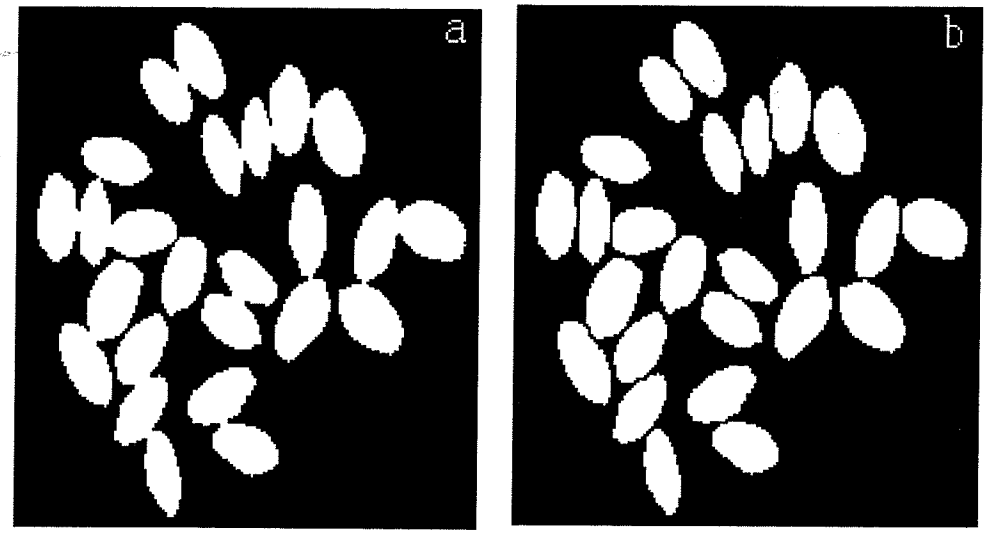

Fig. B14: Example of (a) touching and (b) separated kernels of HRS wheat

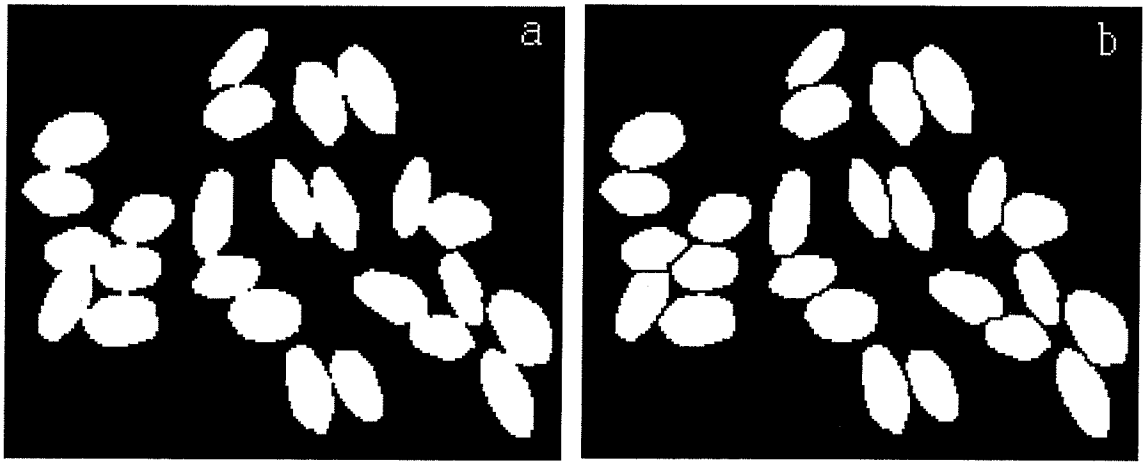

Fig. B15: Example of (a) touching and (b) separated kernels of HRS wheat

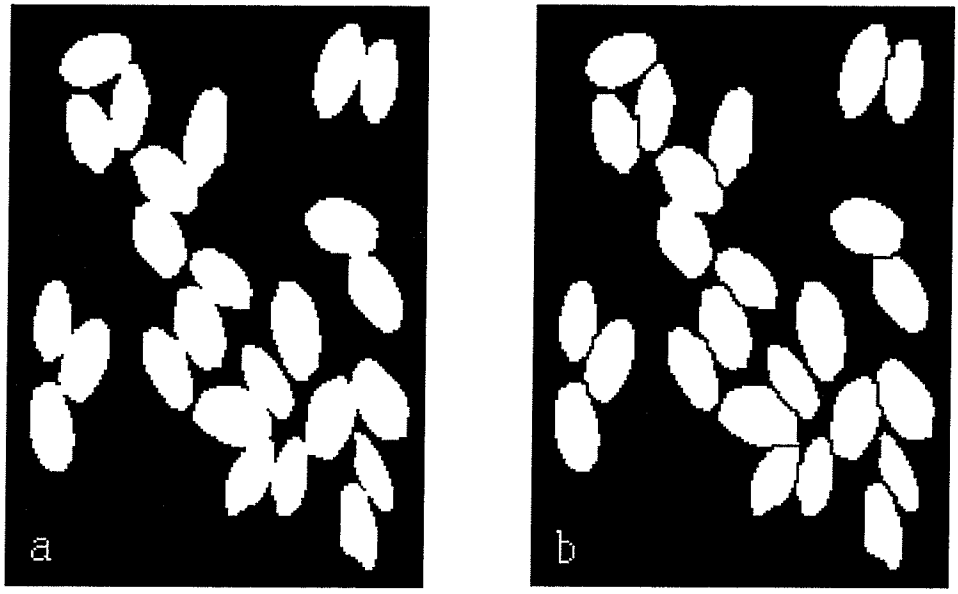

Fig. B16: Example of (a) touching and (b) separated kernels of HRS wheat

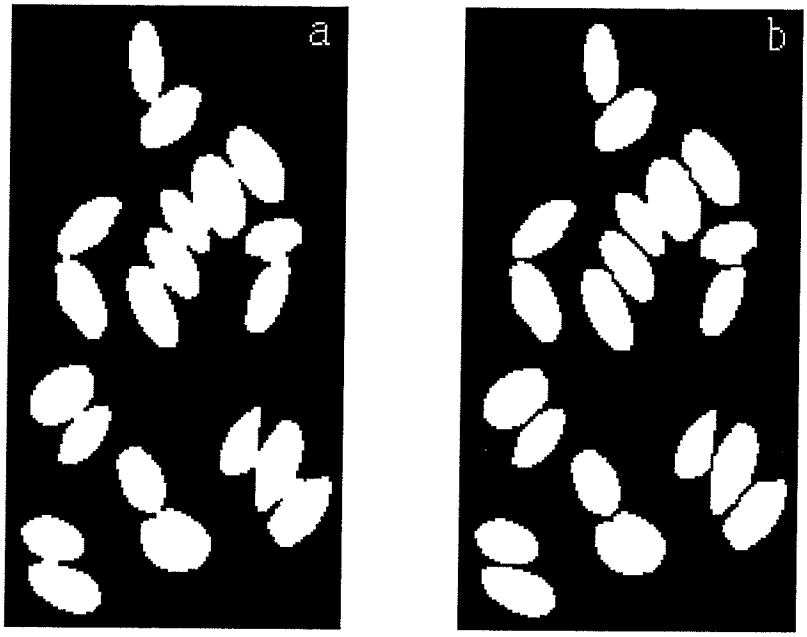

Fig. B17: Example of (a) touching and (b) separated kernels of HRS wheat

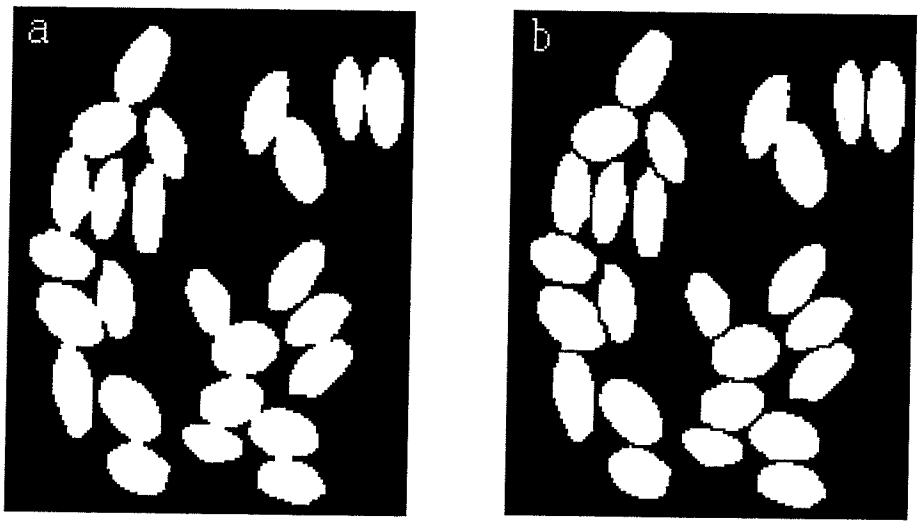

Fig. B18: Example of (a) touching and (b) separated kernels of HRS wheat

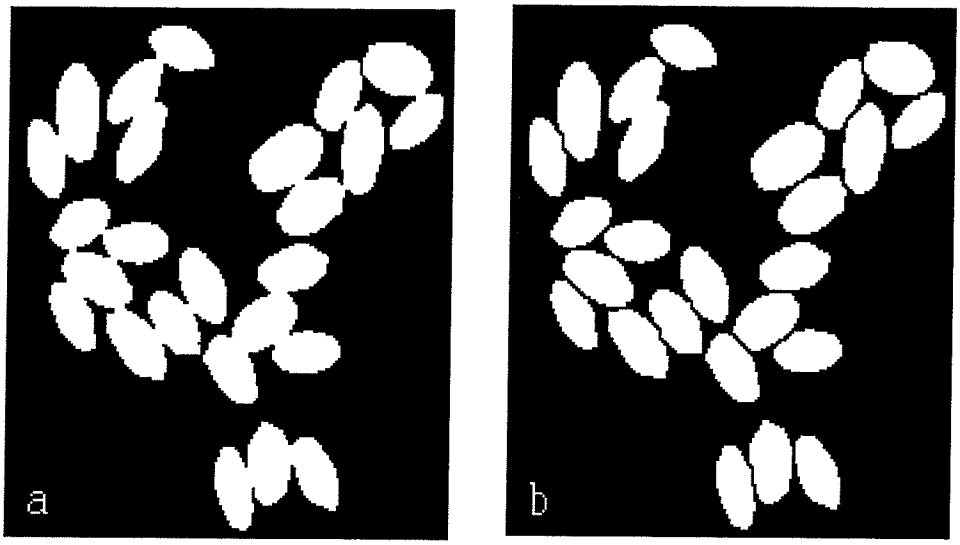

Fig. B19: Example of (a) touching and (b) separated kernels of HRS wheat

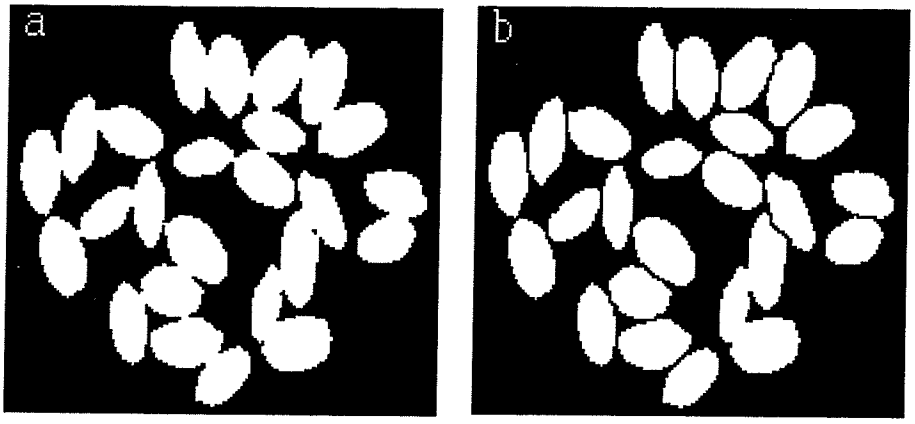

Fig. B20: Example of (a) touching and (b) separated kernels of HRS wheat

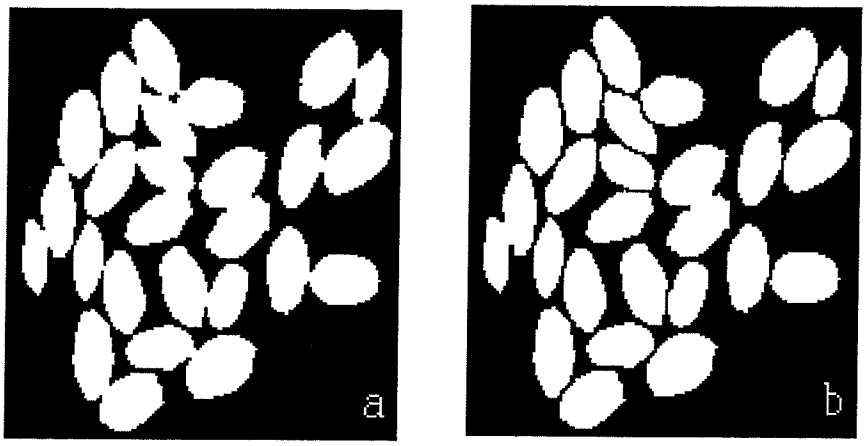

Fig B21: Example of (a) touching and (b) separated kernels of HRS wheat

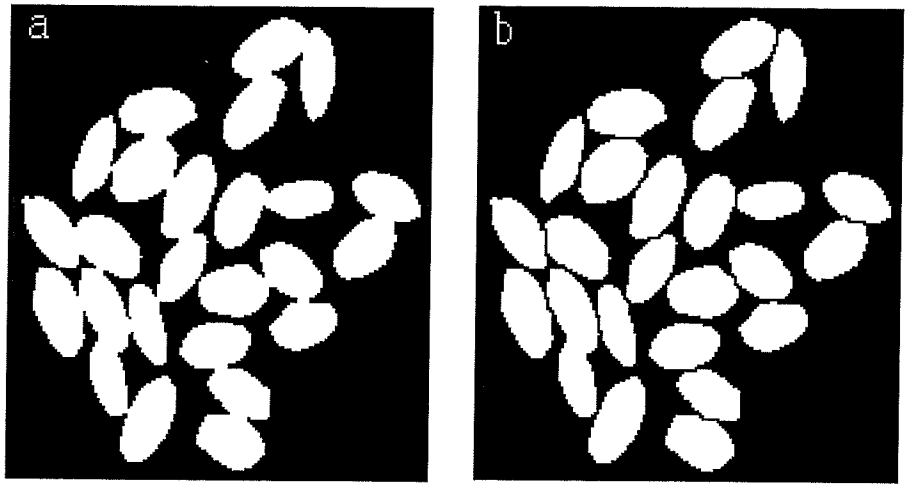

Fig. B22: Example of (a) touching and (b) separated kernels of HRS wheat

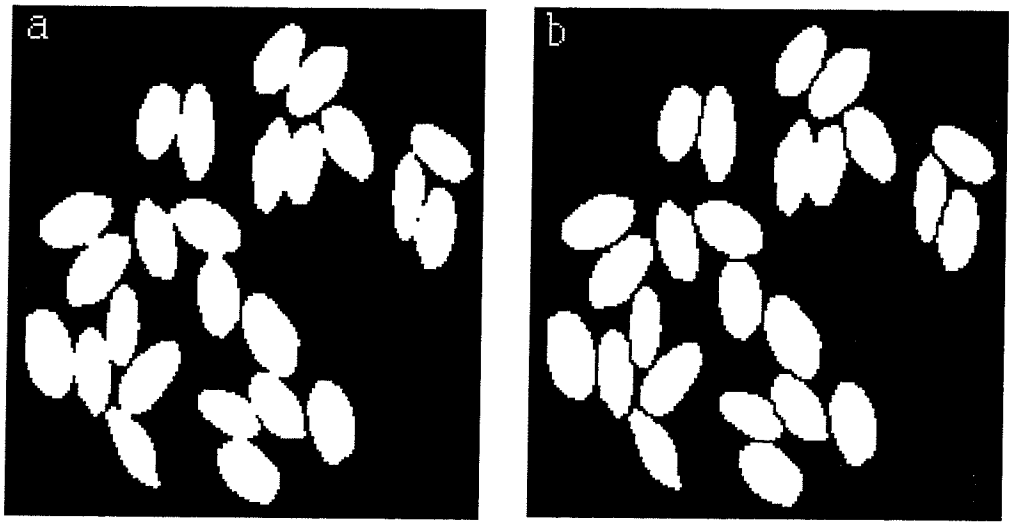

Fig. B23: Example of (a) touching and (b) separated kernels of HRS wheat

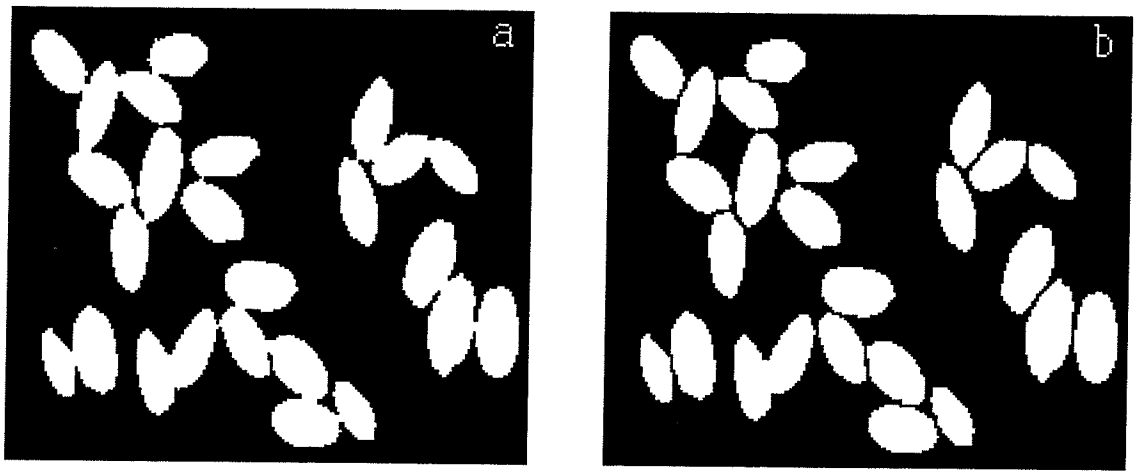

Fig. 24: Example of (a) touching and (b) separated kernels of HRS wheat

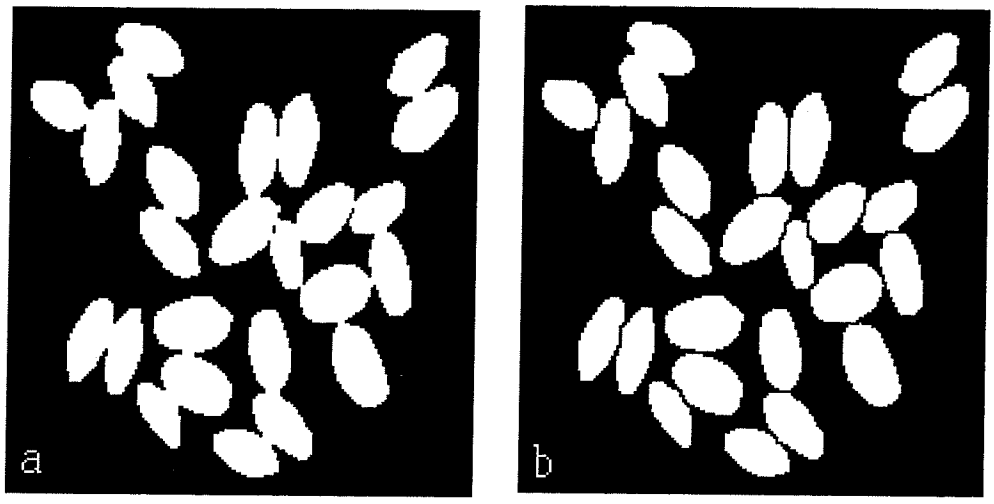

Fig. B25: Example of (a) touching and (b) separated kernels of HRS wheat

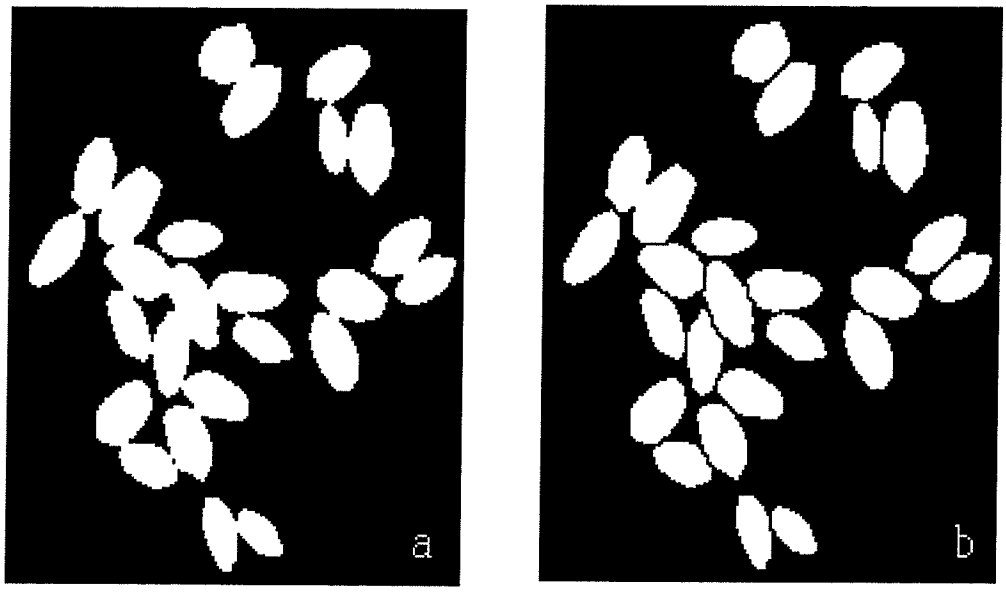

Fig. B26: Example of (a) touching and (b) separated kernels of HRS wheat

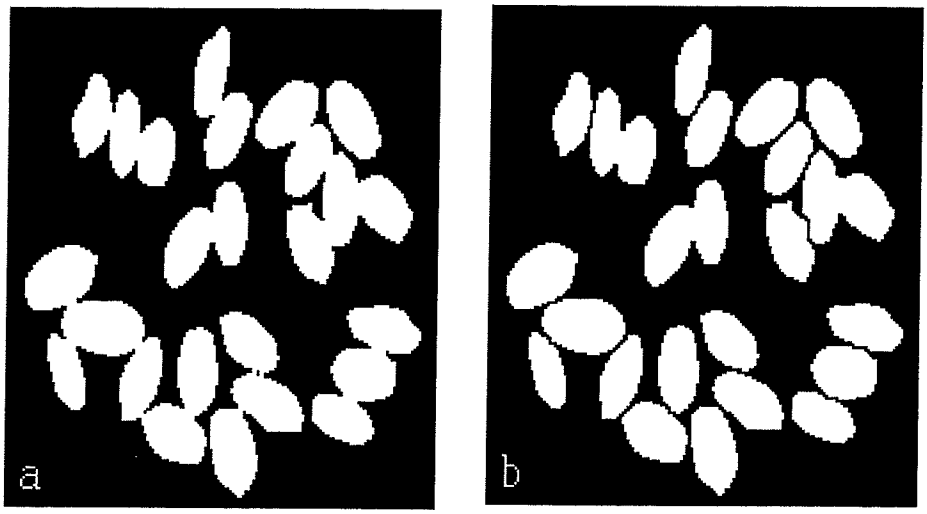

Fig. B27: Example of (a) touching and (b) separated kernels of HRS wheat

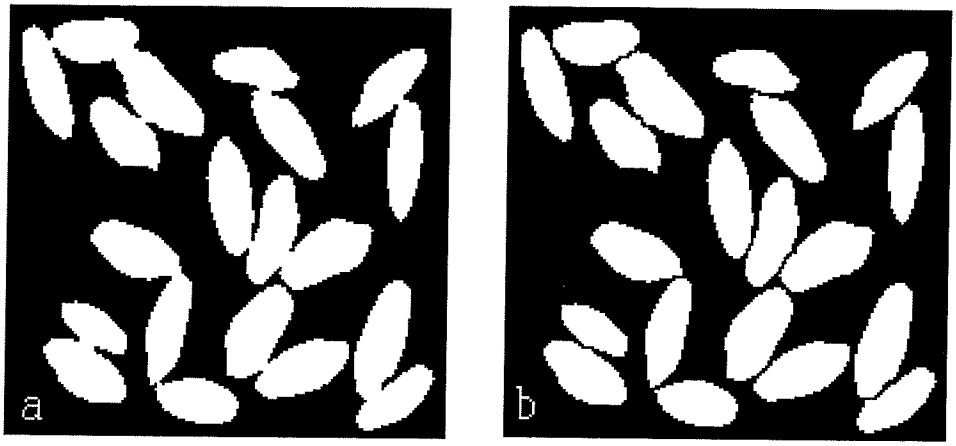

Fig. B28: Example of (a) touching and (b) separated kernels of durum

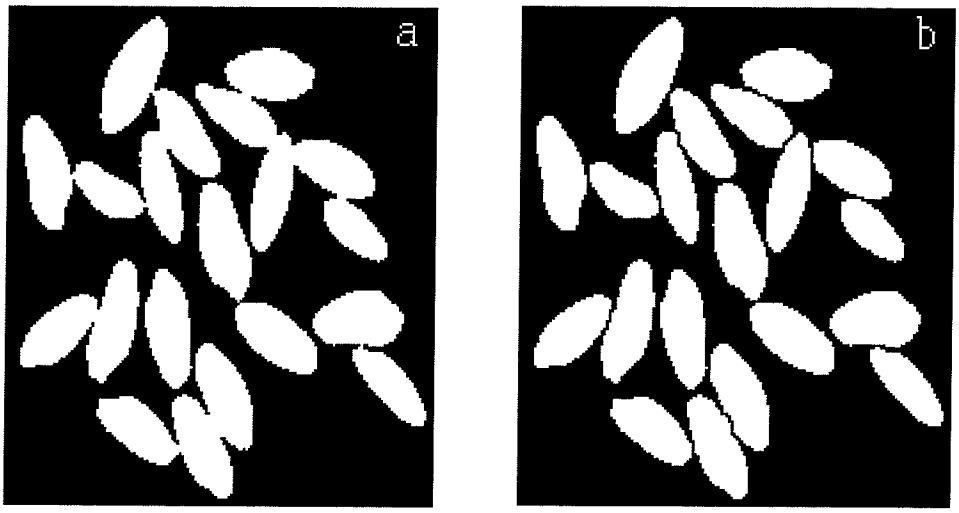

Fig. B29: Example of (a) touching and (b) separated kernels of durum

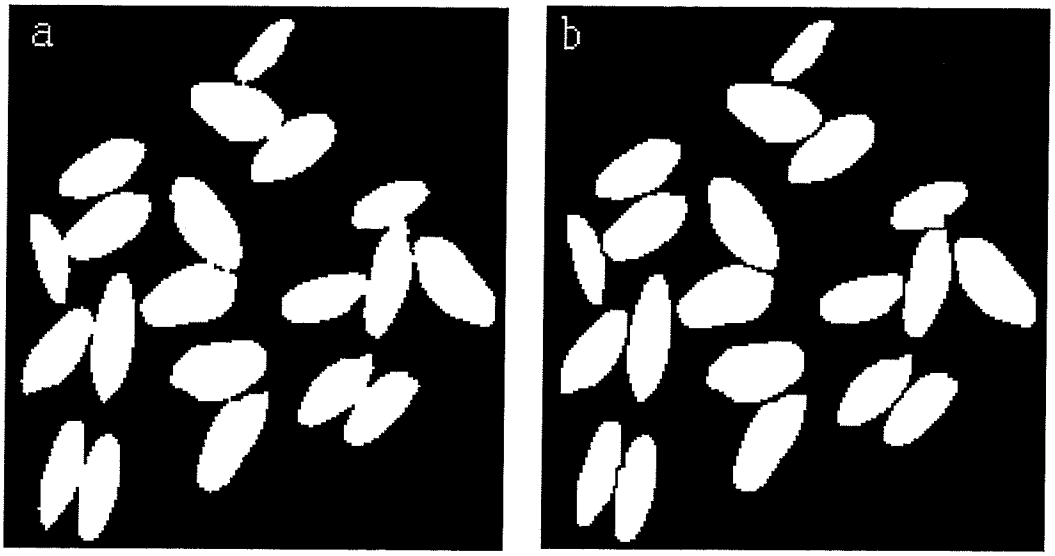

Fig. B30: Example of (a) touching and (b) separated kernels of durum

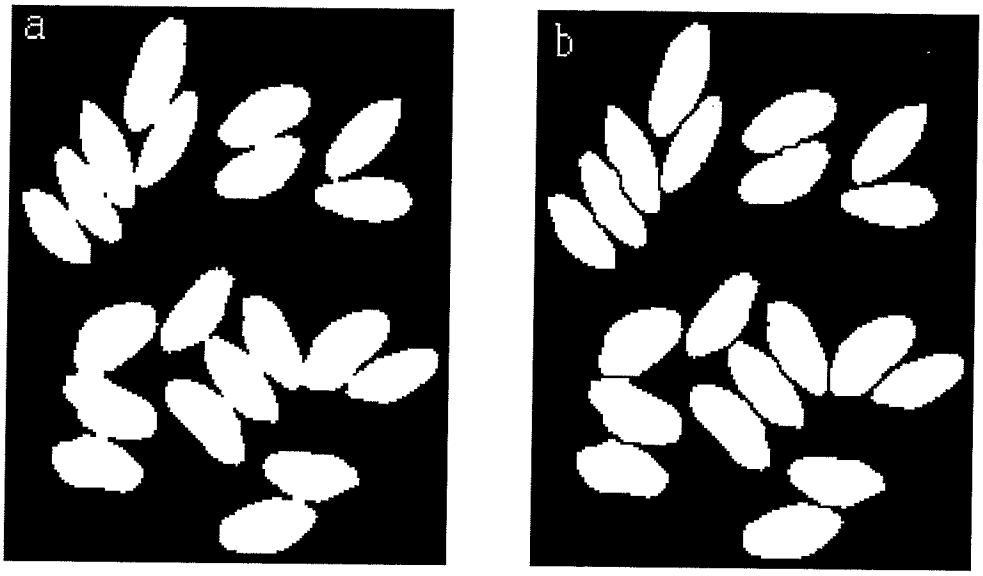

Fig. 31: Example of (a) touching and (b) separated kernels of durum

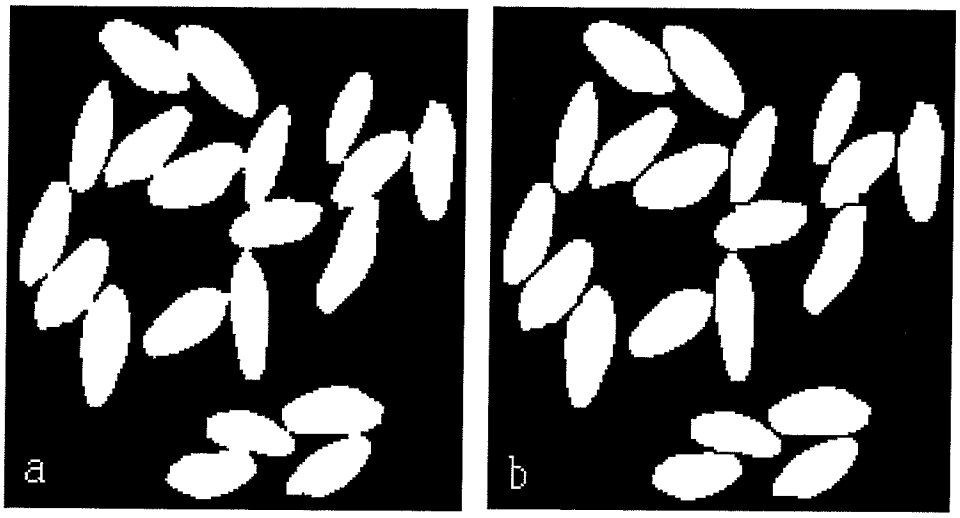

Fig. B32: Example of (a) touching and (b) separated kernels of durum

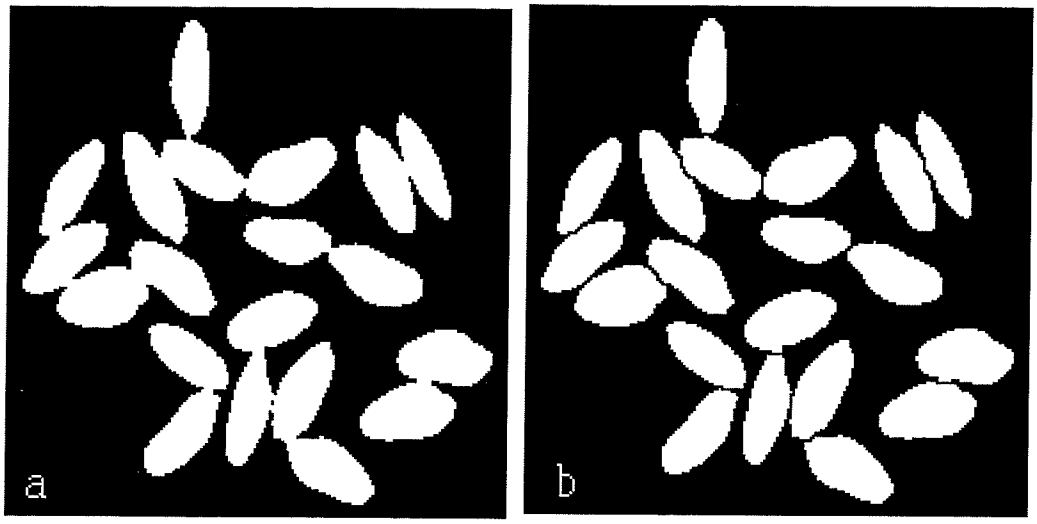

Fig. B33: Example of (a) touching and (b) separated kernels of durum

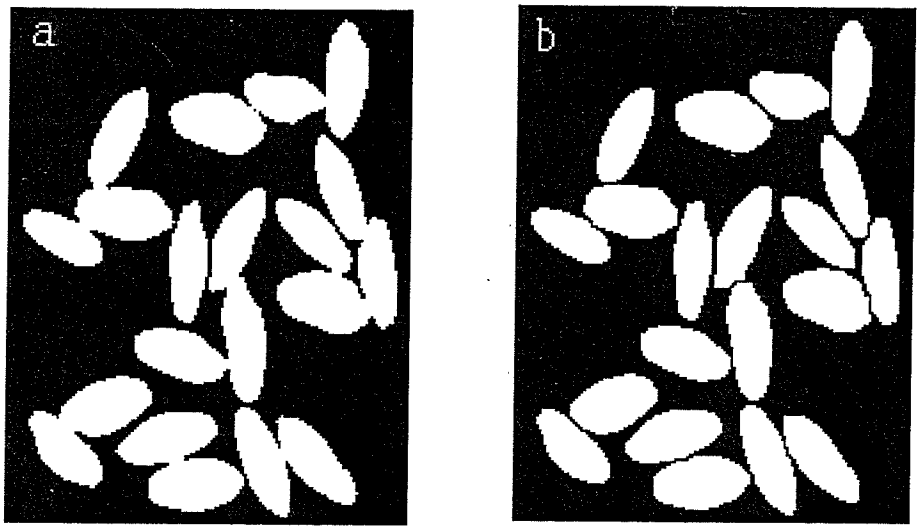

Fig. B34: Example of (a) touching and (b) separated kernels of durum

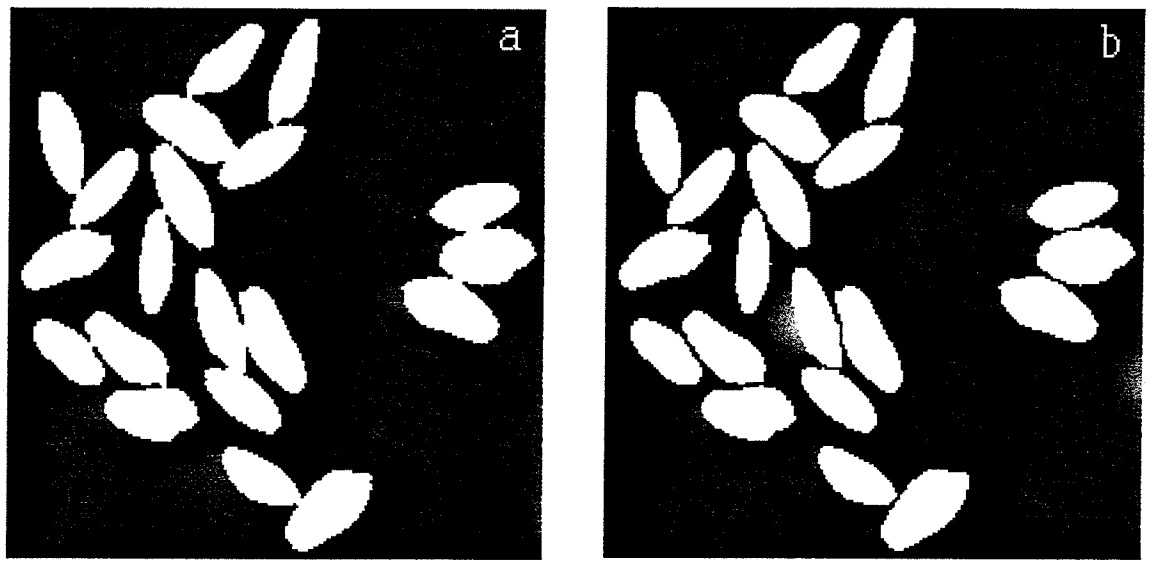

Fig. B35: Example of (a) touching and (b) separated kernels of durum

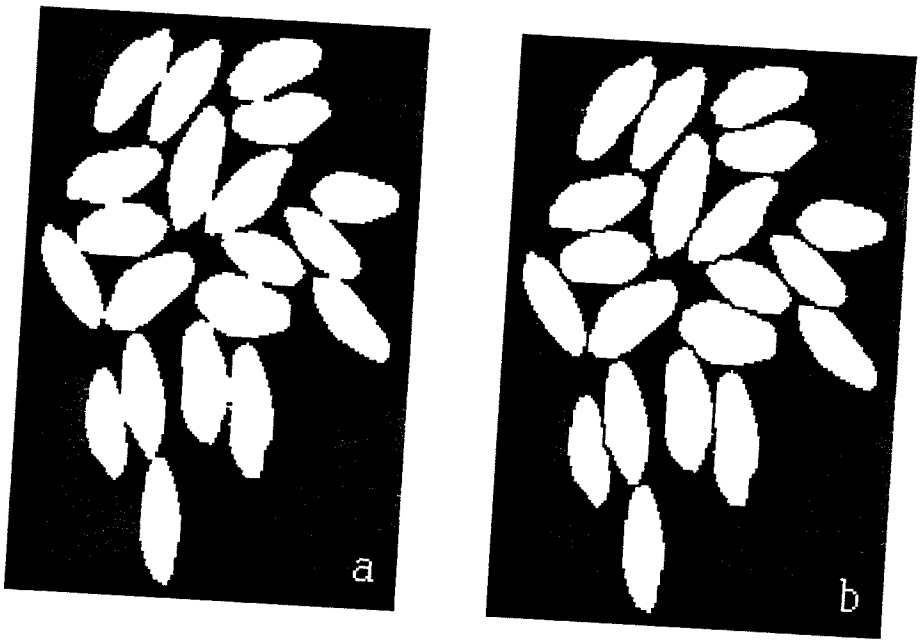

Fig. B36. Example of (a) touching and (b) separated kernels of durum.

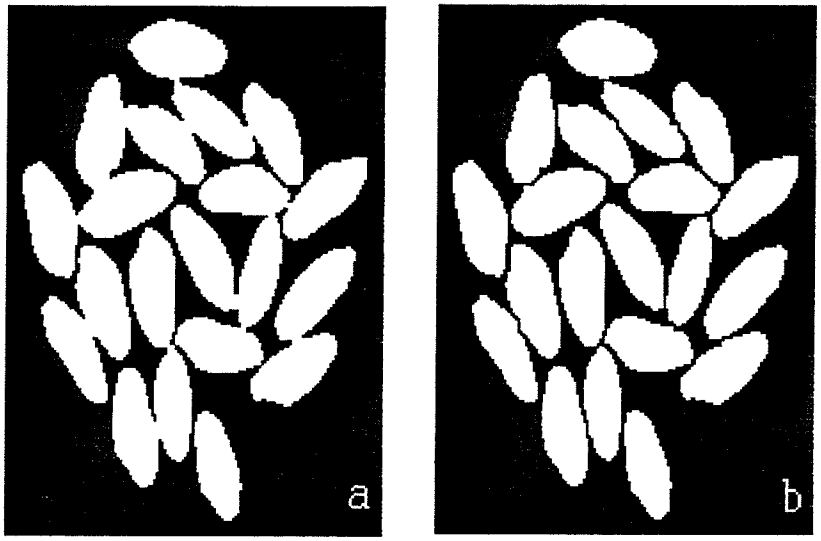

Fig. B37. Example of (a) touching and (b) separated kernels of durum.

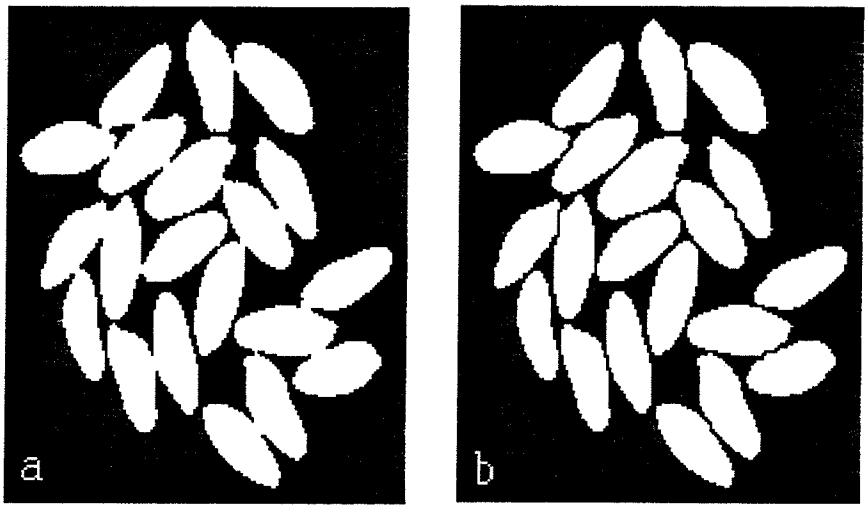

Fig. B38. Example of (a) touching and (b) separated kernels of durum.

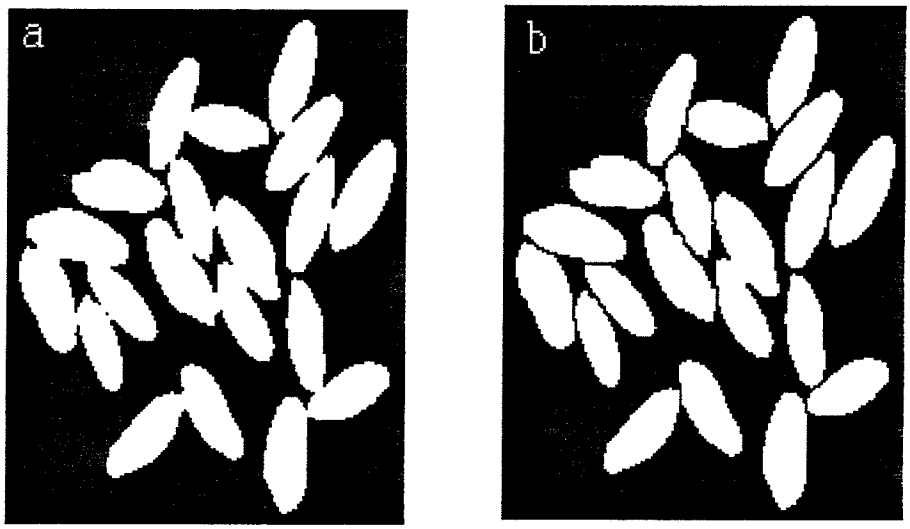

Fig. B39. Example of (a) touching and (b) separated kernels of durum.

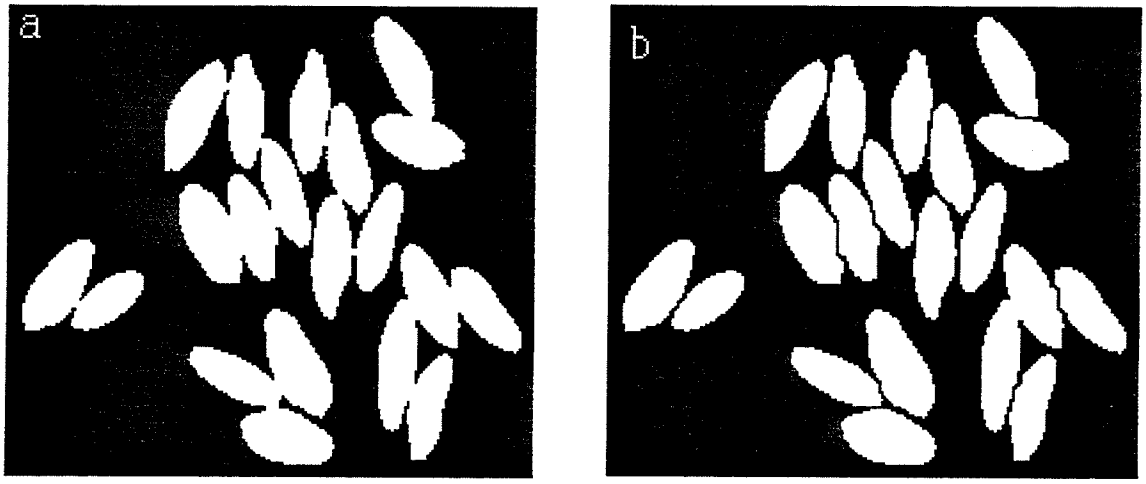

Fig. B-40 Example of (a) touching and (b) separated kernels of durum.

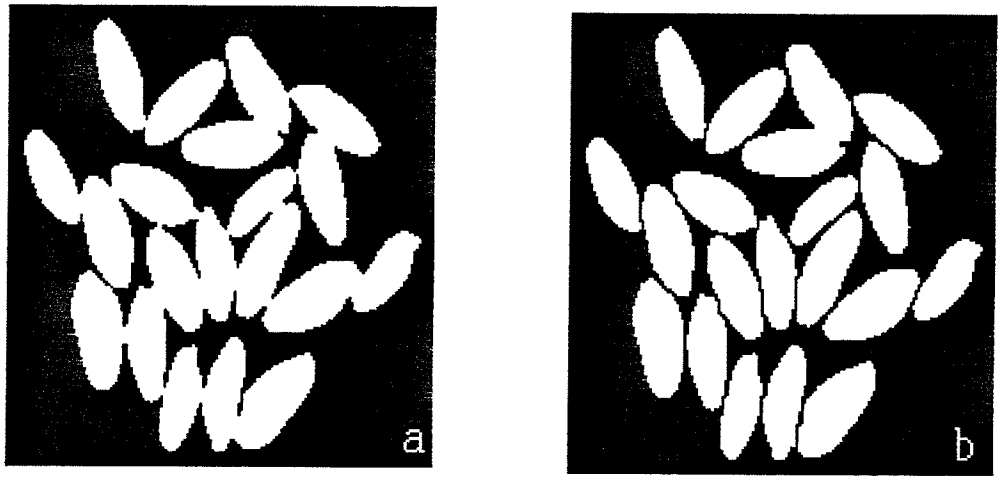

Fig. B-41. Example of (a) touching and (b) separated kernels of durum.

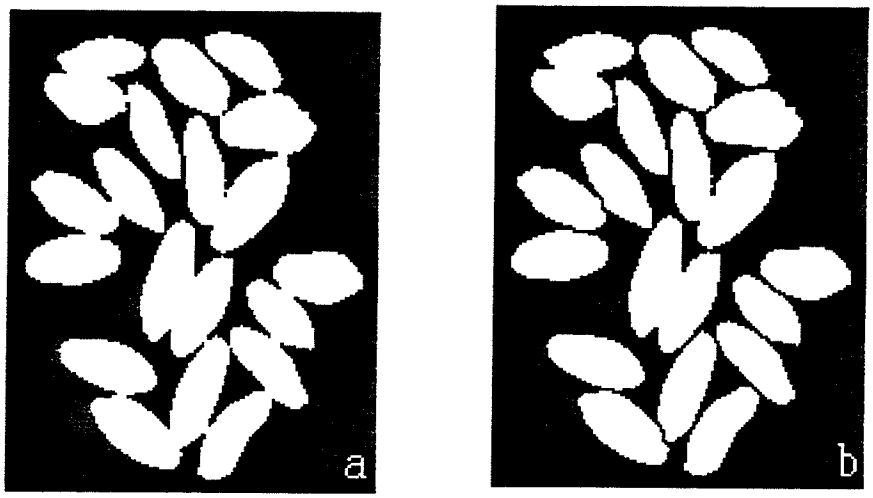

Fig. B-42. Example of (a) touching and (b) separated kernels of durum.

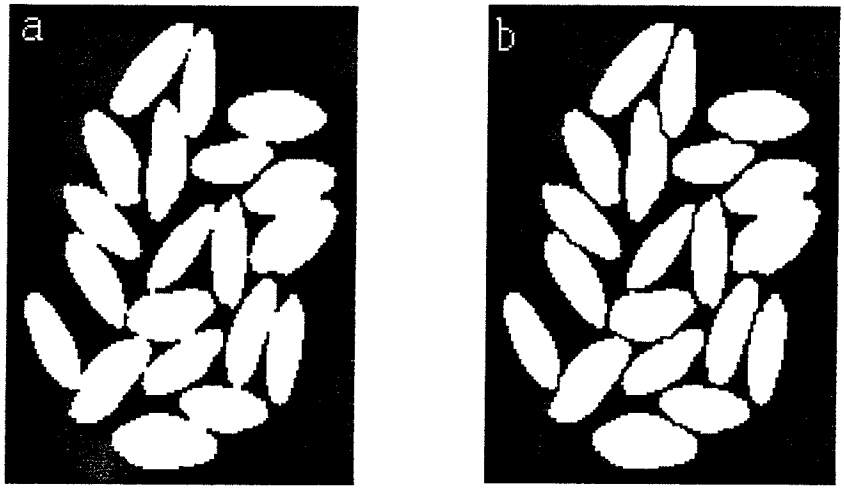

Fig. 43. Example of (a) touching and (b) separated kernels of durum.

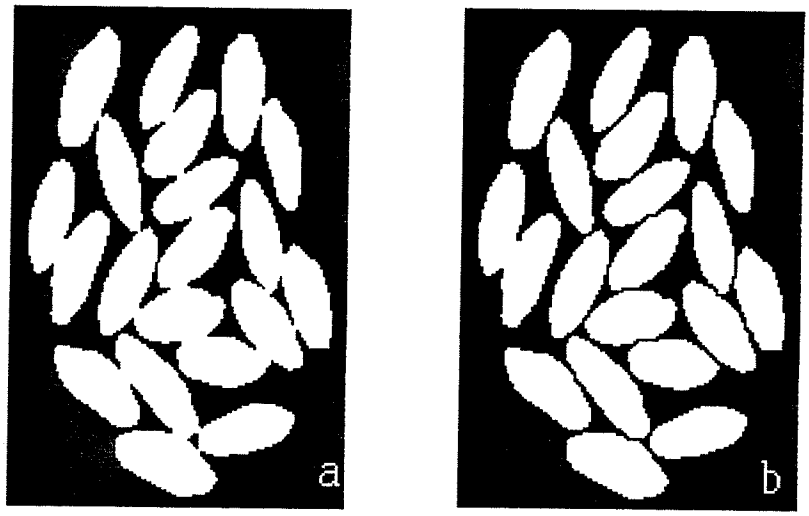

Fig. B44. Example of touching (a) and (b) separated kernels of durum.

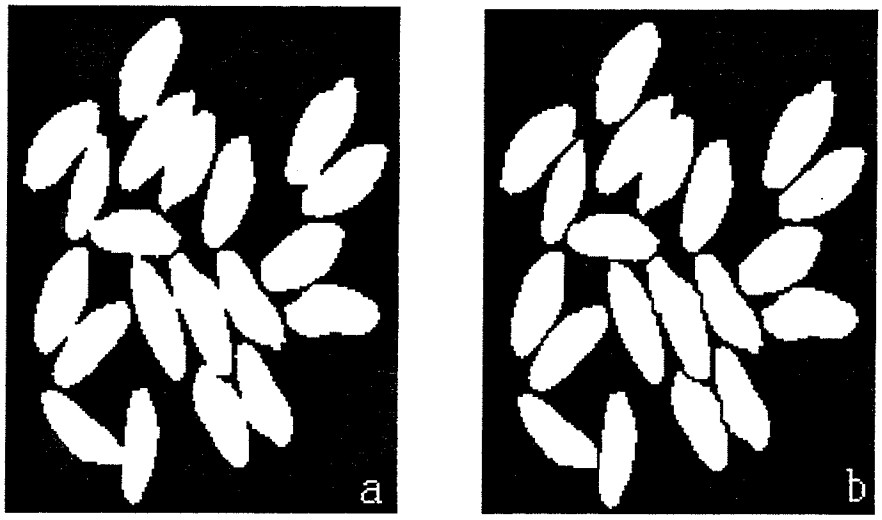

Fig. B45. Example of (a) touching and (b) separated kernels of durum.

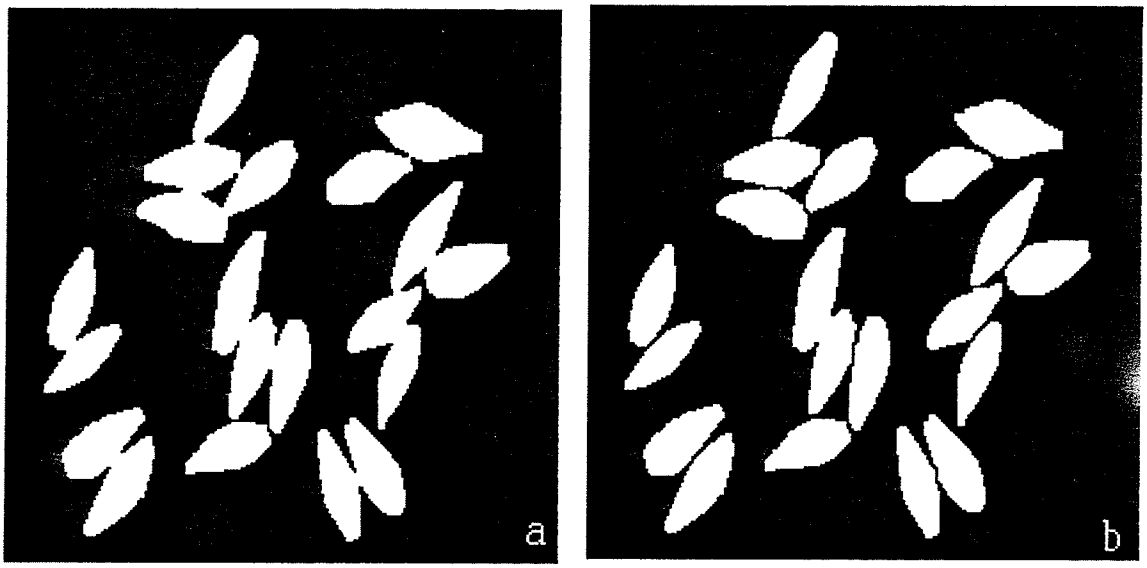

Fig. B46. Example of (a) touching and (b) separated kernels of barley.

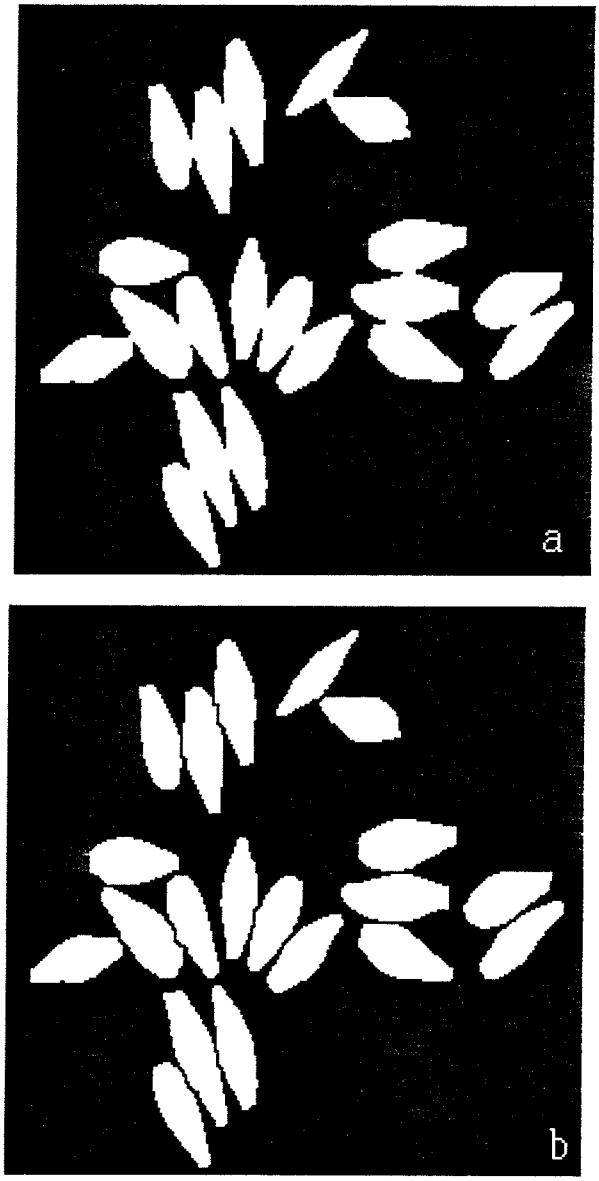

Fig. B47. Example of (a) touching and (b) separated kernels of barley.

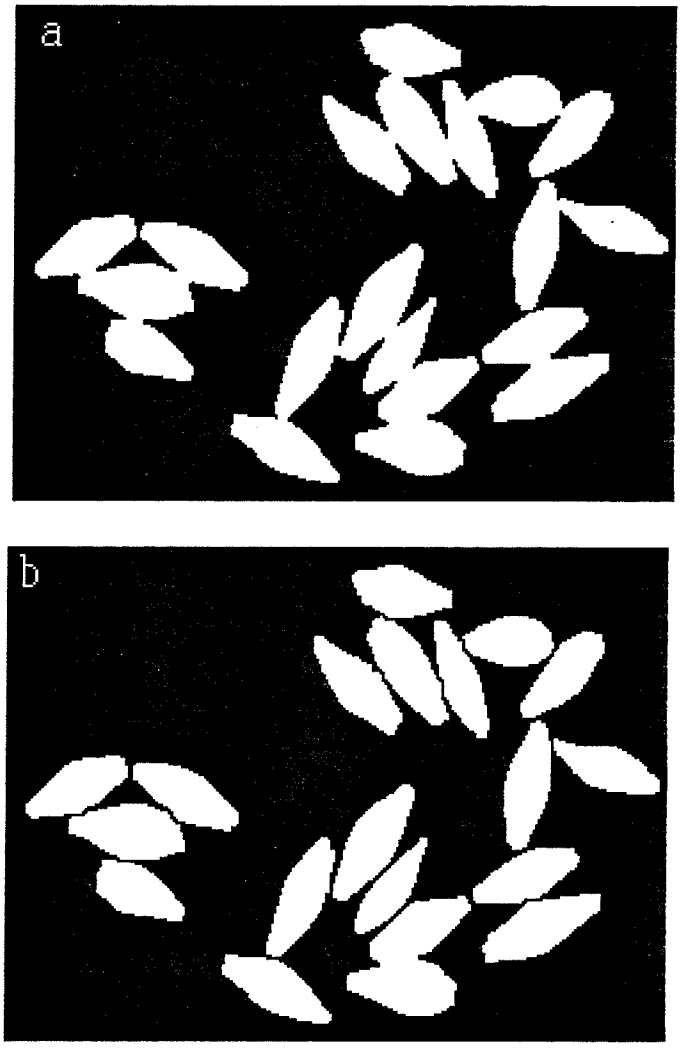

Fig. B48. Example of (a) touching and (b) separated kernels of barley.

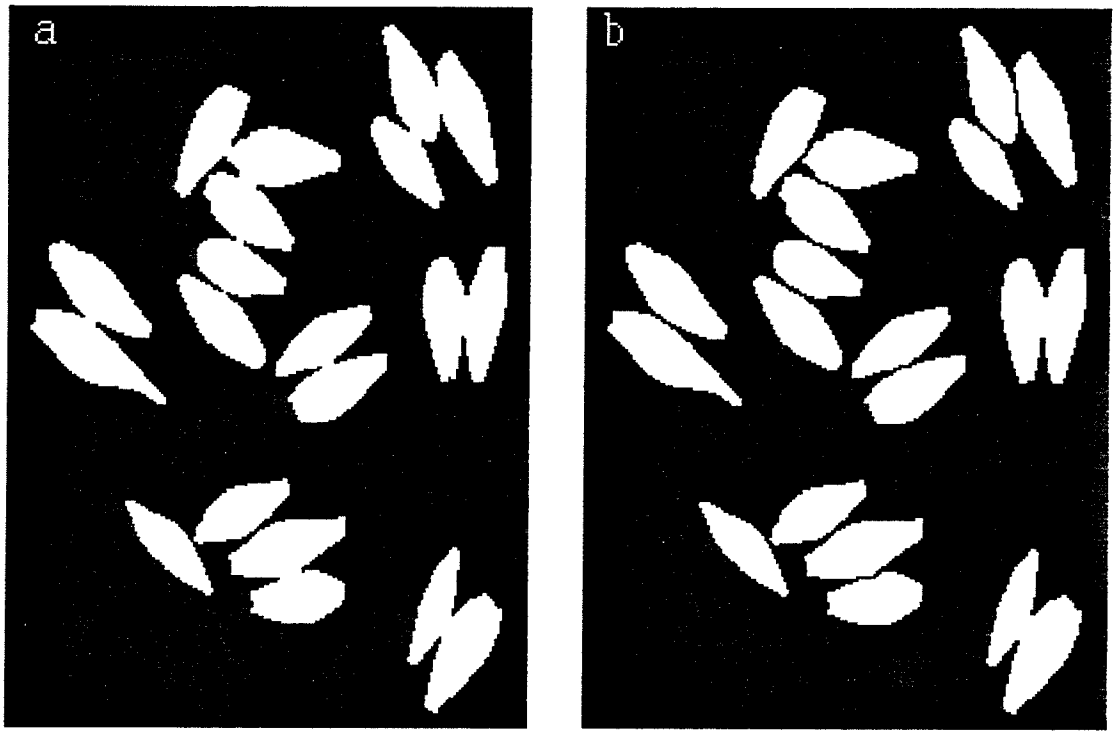

Fig. B49. Example of (a) touching and (b) separated kernels of barley.

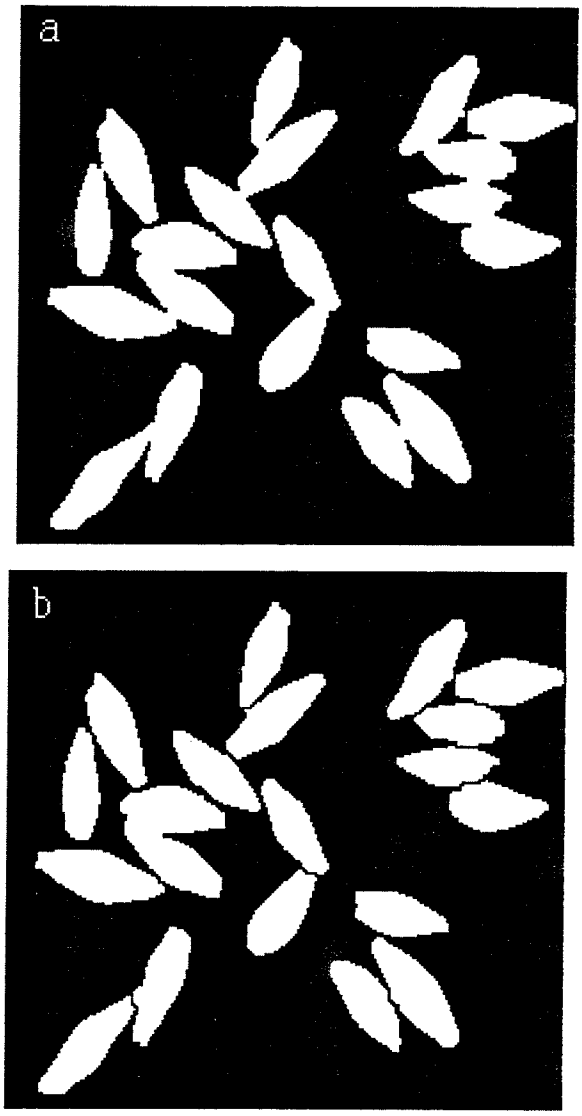

Fig. B50. Example of (a) touching and (b) separated kernels of barley.

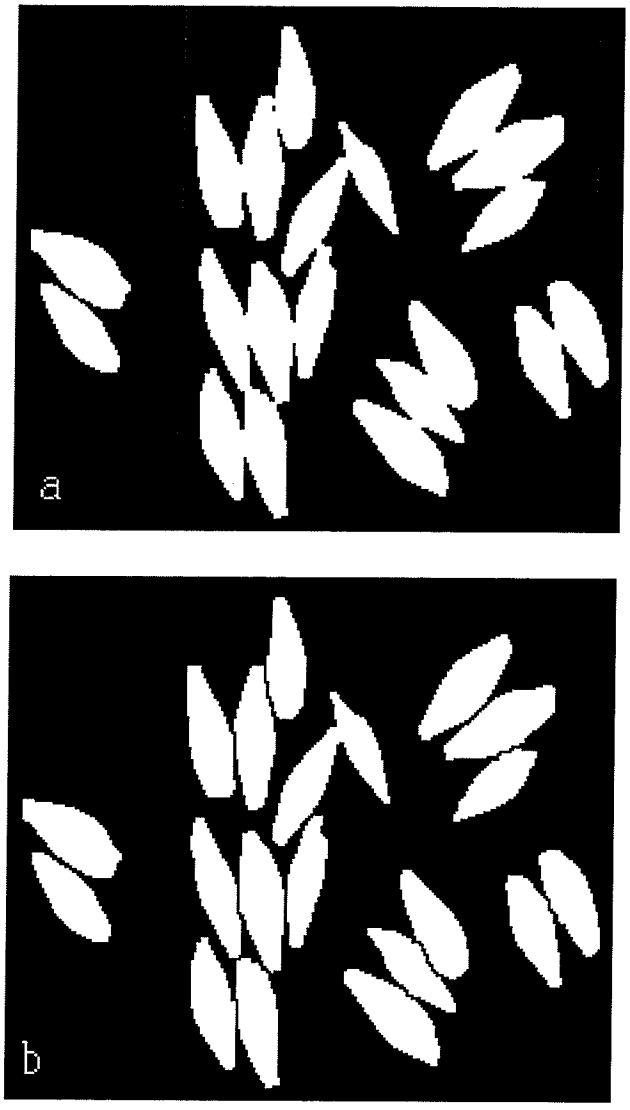

Fig. B51. Example of (a) touching and (b) separated kernels of barley.

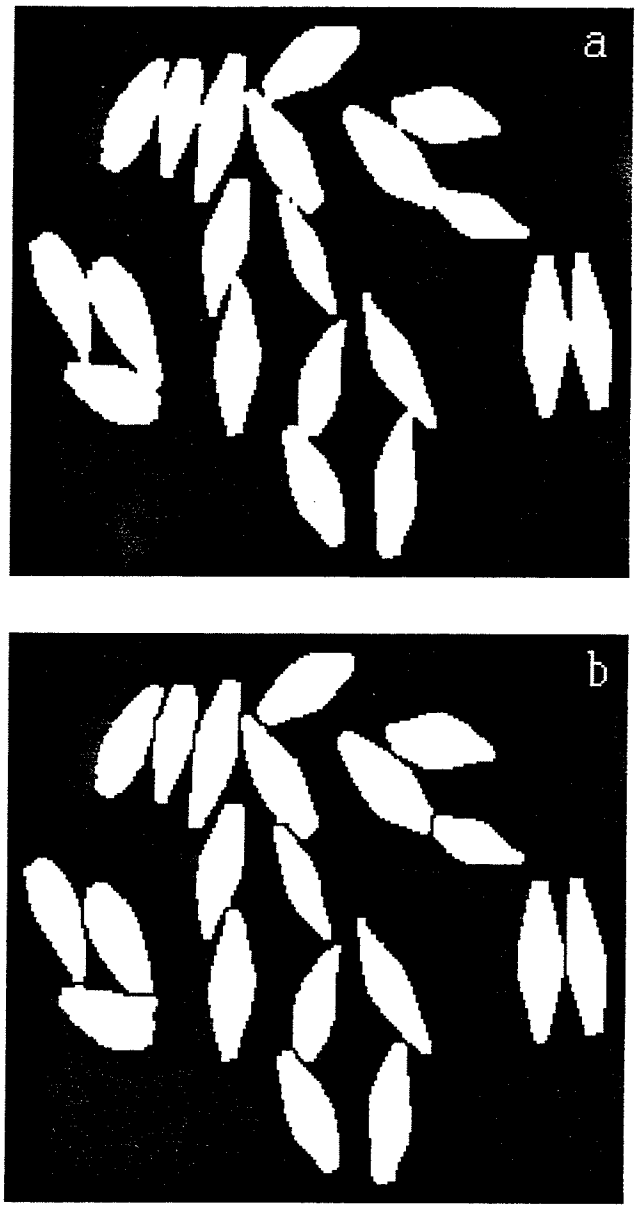

Fig. B52. Example of (a) touching and (b) separated kernels of barley.

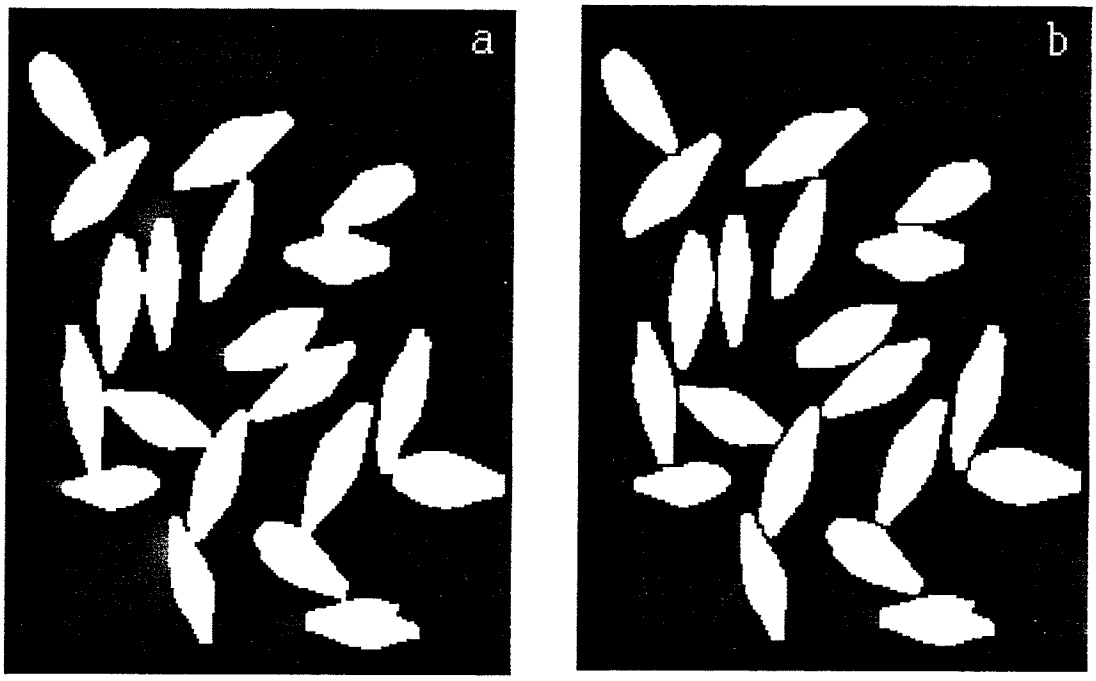

Fig. B53. Example of (a) touching and (b) separated kernels of barley.

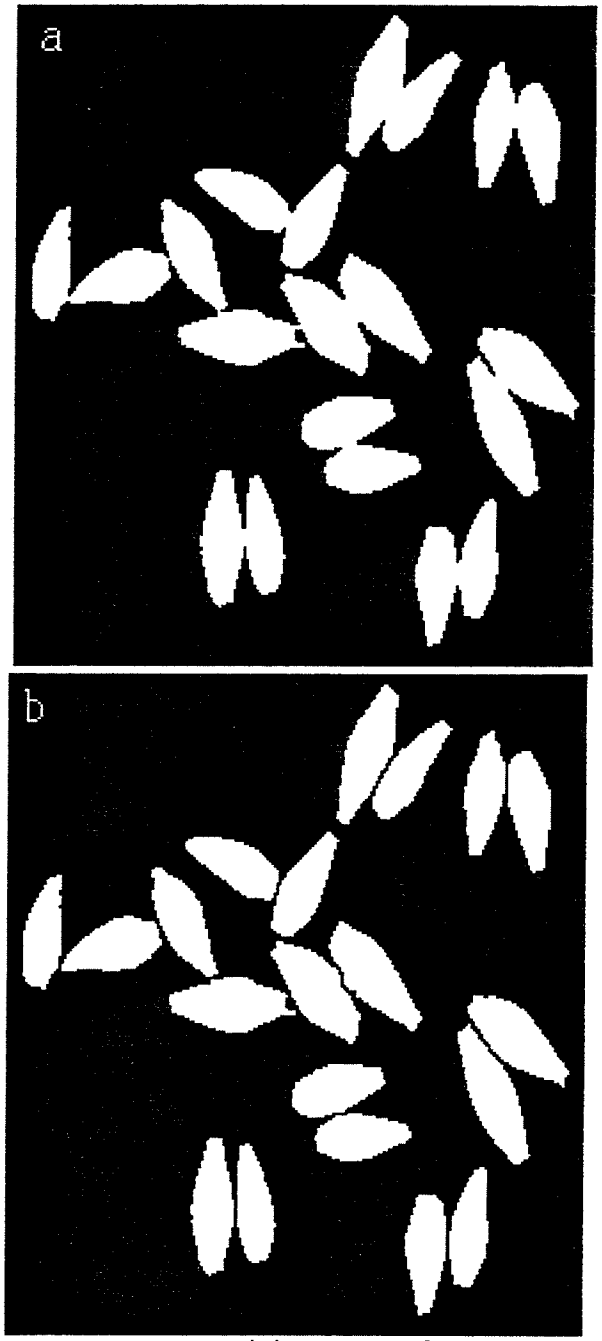

Fig. B54. Example of (a) touching and (b) separated kernels of barley.

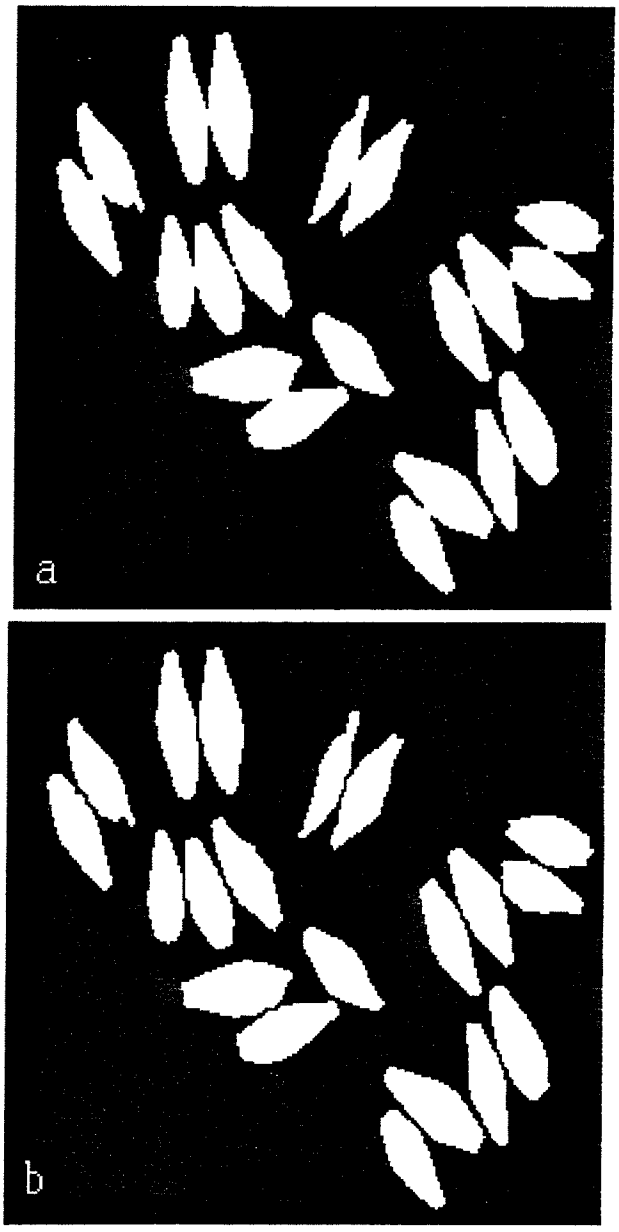

Fig. B55. Example of (a) touching and (b) separated kernels of barley.

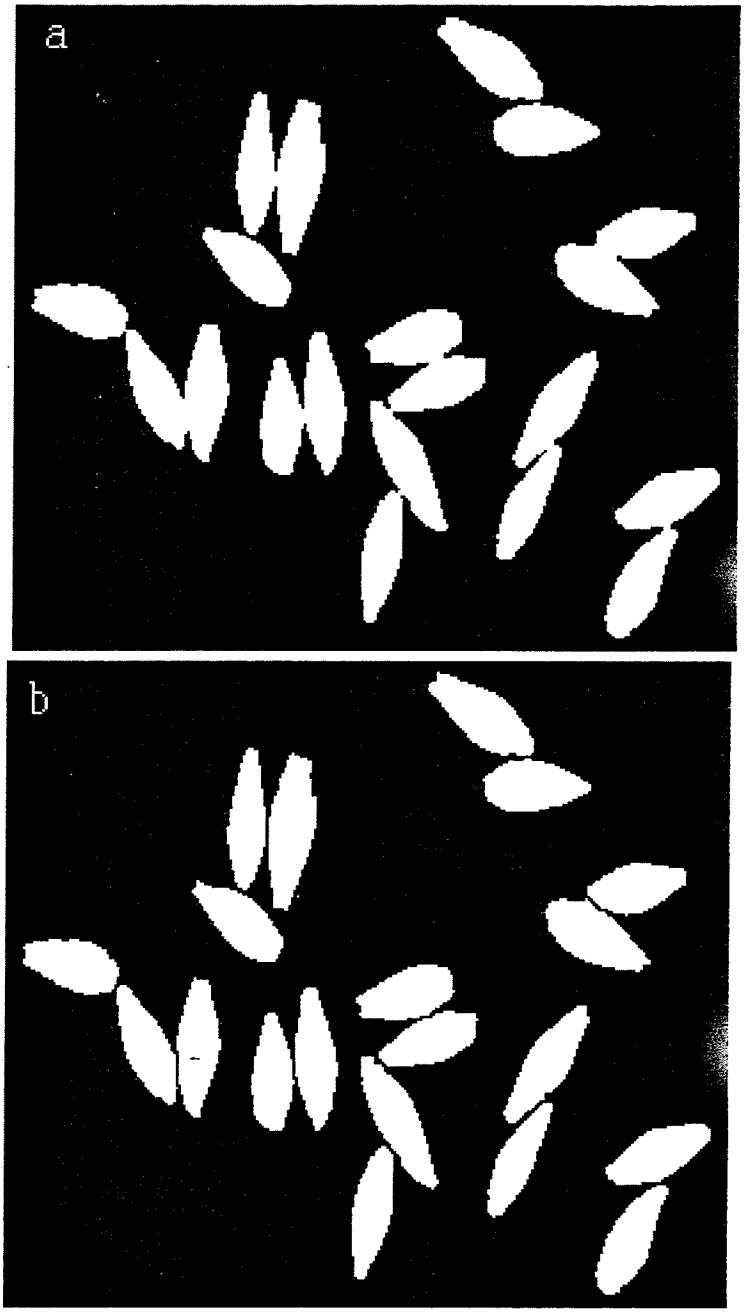

Fig. B56. Example of (a) touching and (b) separated kernels of barley.

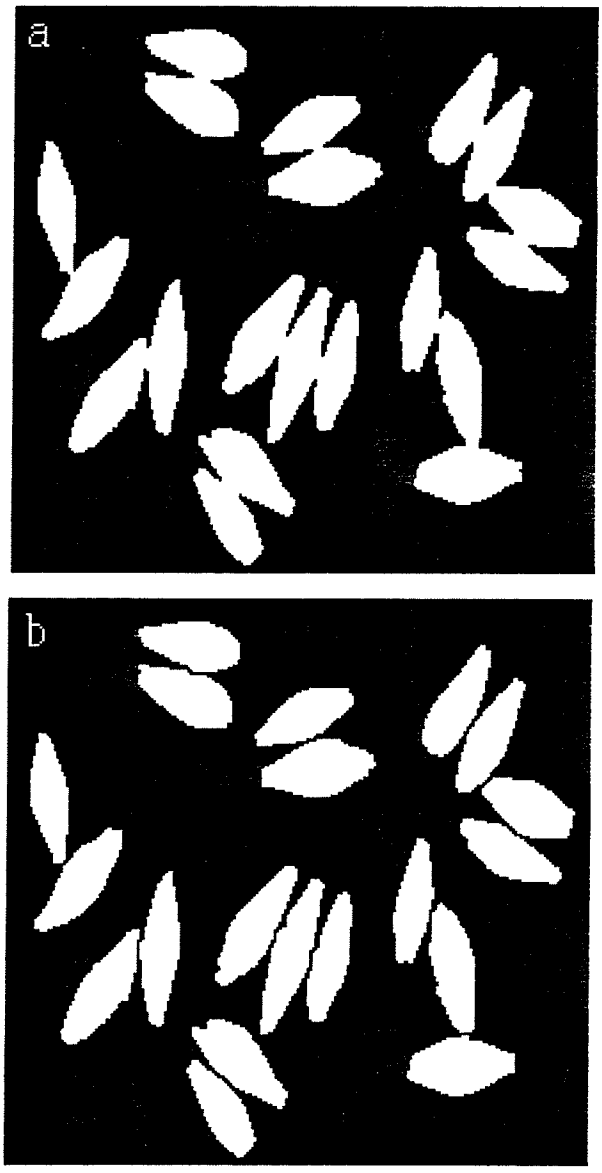

Fig. B57. Example of (a) touching and (b) separated kernels of barley.

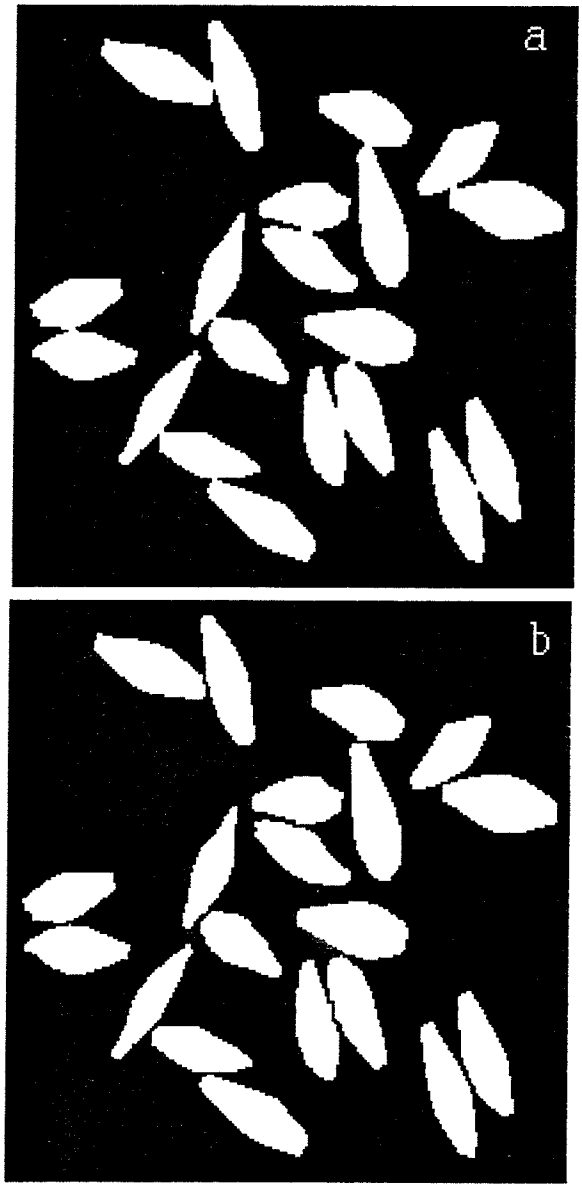

Fig. B58. Example of (a) touching and (b) separated kernels of barley.

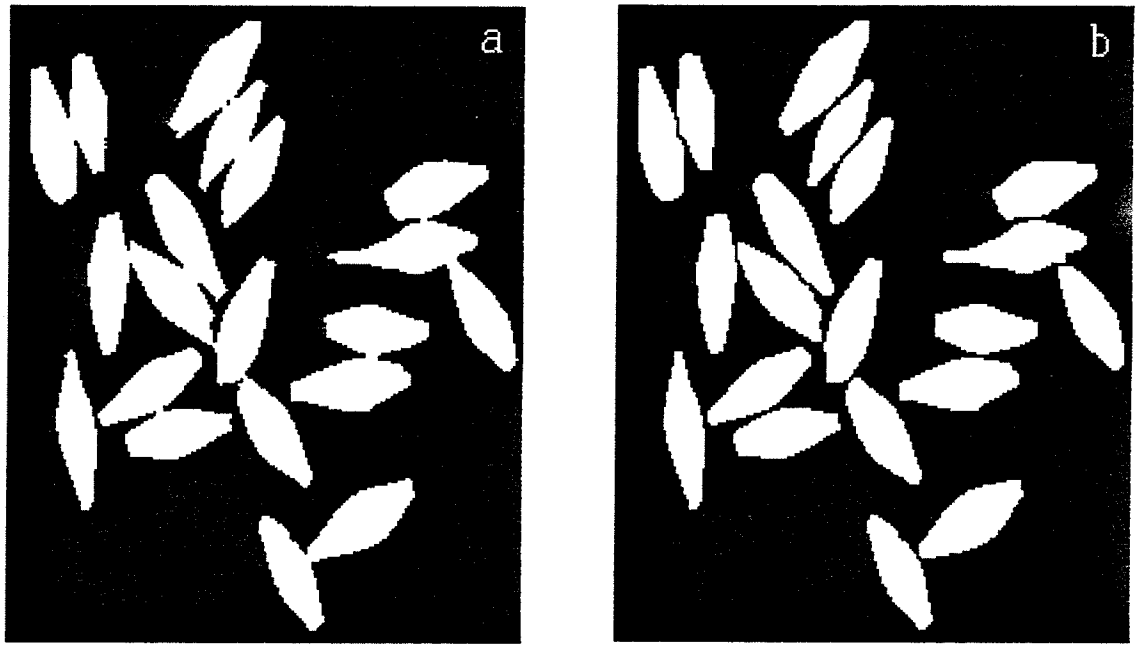

Fig. B59. Example of (a) touching and (b) separated kernels of barley.

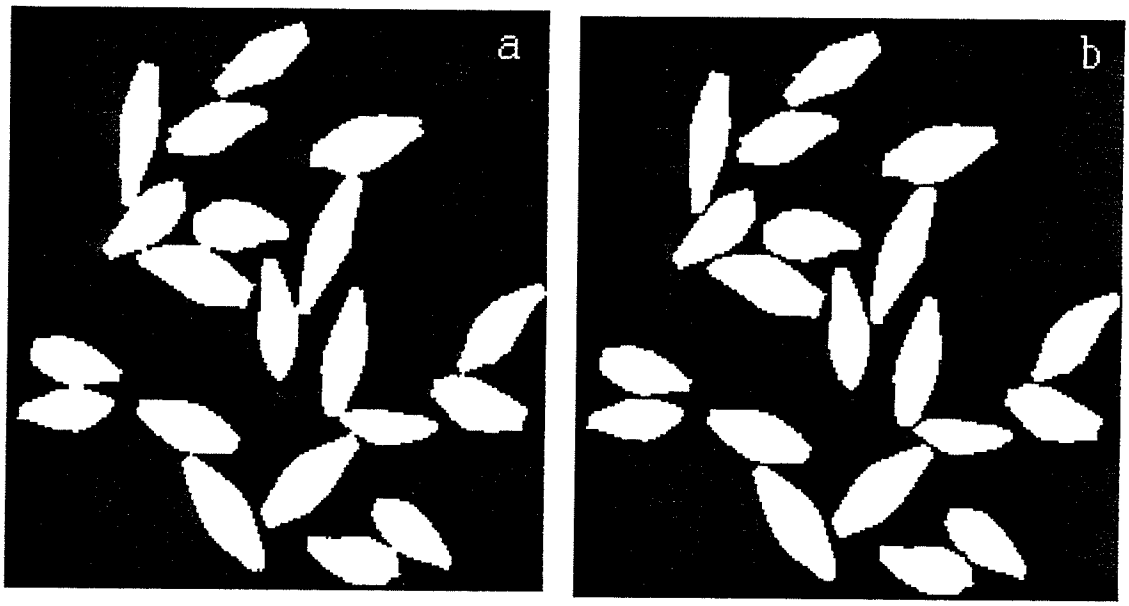

Fig. B60. Example of (a) touching and (b) separated kernels of barley.

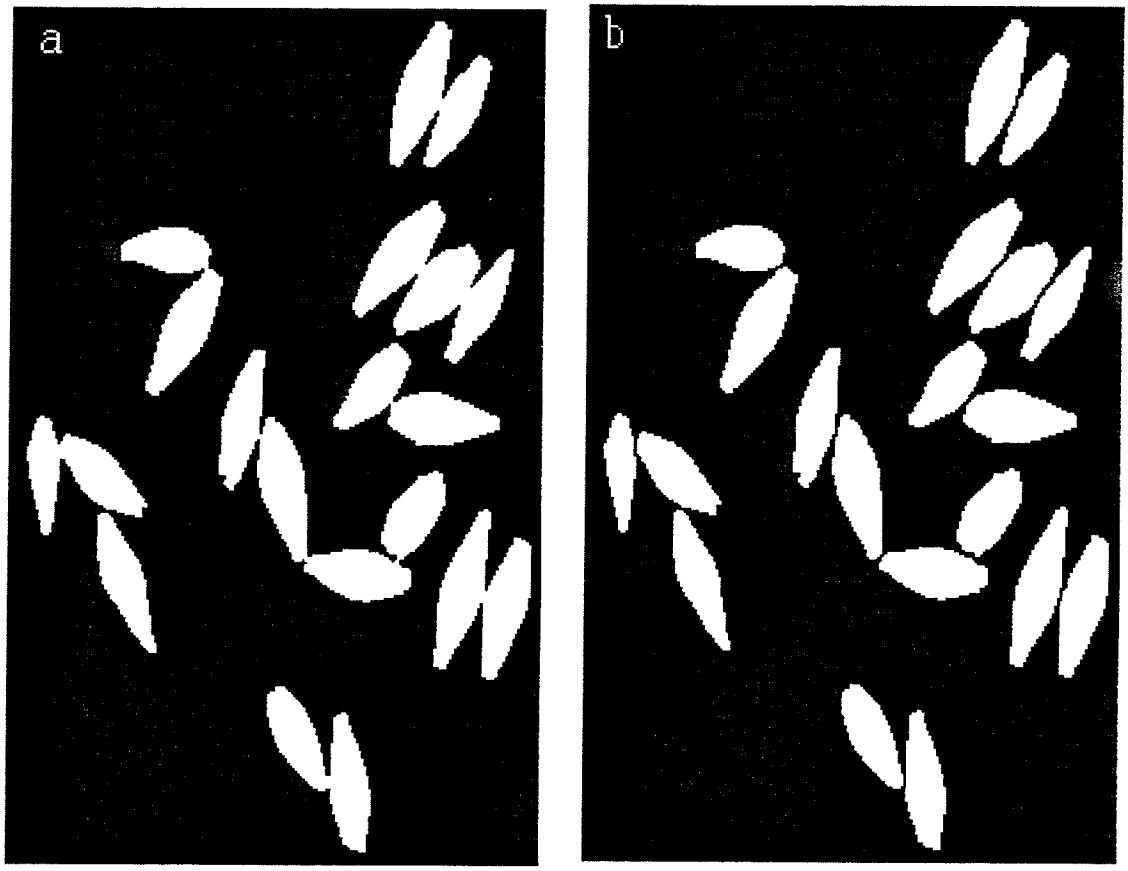

Fig. B61. Example of (a) touching and (b) separated kernels of barley.

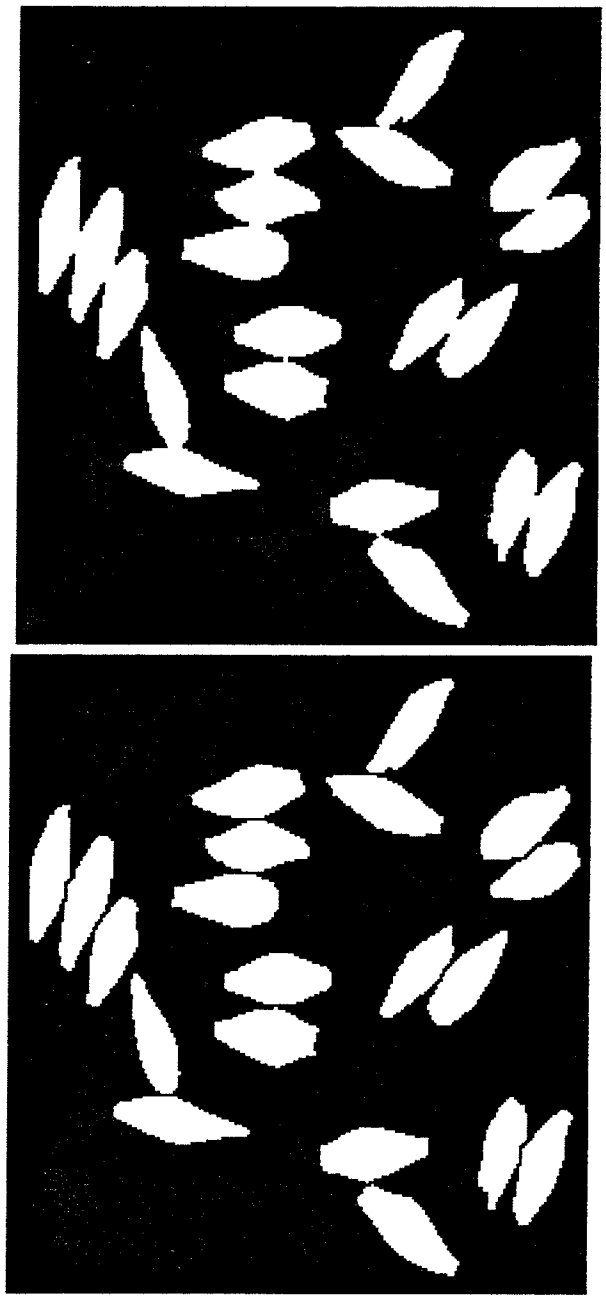

Fig. B62. Example of (a) touching and (b) separated kernels of barley.

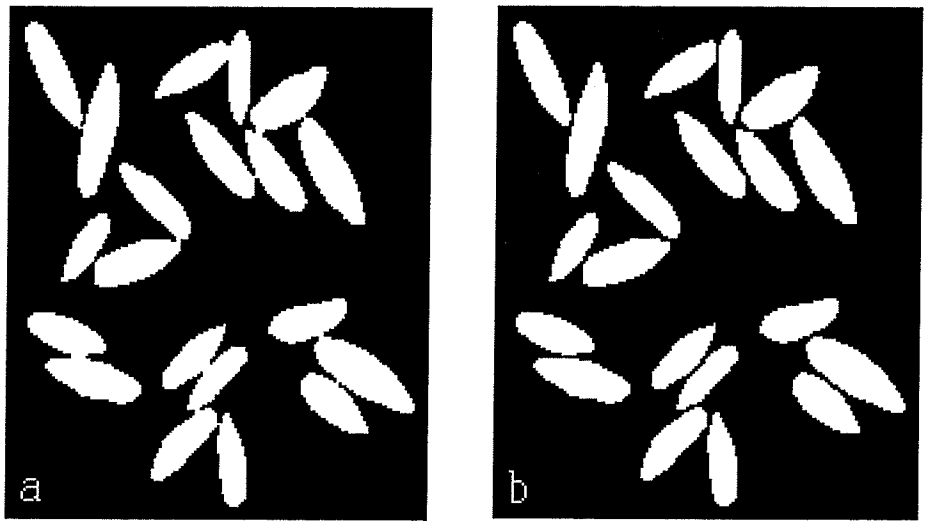

Fig. B63. Example of (a) touching and (b) separated kernels of rye.

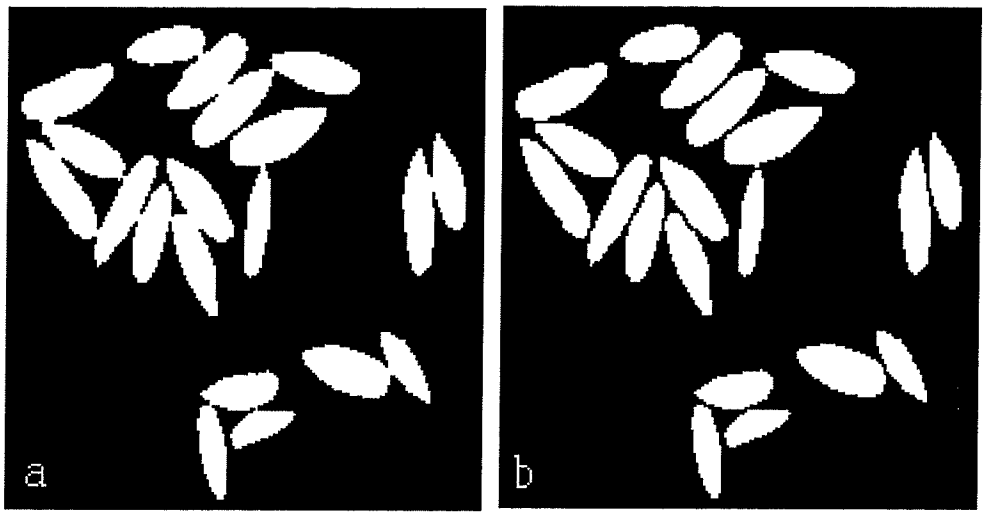

Fig. B-64. Example of (a) touching and (b) separated kernels of rye.

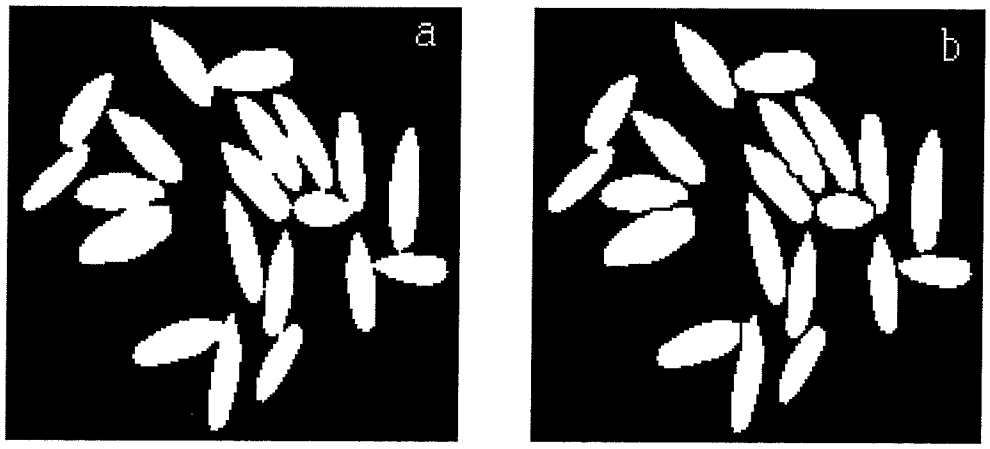

Fig. B65. Example of (a) touching and (b) separated kernels of rye.

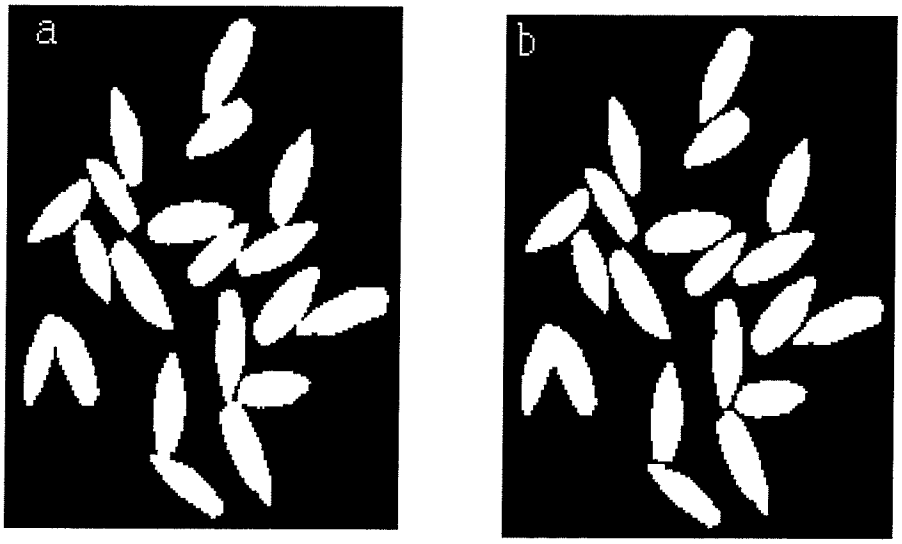

Fig. B66. Example of (a) touching and (b) separated kernels of rye.

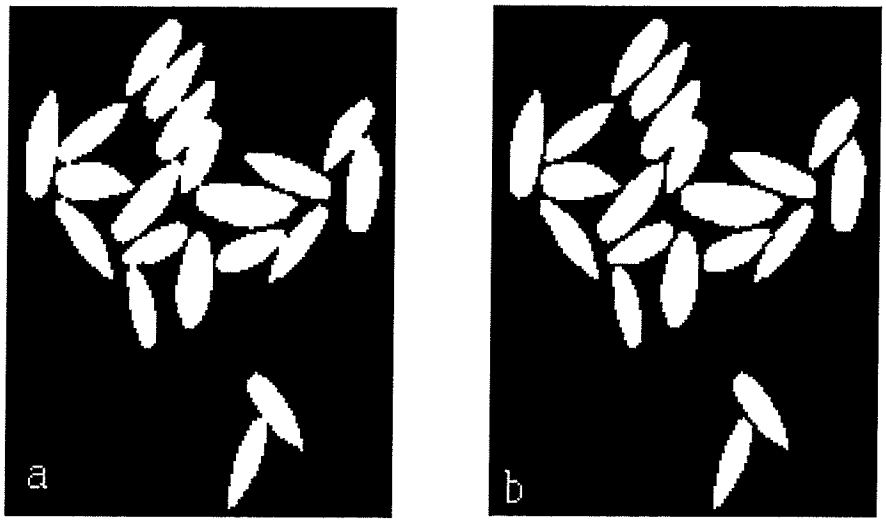

Fig. B67. Example of (a) touching and (b) separated kernels of rye.

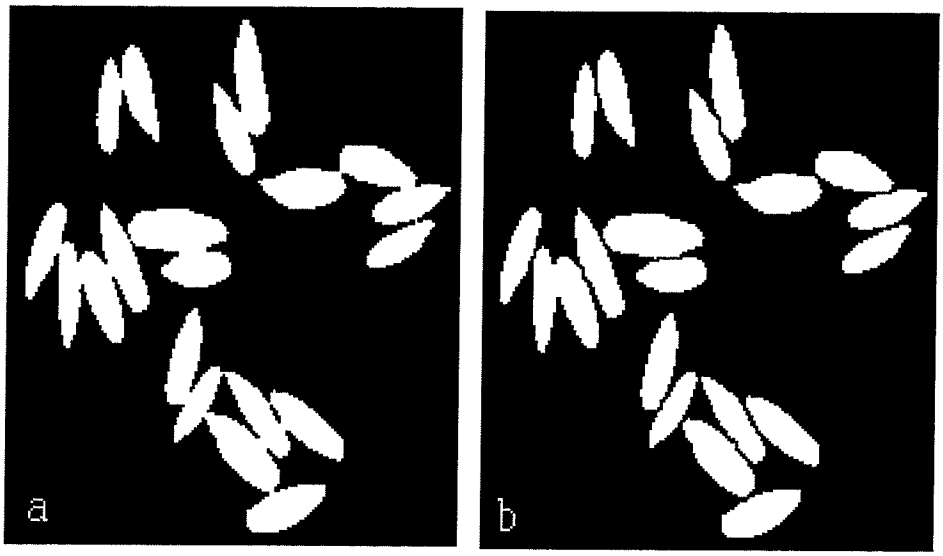

Fig. B68. Example of (a) touching and (b) separated kernels of rye.

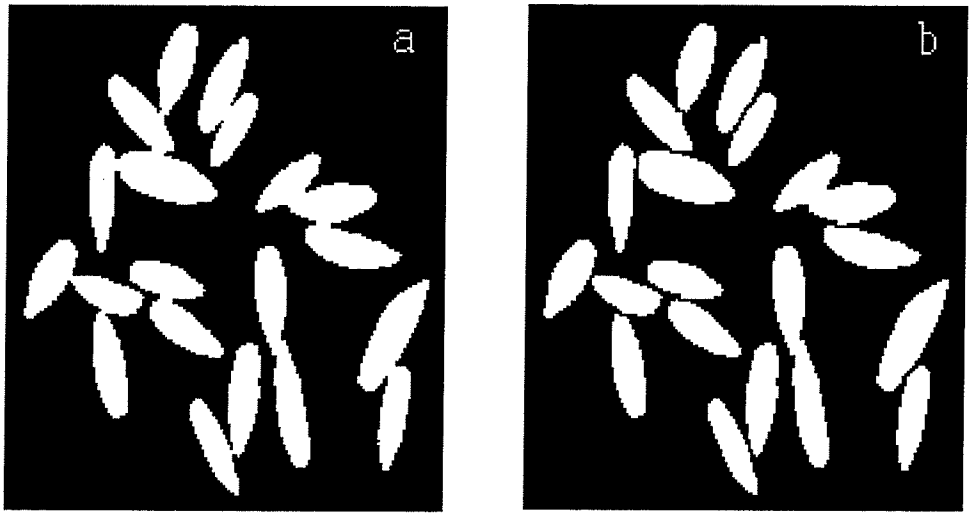

Fig. B69. Example of (a) touching and (b) separated kernels of rye.

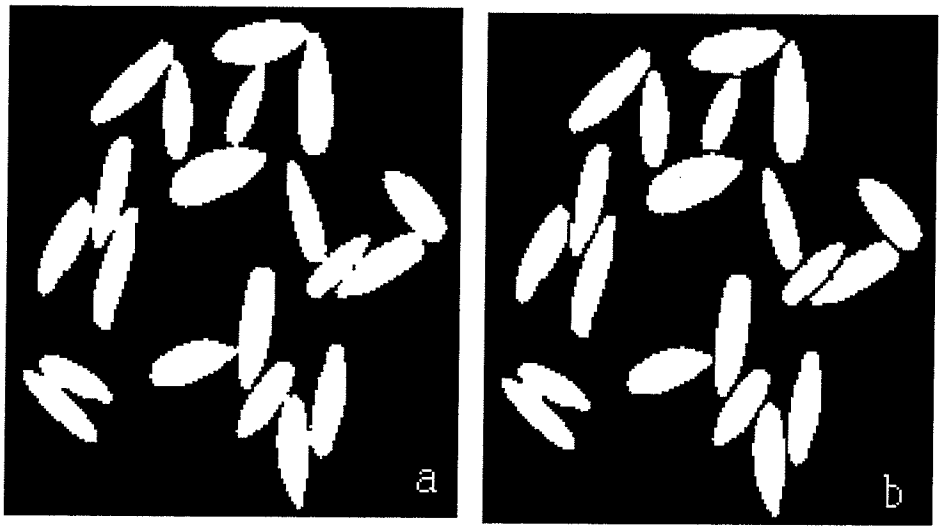

Fig. B70. Example of (a) touching and (b) separated kernels of rye.

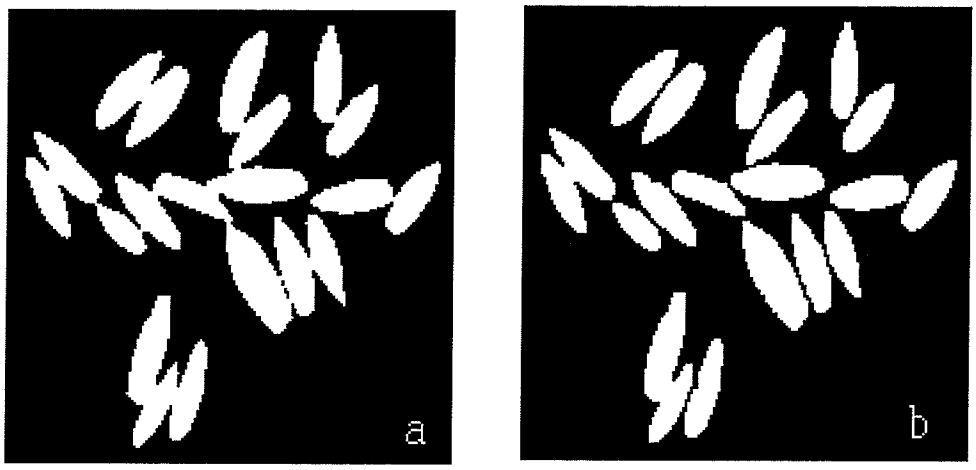

Fig. B71. Example of (a) touching and (b) separated kernels of rye.

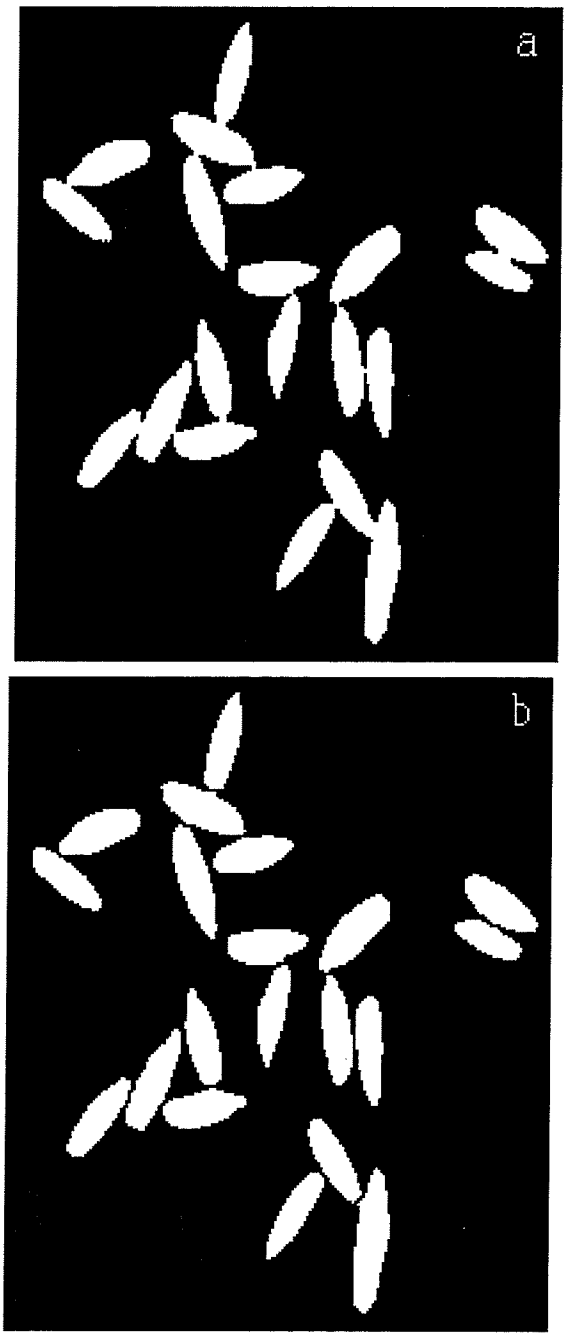

Fig. B72. Example of (a) touching and (b) separated kernels of rye.

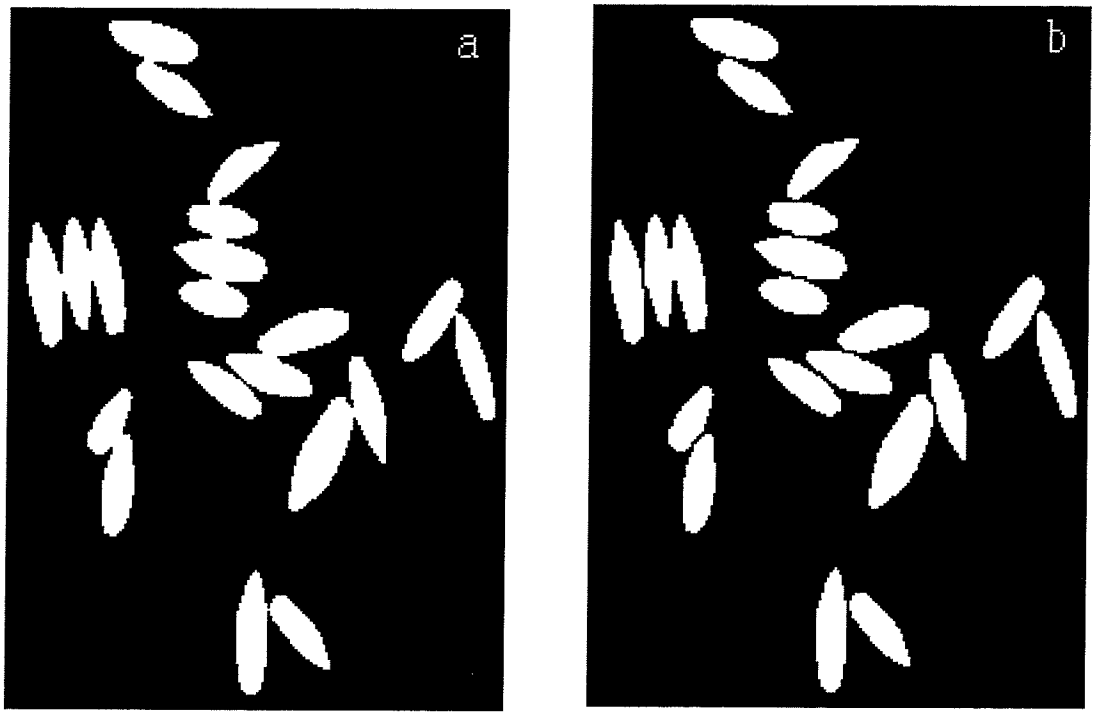

Fig. B73. Example of (a) touching and (b) separated kernels of rye.

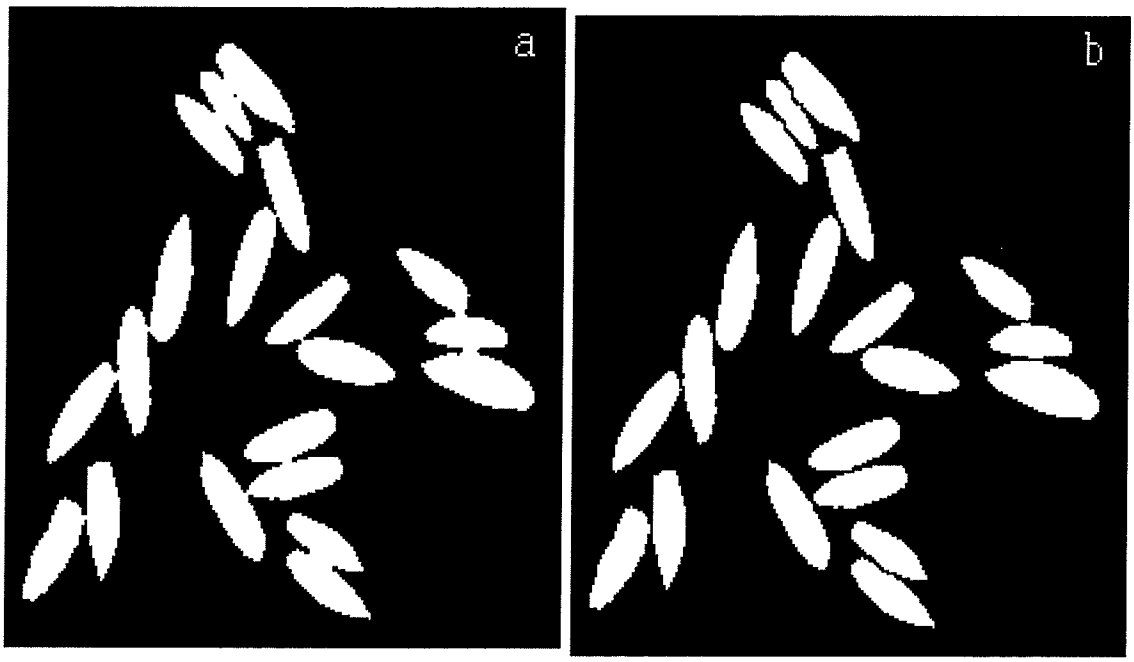

Fig. B74. Example of (a) touching and (b) separated kernels of rye.

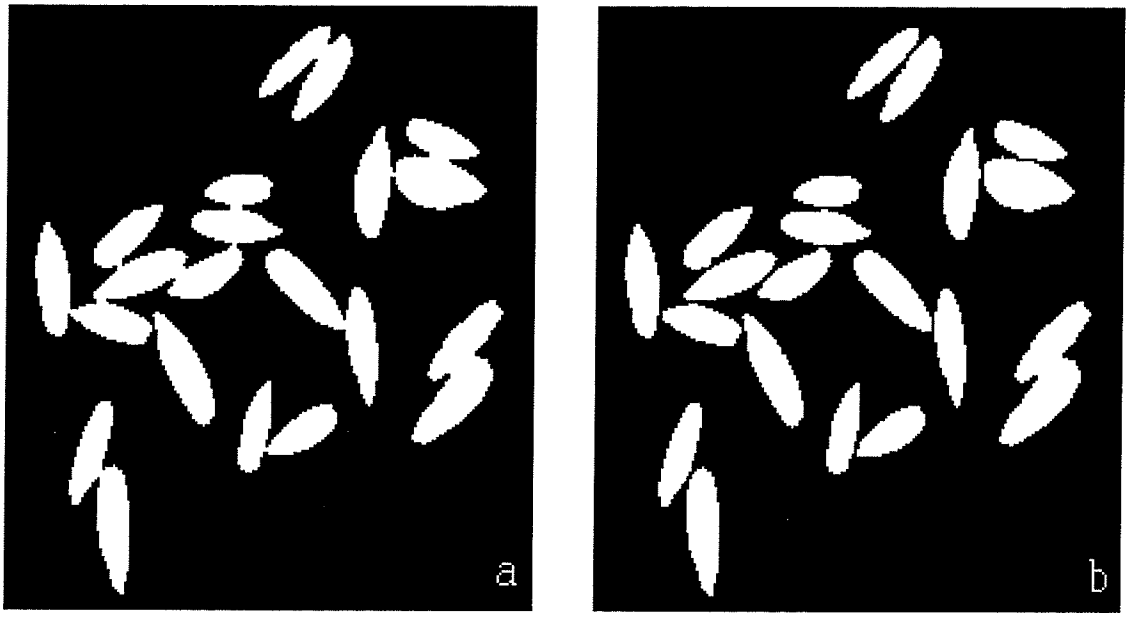

Fig. B75. Example of (a) touching and (b) separated kernels of rye.

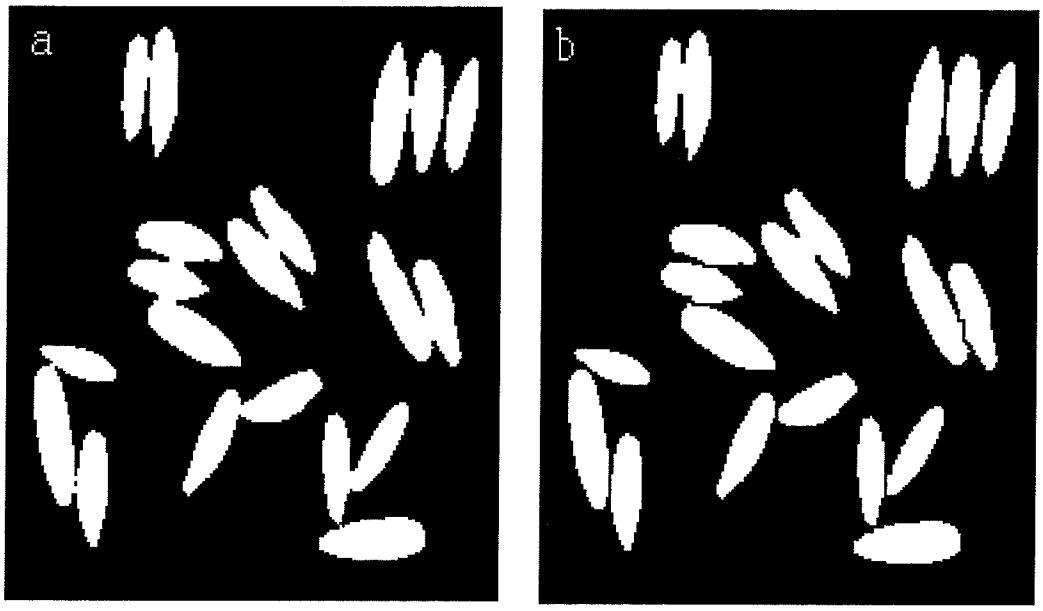

Fig. B76. Example of (a) touching and (b) separated kernels of rye.

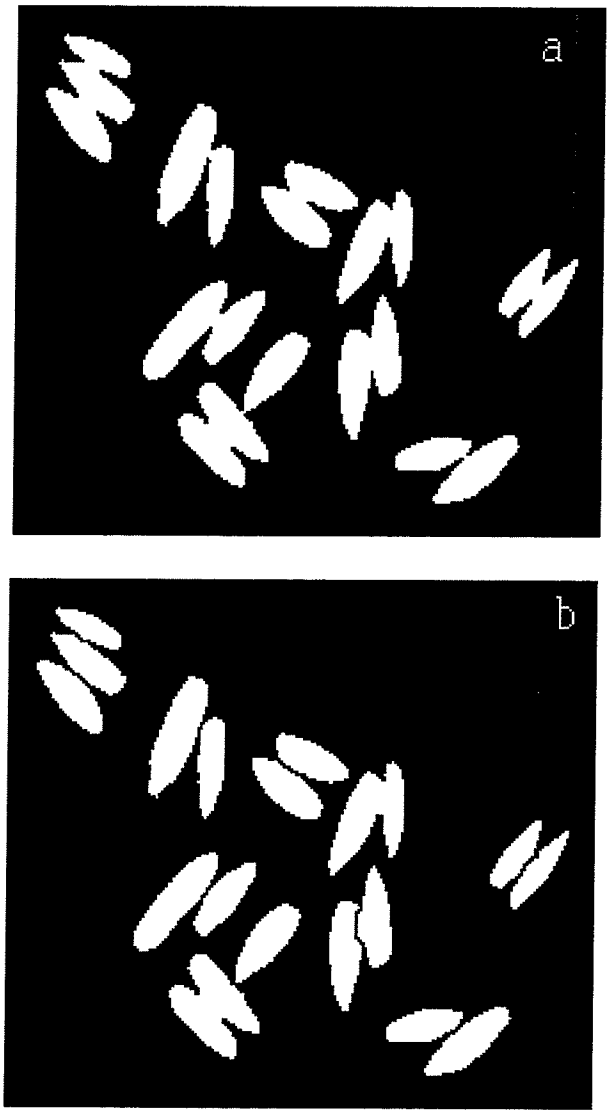

Fig. B77. Example of (a) touching and (b) separated kernels of rye.

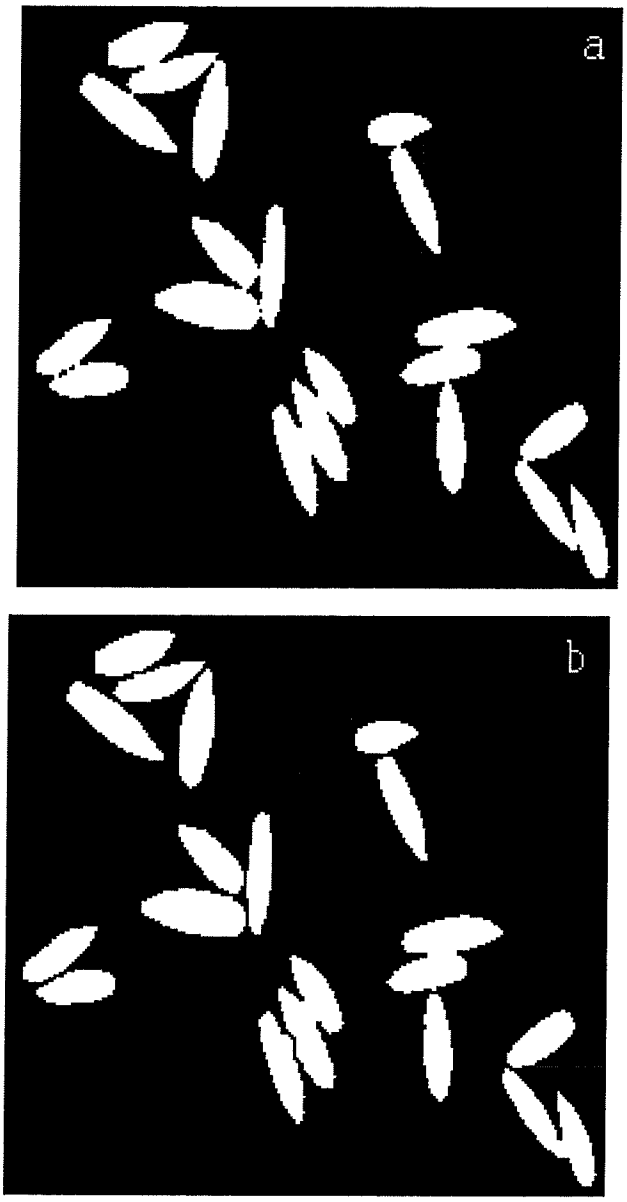

Fig. B78. Example of (a) touching and (b) separated kernels of rye.

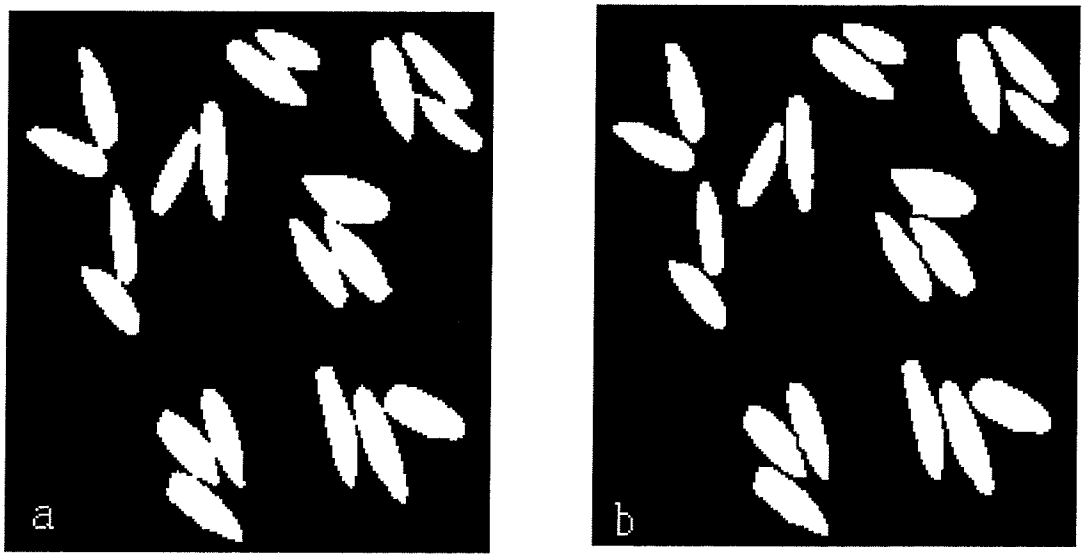

Fig. B79. Example of (a) touching and (b) separated kernels of rye.

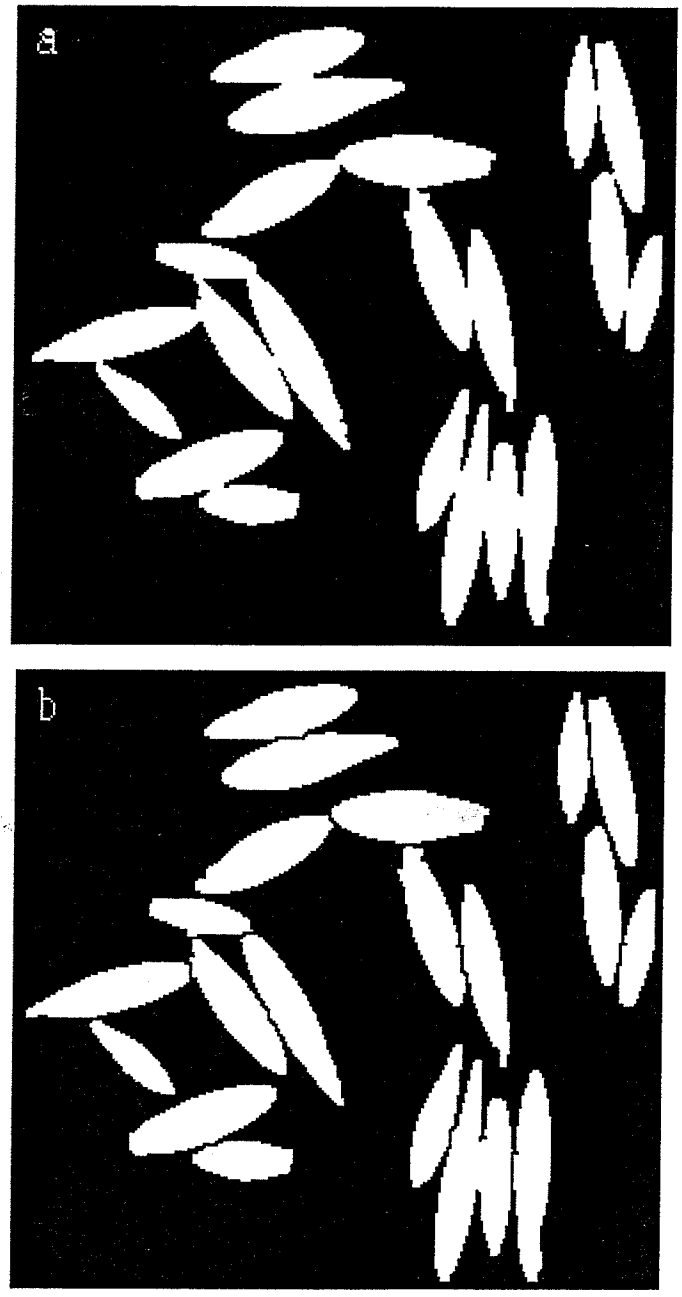

Fig. B80. Example of (a) touching and (b) separated kernels of oats.

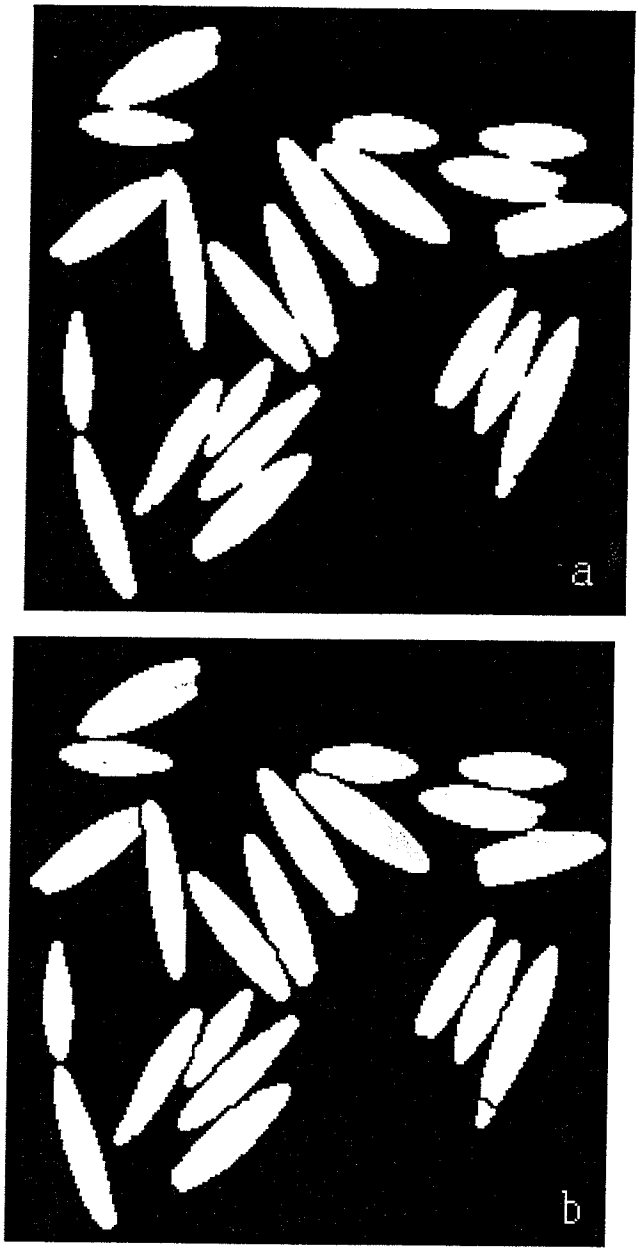

Fig. B81. Example of (a) touching and (b) separated kernels of oats.

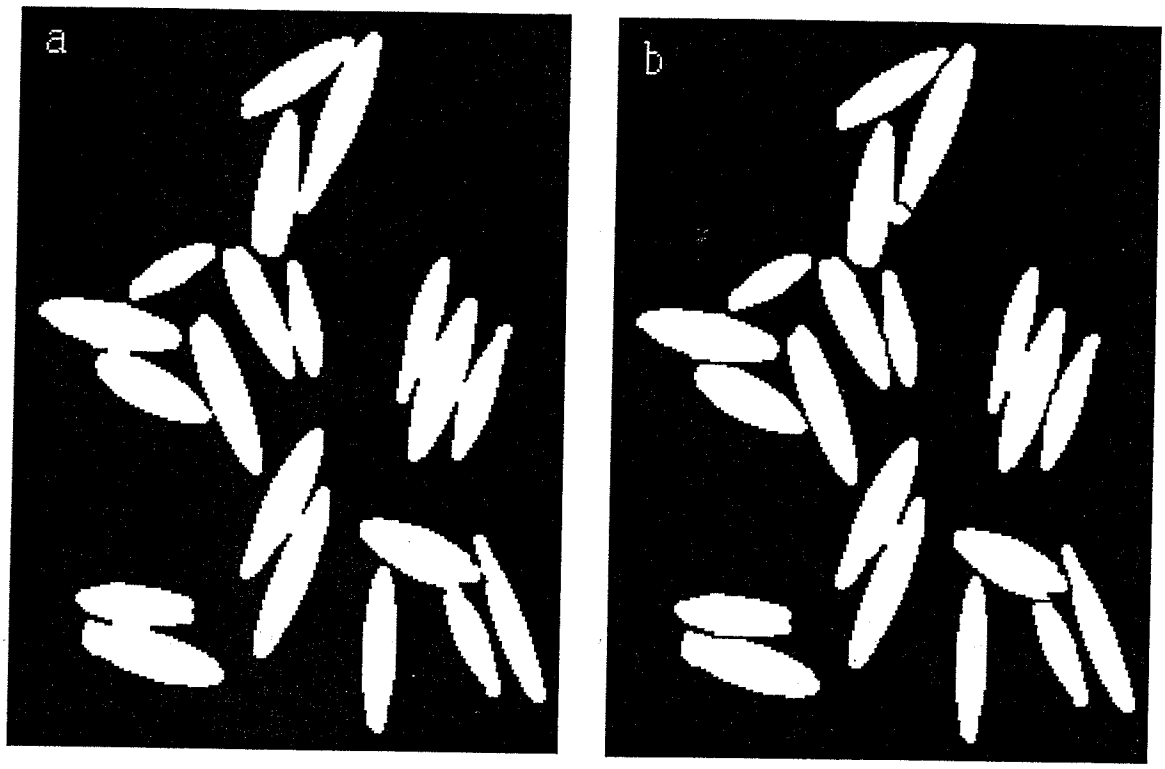

Fig. B82. Example of (a) touching and (b) separated kernels of oats.

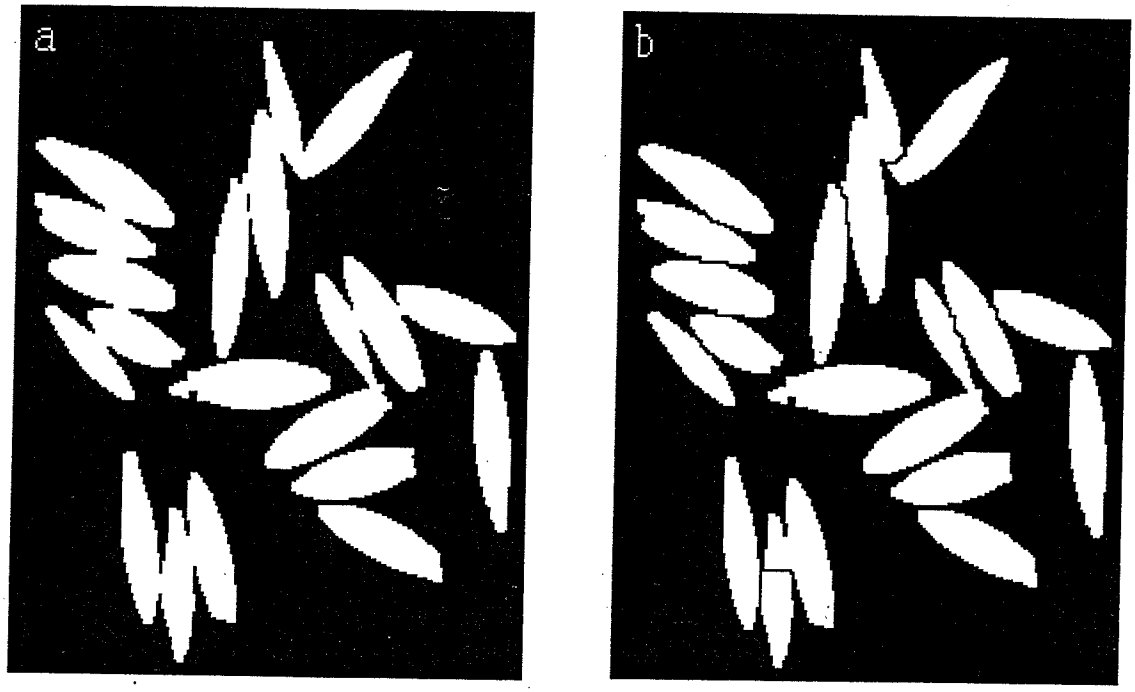

Fig. B83. Example of (a) touching and (b) separated kernels of oats.

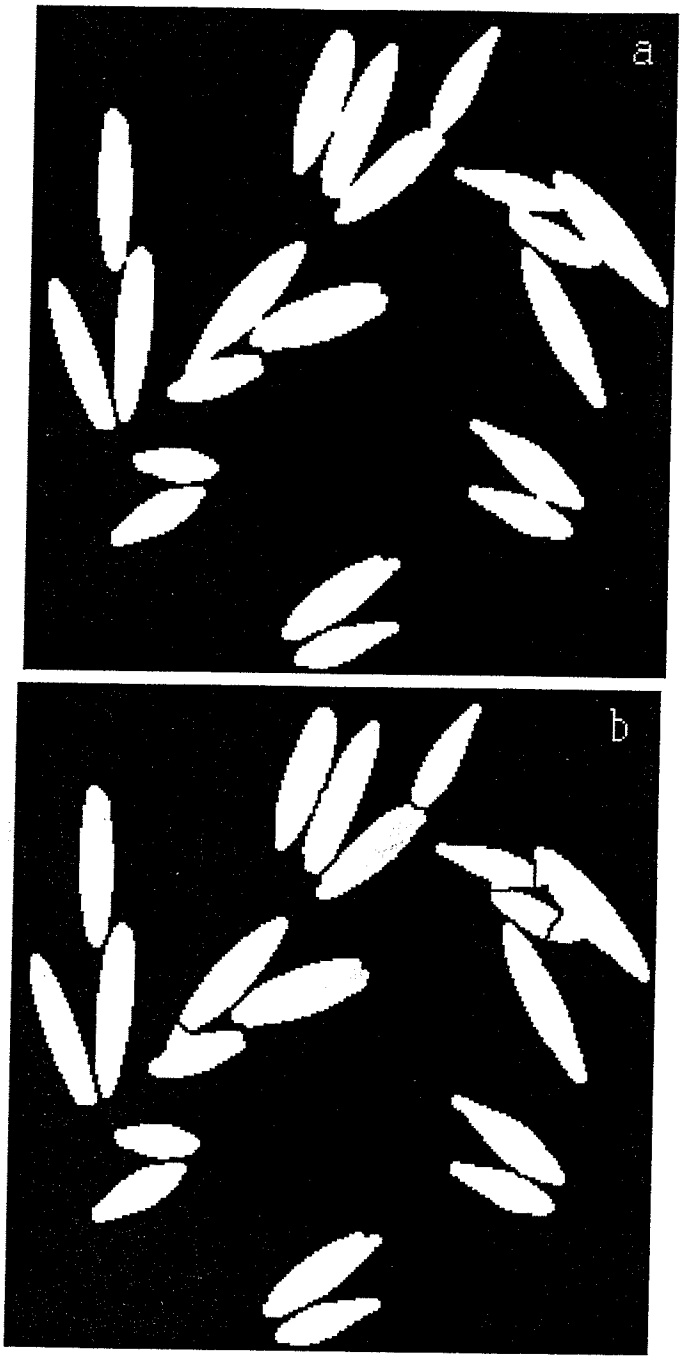

Fig. B84. Example of (a) touching and (b) separated kernels of oats.

Fig. B85. Example of (a) touching and (b) separated kernels of oats.

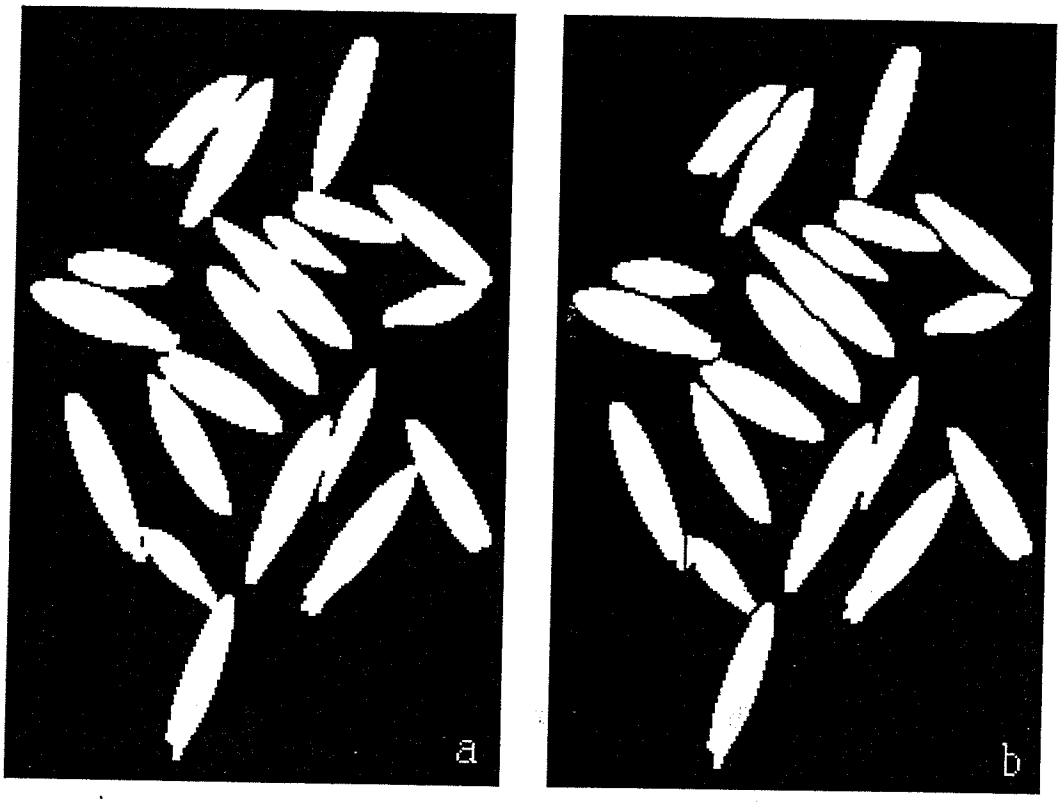

Fig. B86. Example of (a) touching and (b) separated kernels of oats.

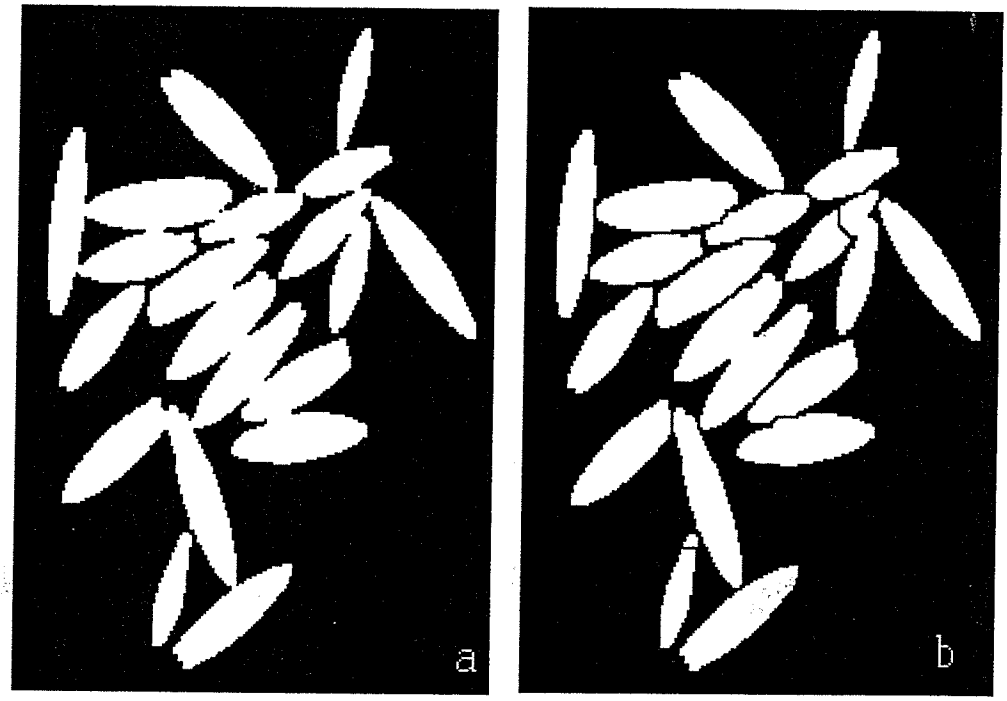

Fig. B87. Example of (a) touching and (b) separated kernels of oats.

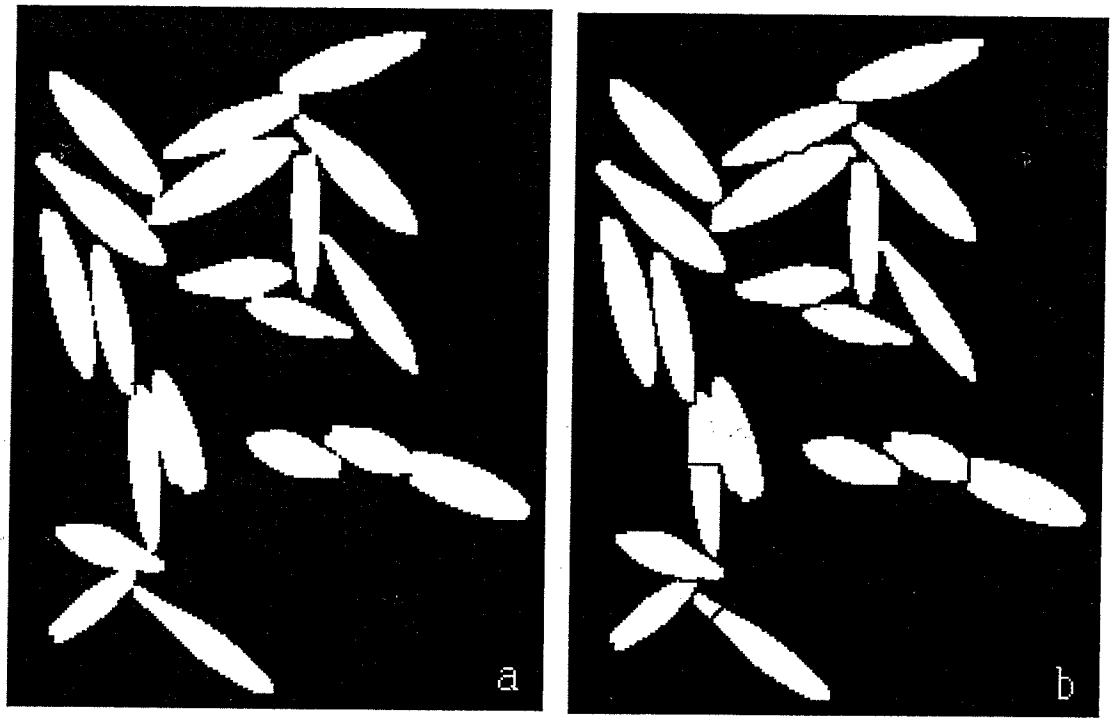

Fig. B88. Example of (a) touching and (b) separated kernels of oats.

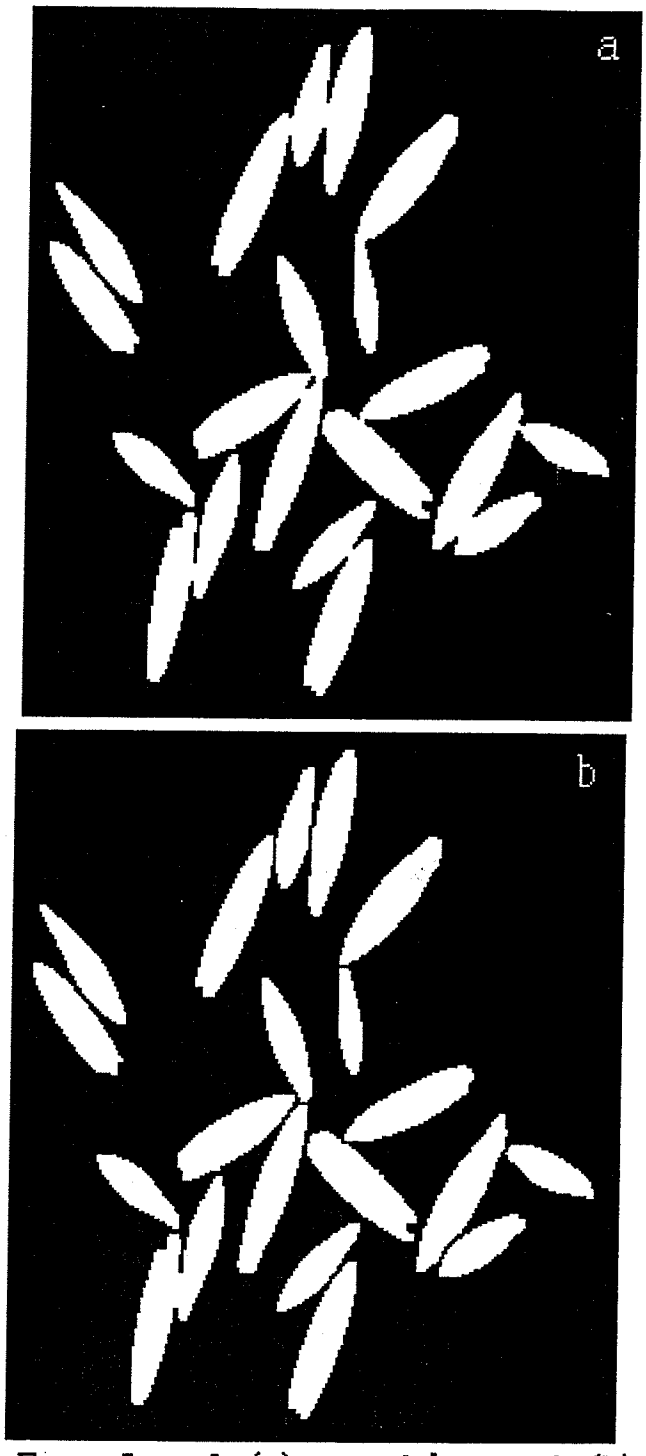

Fig. B89. Example of (a) touching and (b) separated kernels of oats.

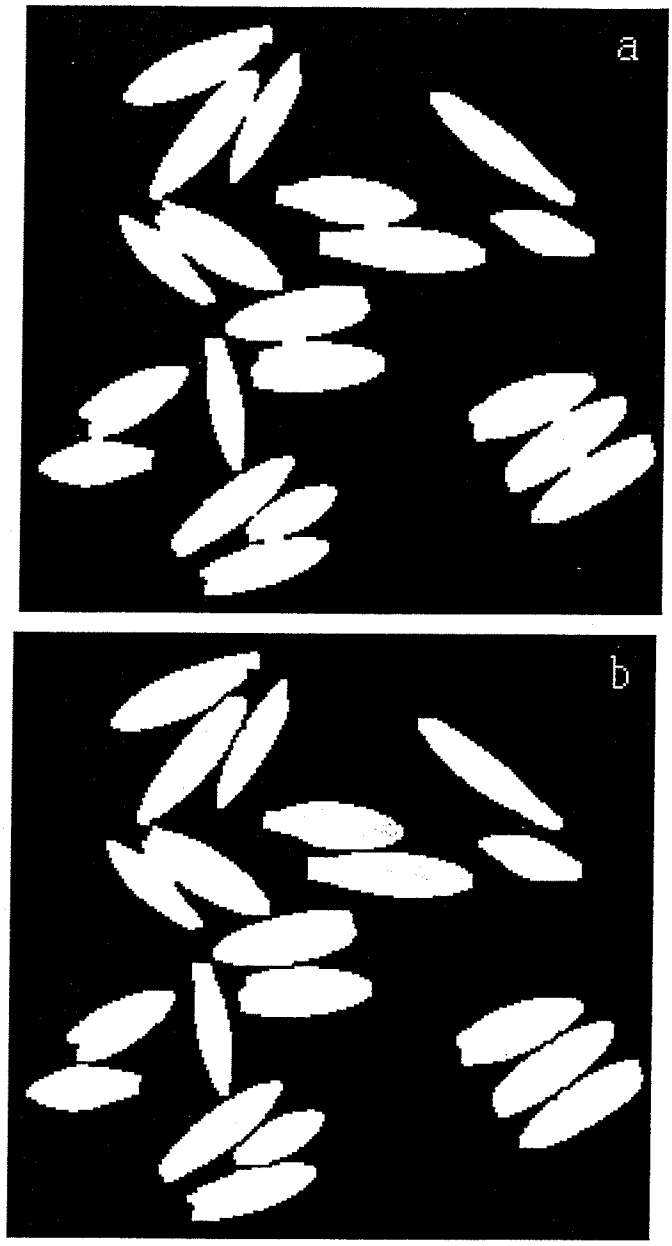

Fig. B90. Example of (a) touching and (b) separated kernels of oats.

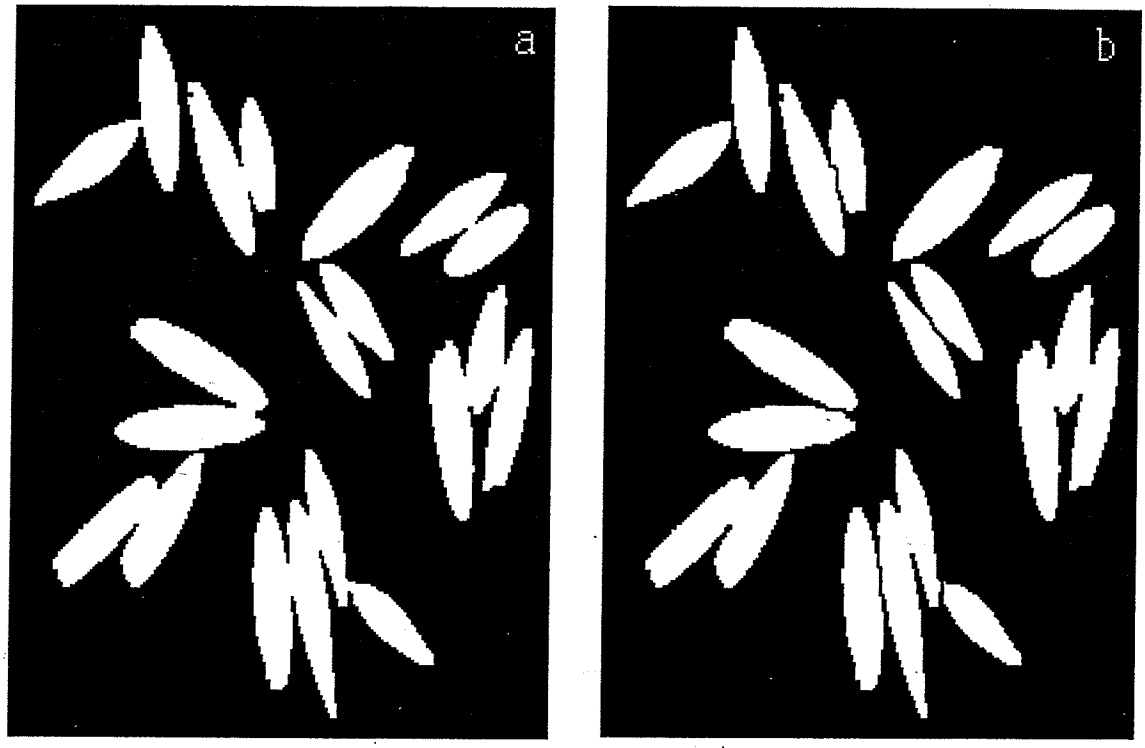

Fig. B91. Example of (a) touching and (b) separated kernels of oats.

Appendix C

Results from the Experiment 1: Precision

Table C1. Mean values of the features from Experiment 1: Precision.

Features	HRS wheat	Durum	Barley	Oats	Rye
Length (mm)	5.83	7.90	10.02	12.35	7.49
Area (mm^2)	16	20	25	25	14
Perimeter (mm)	15.23	18.62	23.38	27.15	16.77
Width (mm)	3.80	3.46	3.75	2.85	2.58
Min. Radius (mm)	1.62	1.44	1.60	1.17	1.05
Max. Radius (mm)	2.93	3.94	5.08	6.36	3.87
Thinness Ratio	14.15	17.49	21.75	29.77	20.77
Rect. Aspect Ratio	1.54	2.28	2.67	4.34	2.89
Radius Ratio	1.81	2.73	3.16	5.43	3.69
H Ratio	5.64	3.28	2.78	2.20	2.67
Area Ratio	1.37	1.39	1.52	1.44	1.44

Table C2. Coefficient of Variation (%)* values of the features from Experiment 1: Precision.

Features	HRS wheat	Durum	Barley	Oats	Rye
Length	2.67	1.42	1.02	1.49	1.29
Area	1.18	2.10	1.37	0.76	1.25
Perimeter	1.13	1.33	1.35	1.99	1.56
Width	3.39	2.22	2.51	3.07	2.73
Minimum Radius	3.61	3.19	2.60	2.87	3.76
Maximum Radius	1.34	1.04	0.83	1.16	1.18
Thinness Ratio	2.06	2.30	2.58	3.73	2.82
Rect. Aspect Ratio	5.35	2.34	2.39	3.32	3.16
Radius Ratio	4.42	3.34	2.52	2.52	3.47
H Ratio	7.57	2.24	1.14	1.37	2.14
Area Ratio	2.55	2.58	2.87	3.13	2.50

* Coefficient of Variation = (Standard Devation / Mean) × 100